University of Naples "Federico II", Italy

Department of Industrial Engineering

Ph.D. in Industrial Engineering

Coordinator: Prof. Michele Grassi

OPTIMIZATION OF THE BUILDING-PLANT SYSTEM FOR NET/PLUS ZERO ENERGY BUILDINGS USING LOW ENTHALPY GEOTHERMAL SYSTEMS

Tutor:
Prof. Francesco Minichiello

Candidate:
Diana D'Agostino

Ph.D. cycle: XXXIII

September 2021

ACKNOWLEDGMENTS

The first deserved thanks go to my Tutor, *Professor Francesco Minichiello*, who from after graduation, took me by the hand and led me into the world of research, teaching me everything I know with passion and dedication.

I thank my children who were born (*Diego*) and raised (*Dionisio*) during my PhD program and who patiently endured and supported me during my long working days, especially during the pandemic.

I thank my husband, *Dimitri*, who, (though I never tell him) is the most patient husband and father in the World, and I am as proud of you as you are of me. Σε παρακαλώ συγχώρεσε την κακή μου διάθεση, μπορείς να αμφιβάλλεις για πολλά πράγματα αλλά ποτέ για την αγάπη μου για σένα.

Big thanks go to my parents, *Paola* and *Diego*, no matter how much I grow up I will always be their little girl, devoting all their energy to making my life as easy as possible. And thanks to my brother Danilo, an example of courage and resourcefulness.

Thanks to *Giovanna* and *Dionisio*, who as patient grandparents contributed to the serenity of my children during the most demanding moments.

Thanks to my friend, colleague, and roommate *Maria*, with whom we shared joys and sorrows, without ever sparing our energy.

Thanks to my lifelong friends *Carla* and *Martina*, and to my new friends Margherita and Bianca Sabrina who made me laugh and gave me moments of absolute carefree without ever lacking their support.

I thank *Professor Carlo Renno*, head of the Laboratory of Applied Thermodynamics of the University of Salerno who shared his experimental activity and with me.

I thank all the *Professors* and *Colleagues* of the Department of Industrial Engineering, including *Fabrizio* for his wisdom and the thousands of coffees shared, *Francesco* who, in addition to having taught me a lot on a professional level, pushed me to overcome my limits and my fears and *Gerry* for being a guide, support and great advisor. Thank you to my colleagues *Francesca*, *Claudia*, *Margherita* and *Davide* for being colleagues and true friends. I love you very much.

Finally, thanks to *all the people* I met during these years, even my undergraduates, as each of them taught me something that I will never forget.

*"La regola secondo me è: quando sei a un bivio e trovi una strada
che va in su e una che va in giù, piglia quella che va in su. È più facile
andare in discesa, ma alla fine ti trovi in un buco. A salire c'è più speranza.
È difficile, è un altro modo di vedere le cose, è una sfida, ti tiene all'erta."*

(Tiziano Terzani)

LIST OF CONTENTS

1 Introduction and aim of the work 12
1.1 Fundamentals on Zero Energy Buildings 13
1.2 Fundamentals on the Geothermal Energy Systems 17
1.3 Aims and originality 19
1.4 Thesis outline 20
2 Ground Source Heat Pump (GSHP) 22
2.1 State of the art 22
2.2 Methodology and application 28
2.2.1 Description of the case study 34
2.3 Results and discussion 41
2.4 Conclusions 52
3 Earth-to-Air Heat eXchanger (EAHX) 55
3.1 State of the art 55
3.2 Methodology and Application 65
3.2.1 Italian climatic zones 68
3.2.2 Climatic zones according to Köppen climate classification 71
3.2.3 The HVAC system description 73
3.2.4 Mathematical model of EAHX 78
3.2.5 Model validation 86
3.3 Results and Discussion 91
3.3.1 Comparison among the six different Italian localities 91
3.3.2 Comparison among the different Köppen climatic areas 111
3.4 Conclusions 119
4 Optimization of a net zero energy building (NZEB) using low enthalpy geothermal systems 123

4.1 Methodology and Application 123
4.1.1 Description of the case study 128
4.1.2 Retrofit scenarios 131
4.2 Results and Discussion 135
4.3 Conclusions 144
5 Conclusions and future developments...147
6 Appendix: experimental CPV/T system..149
6.1 CPV/T description 149
6.2 Applications on case studies...153
6.2.1 Performance analysis on CPV/T coupled to a Desiccant Cooling (DC) system 153
6.2.2 Conclusions 167
Bibliography 169
Publications 178

LIST OF FIGURES

Figure 1. Elements that characterize the definition of an NZEB [8]. 16
Figure 2. Monthly trend of the soil temperature...18
Figure 3. Main classification of the Ground Source Heat Pumps (GSHPs) [20]. 23
Figure 4. Cross sections of geothermal probes: a) single U, b) double U, c) coaxial..24
Figure 5. Cooling and heating operation mode of the GSHP. 25
Figure 6. Maximum performance of heat pumps in winter and summer......25
Figure 7. Detailed HVAC hierarchy in DesignBuilder simulation software [46]. 30
Figure 8. Flowchart of the methodology used. 33
Figure 9. Three-dimensional model of the case study building. 35
Figure 10. Plan of the ground floor and first floor of the case study building. 40
Figure 11. Primary energy consumption for different energy uses in the case of Milan. 44
Figure 12.Primary energy consumption for different energy uses in the case of Palermo...45
Figure 13. Total primary energy consumption in the case of Milan. 45
Figure 14. Total primary energy consumption in the case of Palermo. 46
Figure 15. Percentage reduction of CO_2 emissions for different scenarios in the case of mild climate. 48
Figure 16. Percentage reduction of CO_2 emissions for different scenarios in the case of continental climate. 49
Figure 17. EAHX scheme as pre-cooling technology for summer and pre-heating technology in winter conditions. 55
Figure 18. Office building object of the present analysis:(a) ground floor; (b) first floor. 66
Figure 19. Trend of the external air temperature in the EAHX as the length of the pipe varies for different diameters. 67

Figure 20. The different Italian climatic zones according to D.P.R. n. 412 of 1993. 69
Figure 21.Köppen climate classification map for Italy. 72
Figure 22. HVAC system without EAHX. 74
Figure 23. HVAC system with EAHX. 75
Figure 24. Processes of the humid air into the AHU reported on the psychometric chart during: (a) summer and (b) winter. 76
Figure 25. Schematic of active components in the AHU for primary air in: (a) summer and (b) winter. 77
Figure 26. Computational mesh domain of the investigation on a single buried duct of the EAHX. 80
Figure 27. Average air temperature at the outlet of the buried pipes as a function of time for three different meshing (11124, 15827, 70625 elements). 85
Figure 28. Experimental and numerical values of air temperature alongside one pipe of the EAHX with two inlet volumetric flow rates (135 m^3 h^{-1} and 156 m^3 h^{-1}). 87
Figure 29. Experimental and numerical values of air temperature alongside one pipe of the earth-to-air heat exchanger at an external inlet temperature of 34.9 and 35.9 °C 88
Figure 30. Experimental and numerical values of air temperature alongside the pipe of the earth-to-air heat exchanger. 90
Figure 31. Air temperature along the tube length at different inner tube diameters for: (a) Lampedusa; (b) Catania; (c) Naples; (d) Rome; (e) Milan; (f) Pian Rosa. 95
Figure 32. Air temperature variation in the EAHX as a function of the tube length for an inner tube diameter of 0.2 m in summer. 96
Figure 33. Air temperature variation in the EAHX as a function of the tube length for an inner tube diameter of 0.2 m in winter. 97
Figure 34. EAHX efficiency as a function of tube length for an inner tube diameter of 0.2 m. 98
Figure 35.EAHX efficiency as a function of tube length varying the inner tube diameter in summer for Milan. 100

Figure 36. Capacity of the operating coils as a function of tube length for an inner tube diameter of 0.5 m: (a) during winter, (b) during summer, (c) all over the year....103
Figure 37. Capacity of the operating coils as a function of tube length for an inner tube diameter of 0.3 m: (a) during winter, (b) during summer, (c) all over the year....107
Figure 38. Coils capacity of the operating coils as a function of tube length for an inner tube diameter of 0.2 m: (a) during winter, (b) during summer, (c) all over the year....110
Figure 39. Air temperature variation in the EAHX as a function of the tube length for an inner tube diameter of 0.2 m in: (a) summer; (b) winter....113
Figure 40. Efficiency of the EAHX as a function of the tube length for summer season....114
Figure 41.Coils capacity of the operating coils as a function of tube length for an inner tube diameter of 0.2 m: (a) during winter, (b) during summer, (c) all over the year....117
Figure 42. Geological map of Piana Campana, region of South Italy....124
Figure 43. Workflow of the methodology used....125
Figure 44. Aerial photogrammetry of the existing building....128
Figure 45. Plan drawing of the existing building....129
Figure 46. Thermal zones of the existing building....129
Figure 47. Primary energy consumption of the existing building....135
Figure 48. Yearly primary energy consumption for scenario 1....136
Figure 49. Comparison in terms of primary energy consumptions between existing building and scenario 1....137
Figure 50.Comparison in terms of primary energy consumptions between existing building and scenario 2....137
Figure 51. Comparison in terms of primary energy consumptions between existing building and scenario 3....138
Figure 52.Comparison in terms of primary energy consumptions between existing building and scenario 4....139
Figure 53. Comparison between the different scenarios in terms of primary energy....140

Figure 54. Comparison between the different scenarios in terms of CO_2 emissions..141
Figure 55. Electric energy needs and electric energy production from PV system on monthly basis: a) scenario 2; b) scenario 4. 142
Figure 56. Linear focus experimental plant: a) Triple-Junction solar cell; b) cooling fluid circuit; c) global CPV/T system. 150
Figure 57. Degrees of freedom of the experimental plant. 152
Figure 58. Scheme of the CPV/T coupled to the desiccant cooling system in summer conditions...154
Figure 59. Flow-chart of the model. 155
Figure 60. Scatterplot of the ANN configuration for predicting the DNI. ...156
Figure 61. Thermal (a) and electrical (b) loads annual trend for the case 1. 157
Figure 62. Thermal (a) and electrical (b) loads annual trend for the case 2. 158
Figure 63.Thermal (a) and electrical (b) loads annual trend for the case 3. .159
Figure 64.Thermal (a) and electrical (b) energy production and loads for a summer day..163
Figure 65.Thermal (a) and electrical (b) energy production and loads for a winter day..164
Figure 66. Thermal (a) and electrical (b) energy production and loads for a half season day..165
Figure 67. NPV (Net Present Value) for the proposed CPV/T-DC system in the cases 1, 2, 3. 167

LIST OF TABLES

Table 1. Geographic and climatic conditions of the selected towns [53]. 34
Table 2. Unitary thermal transmittance of the case study building envelope (W/m^2K). 35
Table 3. Design thermal loads of the case study building for both heating and cooling. 39
Table 4. Seasonal average energy efficiency for the analysed solutions.........39
Table 5. Energy consumption for different HVAC proposals for the building located in Palermo. 42
Table 6. Energy consumption for different HVAC proposals for the building located in Milan. 43
Table 7. CO_2 emissions for heating and total energy consumption related to different scenarios. 47
Table 8. Net Zero Energy balance and number of PV modules for Palermo [58]. 50
Table 9. Net Zero Energy balance and number of PV modules for Milan [58]. 51
Table 10. Economic evaluation and SPB-DPB for the two different cities......52
Table 11. Winter and summer design outdoor parameters for the six localities chosen. 70
Table 12. Classification of the chosen Italian cities according to Köppen climatic zones. 72
Table 13. Winter and summer design outdoor parameters for Rio de Janeiro, Dubai, and Ottawa. 73
Table 14. Reynolds numbers evaluated for each couple of diameter and inlet velocity for each air duct. 79
Table 15. Experimental constants of the K-ε ̂model 81
Table 16. Thermal properties of the soil. 82
Table 17. Temperature of the undisturbed soil obtained by Kusuda equation. 83
Table 18. Absolute and relative error on air outlet temperature [90]. 87
Table 19. Absolute and relative error on air outlet temperature [91]. 89

Table 20. Absolute and relative error on air outlet temperature [72]. 90
Table 21. Useful parameters to dimension the probes of GSHP...................126
Table 22. Unitary thermal transmittance of building envelope components in the current state. 130
Table 23. Different energy retrofit scenarios. 132
Table 24. Thermal and energy parameters of the proposed heat pumps.....132
Table 25. Characteristics of EAHX and GSHP systems [99] 133
Table 26. Unitary thermal transmittances of the improved building opaque envelope components. 134
Table 27. Power and number of panels of the PV system necessary to obtain an NZEB for the different scenarios...143
Table 28. Energy costs and savings for different scenarios compared to the existing building. 144
Table 29. TJ cell characteristics. 150
Table 30. Energy loads and energy production together with the electrical and thermal loads cover rate in the case 1. 160
Table 31. Energy loads and energy production together with the electrical and thermal loads cover rate in the case 2. 161
Table 32. Energy loads and energy production together with the electrical and thermal loads cover rate in the case 3. 162
Table 33. CPV/T-DC system costs. 166

1 INTRODUCTION AND AIM OF THE WORK

Nowadays it is well known that in Europe the civil buildings sector represents a large portion (about 36%) of total worldwide CO_2 emissions and 40% of total energy consumption.

This is a key point of *sustainable development.* In fact, to best implement this concept, starting from the reduction of buildings' energy needs is needed.

Over the years this has led to numerous strategies aimed at improving the building-plant system, generating almost or completely self-sufficient building models.

Thus, European Directives have been issued to reduce CO_2 emissions by improving the energy performance of buildings, i.e., the Energy Performance Building Directive, so-called "EPBD"[1] and "EPBD recast"[2]. Particularly, this last Directive introduces the concept of *nearly Zero Energy Buildings* (nZEBs). Citing the EPBD recast, "*The nearly zero or very low amount of energy required should be covered to a very significant extent from renewable sources, including sources produced on-site or nearby.*"

This concept becomes more ambitious with the introduction of the *Net Zero Energy Buildings* (NZEBs) in which the yearly energy required should be entirely balanced through renewable energy sources.

If referring to the civil construction sector, the renewable systems usually suitable are solar photovoltaics and solar thermal systems. These systems should be installed either on the roof of the building or in the immediate vicinity. Furthermore, in widely urbanized contexts, installing renewable energy sources in order to cover the entire energy demand of a building becomes rather complicated.

Nowadays, there are no legislative requirements for NZEBs beyond their mere definition.

Moreover, we have to remember that the only significant presence of renewable energy sources can not lead to an energy efficient building, considering the possible overloading of the national electricity grids that would arise if everyone would decide to install a large number of photovoltaic solar panels.

These are some of the reasons why the fascinating concept of a totally energy self-sufficient building is not yet widespread in urbanized contests.

In addition, the increasingly restrictive energy parameters that are required in the current legislation, lead to ask what the characteristics of the "*optimum design*" of the building-plant system are. Design must be directed not only towards increasingly better performing building envelopes, but also proposing increasingly innovative HVAC system components.

1.1 FUNDAMENTALS ON ZERO ENERGY BUILDINGS

As mentioned in the introduction section, a Net Zero Energy Building (NZEB) is a building in which the non-renewable primary energy request is equal to 0 kWh/m2 on a yearly basis.

At first glance, this topic seems easy to understand, but of course it still lends itself to different interpretations in relation to the different points of view (energy, economic or environmental) from which this type of building can be viewed.

The concept of Zero Energy Building (ZEB) was first proposed as early as 1977, when a group of researchers in Denmark conducted a study on solar energy for a heating system in buildings to counter the problem related to the price of petrol, describing a system sized in such a way as to be self-sufficient especially in the supply of heat.

In 1995, Gilijamse [3] was the first author who, giving importance to energy saving, introduced for the first time the theme of ZEBs connected to the national electricity grid (on-grid), focusing the question on the energy balance between consumption and the yearly production of electricity.

From this, the importance of ZEBs grew more and more, and at the same time the research on zero energy/emission buildings developed. Among the most accredited studies, that of Torcellini et al. [4] highlights three fundamental principles:

• Minimize overall environmental impact by encouraging energy efficient building designs and reduce transport and conversion losses.

• Use of technologies available for the entire duration of the life of building.

• Use of renewable energy sources which are widely available and have a high replication potential for the future.

Therefore, four building classification criteria are defined based on energy performance accounting:

1) Net Zero Site Energy.

Buildings that produce as much energy from renewable sources as it uses in a year. In this case, the "delivered energy", i.e., the energy supplied from the outside to the building system, is null for all energy carriers.

2) Net Zero Source Energy.

The amount of primary energy entering the building on the border is equal to the amount of primary energy outgoing. It is a building that produces (or purchases) as much energy from renewable sources as it uses primary energy in a year.

3) Net Zero Energy Costs.

The amount that the managers of the territorial energy infrastructures pay to the owner of the property for the energy he self-produced on site from renewable energy sources and poured into the grid ("exported energy") is at least equal to the cost that the owner of the property pays to the operators itself for the energy he needs during a calendar year ("delivered energy").

4) Net Zero Energy Emissions.

A building that, over the course of a year, produces as much renewable energy with zero emissions as is needed to offset the carbon dioxide emissions associated with the energy it uses. Naturally, the emission balance must be carried out using the conventional values of the emission factors for the different energy carriers.

Despite all these definitions, there are common criteria that contribute to the definition of the NZEB target [5] [6]:

- The position and orientation of the building must help to control the contributions of solar radiation on the opaque and transparent envelope and favour the natural ventilation.

- The thermal mass of the building allows to reduce temperature variations due to external climatic conditions (mainly in summer), and the building envelope must ensure adequate air tightness.

- Thermal regulation systems are aimed at maintaining the internal conditions of the project, with the aim of both guaranteeing internal comfort and limiting energy consumption.

- Solar shading systems are essential to avoid overheating in summer.

According to the state of the art, traditional HVAC i.e., heating, ventilation and air conditioning systems are responsible for nearly half of a building's total energy consumption [7]. For this reason, in addition to optimal characteristics of the envelope components, it is also necessary to improve the systems by equipping the building with advanced systems, with high energy efficiency and based on the use of renewable energy sources. Among the most adopted solutions are Dedicated Outdoor Air Systems (DOAS), mechanical ventilation systems with heat recovery units, heat pumps for heating and cooling, passive daylighting technologies, photovoltaic systems and solar thermal systems [7]. Figure 1 shows the most important elements to take into account in order to define an NZEB.

It is deduced that the energy needs for cooling and heating, domestic hot water and ventilation must be calculated and managed in the best possible way to ensure both the comfort of the occupants and the reduction of energy consumption.

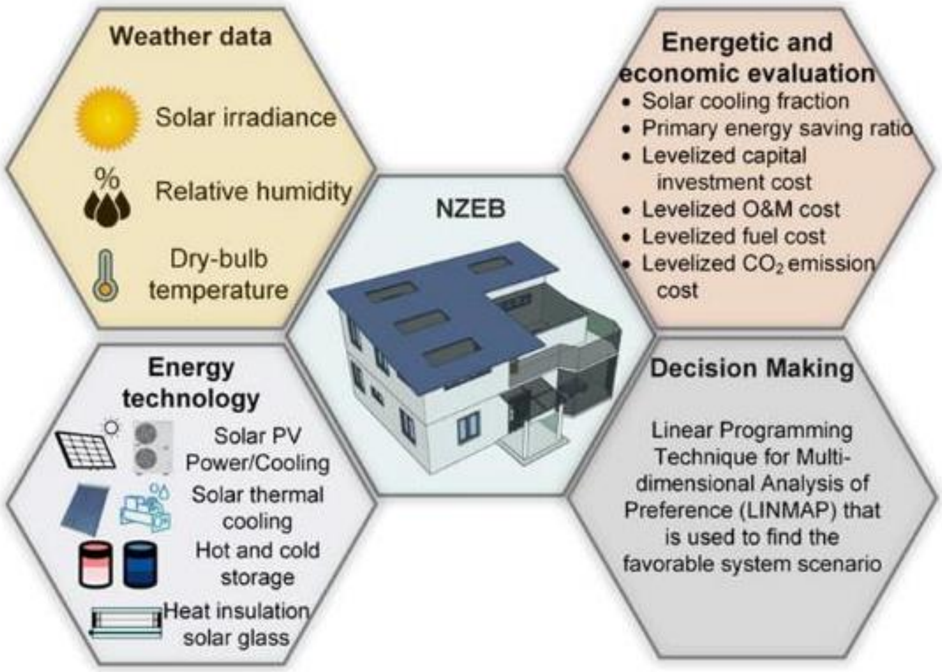

Figure 1. Elements that characterize the definition of an NZEB [8].

By applying these rules, an NZEB has a very low energy requirement, completely satisfied by renewable energy sources [9],[10],[11]. As highlighted by Harkouss et al. [10], the systems used to generate electricity to cover the entire electricity needs and ensure zero energy balance often include fixed, concentrating and tracking photovoltaic panel systems, residential wind turbines and biomass cogeneration, preferably with on-site production.

Obviously, the NZEB can also use renewable sources not produced on site, such as in the case of photovoltaic power plants nearby, or through the purchase of electricity produced by hydroelectric or wind power plants [12].

Since the most applicable and widely used renewable energy supply options are not programmable, Tummia et al. [13] show how the large-scale diffusion of NZEBs can seriously affect their stability of existing electricity grids, with an impact on both operating costs and environment.

For this reason, in addition to the production of electricity from renewable sources, it is also necessary to resort to the production of thermal energy produced from renewable energy sources, such as solar energy, air energy or geothermal energy. Besides, most studies present in literature on existing NZEB cases studied are relatively particular for a specific place, often very sunny, without studying the impact on different climatic conditions, for which the promotion of renewable geothermal energy instead of the exclusive use of only solar energy would be a big step forward for the development of these buildings.

1.2 FUNDAMENTALS ON THE GEOTHERMAL ENERGY SYSTEMS

Geothermal energy is a renewable energy source that can be used for summer and winter air conditioning of buildings, the production of domestic hot water, industrial cycles and food processes.

After solar energy, the energy stored in the ground is the most relevant source of renewable energy on the Earth as it is a large quantity and is almost inexhaustible. Part of the heat of the Earth propagates in the rocks. This geothermal flux is subsequently dissipated with a thermal flux of approximately 0.065 W/m^2 [14]. The geothermal gradientgiven by the derivative of the temperature T with respect to a direction (x, y, z). In the case of the Earth, due to its symmetry, this gradient becomes a total derivative which is the same for all directions. This gradient, reaches a depth of about 100 m, increases the temperature of the soil by about 3°C every 100 meters. Furthermore, this gradient is not a constant value all around the globe due to thermal anomalies that make the gradient higher or lower [15]. Based on different uses and different temperatures of the ground, the geothermal energy can be classified in:

- High enthalpy. Temperature of the thermo-vector fluid is higher than 150 °C. This energy is used for energy production or in the industrial sector.

- Medium enthalpy. Temperature of the thermo-vector fluid is between 150 °C and 100 °C. This energy is used in the industrial sector or agricultural systems.

- Low enthalpy. Temperature of the thermo-vector fluid is below 90 °C. This energy is used mainly for direct use in civil sectors, particularly in air-conditioning systems or in spa use.

This last type of geothermal energy in common international literature is called Shallow Geothermal Energy (SGE) or Near Surface Geothermal Energy (NSGE), although the terms Low Temperature and Low Enthalpy are still pervasive [16].

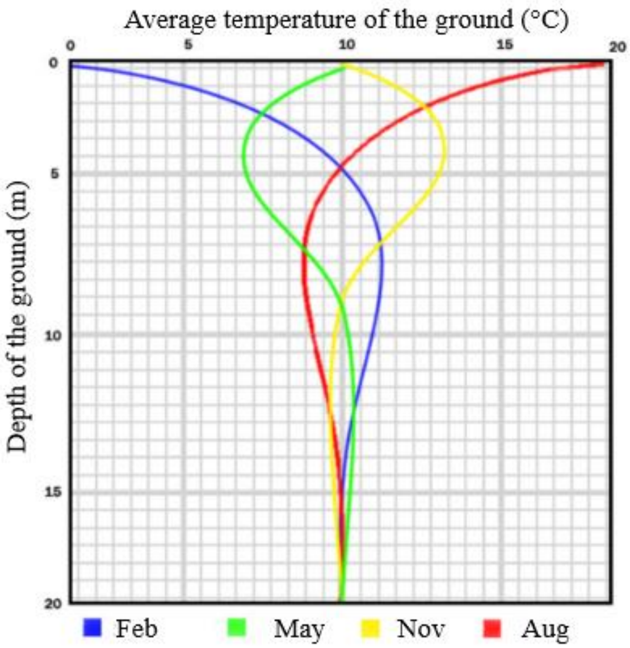

Figure 2. Monthly trend of the soil temperature.

One of the greatest advantages of using the energy of the ground is certainly the continuous availability which is independent of climate factors that penalize other renewable energy sources [15].

As can be seen in Figure 2, the ground temperature reaches an almost constant value after 15 meters (undisturbed temperature) equal to the arithmetic average of the outside air temperatures in a calendar year. In fact, the ability of the ground to absorb solar radiation allows to reduce the the daily variation of the external temperature after very short depth until the seasonal variation is very small after few meters. Furthermore, this temperature is usually higher in winter and lower in summer than the outside air.

As already mentioned, low enthalpy geothermal energy is mainly used for heating and cooling in buildings, production of domestic hot and/or cold water in industrial processes and for food conservation. In the case of heating systems, domestic hot water production and process "heat", the subsoil at low depth constitutes as a source for the extraction of heat; in the case of cooling and process “cold”, the subsoil, on the other hand, constitutes as a drain for the dissipation of heat.

The heat transfer can be carried out through water wells, vertical probes, special foundations or even surface excavations developed horizontally (called horizontal probes or exchangers).

Two systems that exploit the low enthalpy geothermal energy are heat pumps coupled with geothermal probes or earth-to-air heat exchangers. Both systems are coupled with different distribution plants linked to HVAC systems.

Due to different applications, its vast untapped potential and high growth in recent years, geothermal energy is set to become one of the foundation of the energy transition. From 2020 to 2030 it will be the "Geothermal Decade". An appropriate European and national policy framework can and must encourage this trend if European countries are serious about becoming carbon neutral by 2050 "[17].

1.3 AIMS AND ORIGINALITY

During these three years of PhD course, the research, summarized in this thesis work, has been extended mainly to evaluate the energy efficiency of HVAC plant solutions that exploit the low enthalpy geothermal energy of the ground. All this in order to provide a valid alternative for common building-system solutions (often not adequate to all climatic conditions) and thus to more easily made the complete self-sufficiency of the NZEB buildings and consequently the widespread diffusion of the Net/Plus ZEB in the near future.

The thesis focuses mainly on the study of two components:

1- the Ground Source Heat Pump (GSHP), i.e., a heat pump which uses the ground as external source through buried probes.

2- the Earth-to-Air heat exchanger (EAHX), i.e., a system in which the outdoor air is pre-heated or pre-cooled trough buried pipes (in which there is a heat exchange between air and ground) to reduce the heating and cooling energy consumption in buildings.

After analysing several articles dealing with these technologies, to date, to the best of my knowledge, information on the comparison of these two systems lack, as well as their their impact on the energy performance of the NZEB buildings. The scientific community highlights the significant contribution of the systems that exploit the geothermal energy sources in the energy saving in buildings. In the light of this, I have focused my thesis on the study and then on the comparison of a GSHP and EAHX mainly when retrofit strategies applied on different existing buildings are proposed.

The present work first energetically analyses these two technologies separately, comparing them to more common alternative components. Lastly, the performance of these systems is compared with each other, in order to obtain an NZEB.

1.4 THESIS OUTLINE

Following the main objectives discussed in the previous sections, the presented dissertation is organized as follows.

In Chapter 2 the Ground Source Heat Pump (GSHP) is investigated. Particularly, after carrying out a literature analysis, by means of dynamic energy simulation, the contribution that this technology can provide in terms of energy saving, reduction of CO_2 emissions, and the reduction of the surface to be allocated to a photovoltaic solar system in an NZEB is evaluated when it is compared with more common heat generators. Finally, an economic analysis is also carried out using the PayBack Period indicator.

In Chapter 3 the Earth-to-Air Heat Exchanger (EAHX) is investigated. The performances of this exchanger are firstly evaluated through a 2D mathematical model under different outdoor air temperatures considering different lengths, diameters, and air velocity. The results are applied to a case study, where the EAHX is a component (to pre-treat the air) located upstream an Air Handling Unit (AHU) inside a HVAC system, in order to demonstrate how this simple component can ensure relevant energy saving.

In Chapter 4 the two technologies that exploit the low enthalpy geothermal energy are implemented in the retrofit strategies of an existing building located in Naples, (South Italy) in order to obtain the NZEB target. The contribution of the GSHP and the EAHX on the energy performances of the NZEB are evaluated first separately and then together, from different points of view.

Chapter 5 outlines the main conclusions and future developments.

Lastly the Appendix presents a brief description and main results of an experimental activity on a Concentrated Photovoltaic/Thermal (CPV/T) system carried out during the last year of the PhD course.

2 GROUND SOURCE HEAT PUMP (GSHP)

2.1 STATE OF THE ART

The ground source heat pump (GSHP) is one of the high efficiency systems that are suitable for reducing energy consumption.
The ASHRAE (American Society of Heating, Refrigerating and Air-Conditioning Engineers) has established a standard classification that is, to date, the reference worldwide. The ASHRAE standard defines the Ground-Source Heat Pumps (GSHPs) family to identify geothermal heat pumps in a general way [18].
According to the ASHRAE nomenclature, three main categories of GSHP systems are distinguished (Figure 3), depending on the characteristics of the heat transfer fluid:

- GWHP – Groundwater Heat Pump: the heat transfer fluid consists of groundwater which is captured and released once the heat exchange cycle has ended.

- SWHP - Surface Water Heat Pump: the heat transfer fluid consists of surface water which, also in this case, is captured and released once the heat exchange cycle has ended.

- GCHP - Ground-Coupled Heat Pump: the heat transfer fluid flows in a closed circuit in contact with the ground.

Depending on the mode of exchange, geothermal systems are divided into two categories:

- Open loop.
- Closed loop.

With reference to GWHP, open loop systems exploit groundwater circulating in the subsoil for heat exchange and typically consist of a doublet of wells (intake and yield) or a greater number of wells in larger plants. In these systems, the underground water is first withdrawn from a well, then sent to the heat pump for heat exchange and finally it is discharged at a slightly different temperature which is lower in winter and higher in summer. The water can either be reintroduced back into the groundwater through a yield well to avoid depleting the aquifer or discharged into an adjacent surface water body.

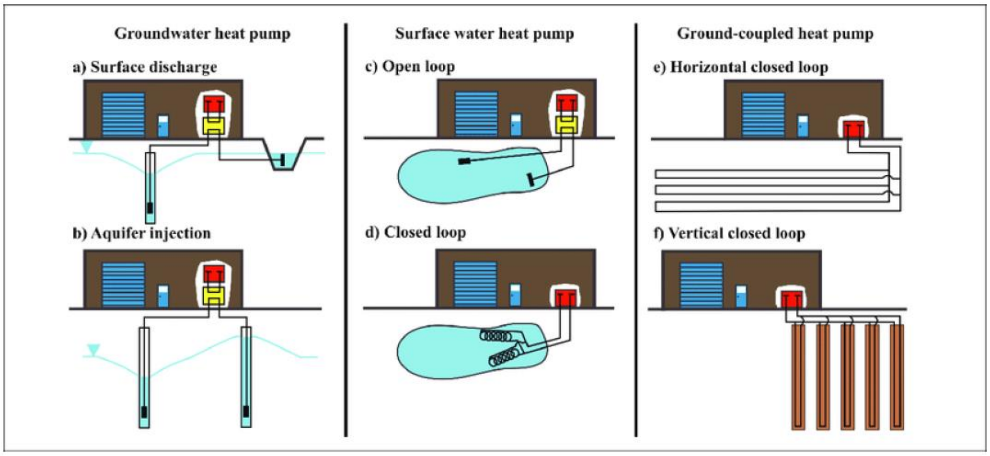

Figure 3. Main classification of the Ground Source Heat Pumps (GSHPs) [19].

Closed loop systems, on the other hand, exchange heat with the ground through a heat transfer fluid circulating in pipes installed underground.
Ground-coupled heat pumps use closed-loop ground heat exchangers and the pipes can be of various types:

- Vertical probes. In this type of circuit, the heat exchange with the subsoil is carried out by means of a heat transfer fluid. This fluid is continuously circulated inside special pipes cemented within vertical boreholes and transfers the heat captured from the subsoil (in heating mode) to the surface and from there to the heat pump. The cementation of the probe is carried out with special cement mortars, defined grout, which have the function of mechanical protection, insulations of the various aquifers that may be crossed, and of guaranteeing the physical continuity of the heat exchange between the ground, the pipes and the circulating heat transfer fluid inside them [19]. Vertical probes generally have depths between 50 and 250 m

(typically 100 m), depending on the local geological and hydrogeological conditions, and a diameter of 100-200 mm [20].
The pipes can be made of polyethylene, high density polyethylene (HDPE) or cross-linked polyethylene (PEX) and can have different configurations (Figure 4).

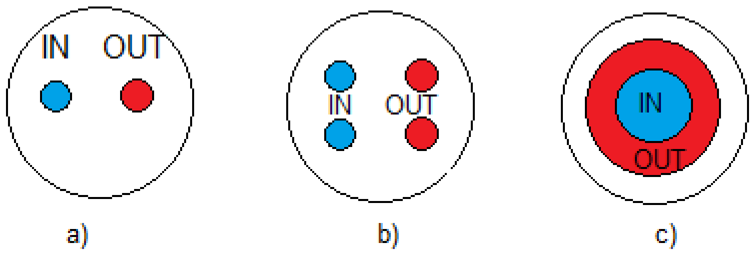

Figure 4. Cross sections of geothermal probes: a) single U, b) double U, c) coaxial.

- Horizontal probes. The surface occupied by a horizontal system is approximately equal to about double the surface of the building to be heated. The performance of this type of system depends heavily on fluctuations in the temperature of the outside air, the intensity of solar radiation incident on the surface of the ground and also on the possible presence of snow on it [21]. The heat exchange takes place with the ground at reduced depths, usually 2-3 m, by means of polyethylene pipes with a diameter of 32 or 40 mm.

The GSHP usually has a higher coefficient of performance (COP) than the more common air source heat pump, due to the more favourable and stable thermal level of the soil compared to the outside air [22]. In fact, as Figure 5 shows, particularly for the great depths at which geothermal heat pumps with vertical probes work, the soil temperature is higher in winter and lower in summer than that of the outside air. This improves the ideal COP of the heat pump and therefore also the achieved COP or EER (see Figure 6). It has been demonstrated that geothermal heat pumps offer a 30-70% reduction in energy consumption in heating mode and 20-50% reduction in cooling mode [23], compared to conventional solutions. Marrasso et al. [24] also highlight how the geothermal heat pump is one of the best strategies for energy refurbishment of condominiums. In fact, this technology allows energy benefits and lowers the environmental impact on both a local and global scale to reduce urban air temperatures.

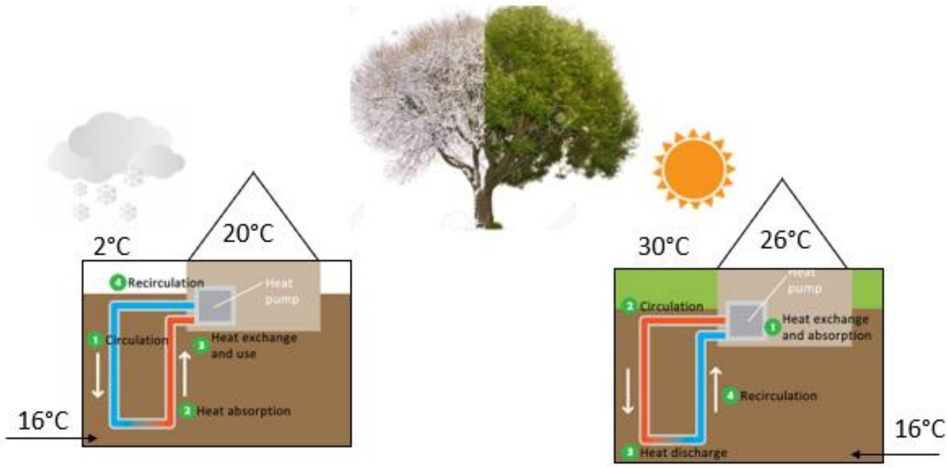

Figure 5. Cooling and heating operation mode of the GSHP.

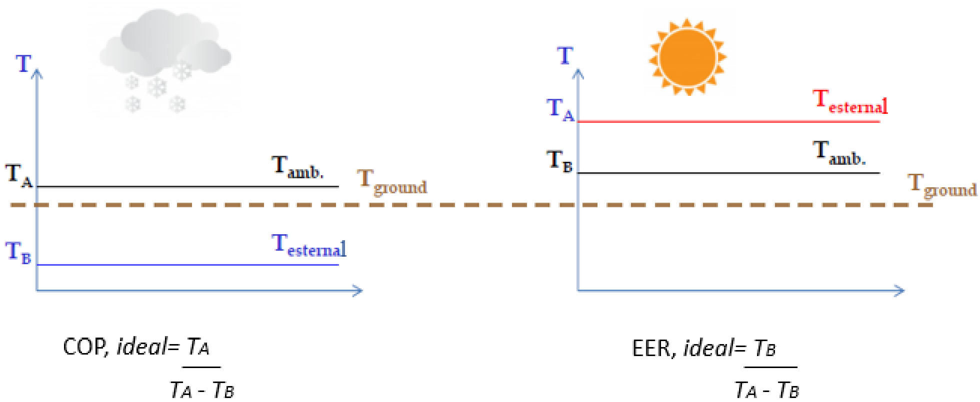

Figure 6. Maximum performance of heat pumps in winter and summer.

Although it is a system that exploits the soil and may have considerable surface requirements, there are innovative systems that exploit the foundations of buildings for the implementation of geothermal probes. Based on innovative geothermal systems, Massarotti et al. [25] propose a low-enthalpy geothermal system in the energy retrofit of an important historical building in South-Italy, demonstrating how the GSHP can reduce the CO_2

emissions more than 53% when compared to technologies that use fossil fuels. Despite the difficulty often encountered in finding an available surface on which to lay the probes on site, Kotarela et al. [26] highlight that the combined use of a photovoltaic system and geothermal heat pump is one means of reducing dependence on fossil fuels while simultaneously avoiding overloading of the electricity grid. In Carotenuto et al. [27], innovative ground systems are analysed using the finite elements method. In this geothermal system configuration, freezing probes are inserted in foundation pylons to exploit the low enthalpy of the ground. It is also important to bear in mind that geothermal heat pumps, both in summer and winter, exploit the renewable energy of the soil. Revesz et al. [28] investigates the GSHP in urbanized cities where the heat from an underground tunnel (the ground surrounding the infrastructure) could be exploited to improve the heating mode operation of a GSHP. Thus, the advantage of this technology can be used to satisfy the need to exploit renewable energy sources for civil and non-civil use.

One of the main problems related to the use of heat pumps is their primary energy consumption, which depends on the way in which the compressor shaft is powered. In this regard, heat pumps are usually classified as electric heat pumps (EHP - Electric Heat Pump) or gas heat pumps (GEHP - Gas Engine Heat Pump, or GHP – Gas Heat Pump). Most of the current models of heat pumps are driven by electric motors that use electricity as the driving force. Recently gas heat pumps have been used as an alternative to conventional electric heat pumps. A study was carried out on three residential buildings in different climatic areas based on the comparison between the two types of heat pumps used in a geothermal system [29]. Regardless of the study area, it was found that the technical differences between electric heat pumps and gas heat pumps are significant. The use of an electric heat pump in the geothermal system results in higher COP values, a reduction in annual energy consumption, even if it requires longer geothermal probes.

In the literature, this system is coupled with several innovative complementary systems. In Buonomano et al. [30], geothermal energy coupled with solar energy is used and investigated in a trigeneration plant. Huang et al. [31] investigate the optimization of a large scale solar-assisted ground source heat pump for district heating, finding an optimal match between the size of the ground heat storage, the collector area, and the tank

volume. In [32] and [33] the coupling between the GSHP and the photovoltaic/thermal system is analysed, demonstrating how the use of these systems together increases the thermal efficiency of the collectors; the electrical efficiency of the cells remains high without the risk of cell damage due to overheating. Many scientific articles examine energy conversion plants based on GSHPs and photovoltaic plants used in villas or condominium buildings and whose primary energy requirement is in the range 57-67 kWh/m^2 [34], [29] and [35]. Due to its characteristics and high efficiency in terms of energy saving, CO_2 emissions reduction, and renewable energy source use, this system can easily be implemented in buildings to achieve the NZEB target more easily. However, little research has been undertaken about this coupling in literature.
In Fedajev et al. [36] , with reference to a nearly Zero Energy Building (nZEB), the influence of different heat exchangers linked to a GSHP and thermal storage is examined, for the very harsh climatic conditions of Finland; the importance of the thermal storage to achieve the goal of NZEB is shown.
In a review article, Gao et al. [37] highlights the different potentialities of the technologies that can be coupled to the geothermal heat pump, suggesting this technology can be used in zero energy buildings.

In the technical-scientific literature to date, little examination has been made on the contribution of GSHPs to obtain a zero-energy balance in an NZEB and their influence in reducing the photovoltaic surface to be used in densely urbanized cities. Often these systems are analysed separately without any reference to the reduction of photovoltaic panels to be installed. Therefore, this chapter analyses the contribution of this technology by comparing the GSHP to other systems, such as an invertible (”reversible”) air source heat pump or a condensing boiler coupled to a chiller, in order to obtain the satisfaction of an NZEB balance in different climatic conditions and to evaluate the photovoltaic surface needed to achieve the status of NZEB compared to the available area on the roof of the building. To this aim, a case study building used as a bed and breakfast (B&B) virtually located in two Italian towns with different climatic conditions is analysed. Using the dynamic energy simulation software, DesignBuilder, a detailed energy analysis is carried out. The procedure is partially validated by comparing the building energy requirements with data found in literature. Moreover, other important results are obtained in terms of primary energy consumption, reduction of CO_2 emissions, and percentage of renewable energy used for the various solutions. Finally, a technical-economic analysis using the discounted payback is performed.

2.2 METHODOLOGY AND APPLICATION

To evaluate the contribution of a GSHP in an NZEB, a case study was analyzed. The seasonal and yearly energy consumption and CO_2 emissions of the building-plant system are evaluated.

The first step is to design a building characterised by low energy needs. Therefore, optimal thermal characteristics for the building envelope must be chosen to minimize the thermal losses in winter, while the free heat gains should be maximized in winter and minimized in summer. To this end, optimal thermal insulation, excellent phase shift and attenuation values, compact form, and innovative technologies should be selected [38].

Subsequently, the HVAC (heating, ventilation and air-conditioning) and other building energy systems must be chosen and designed to minimize the primary energy requirements by using energy-efficient solutions [39].

The building of the case study is virtually located in different Italian climatic zones and the energy analysis is performed through a dynamic building energy performance simulation software, i.e., DesignBuilder [40], based on the EnergyPlus calculation engine. The U.S. Department of Energy with ANSI/ASHRAE have obtained validation test results [41] for DesignBuilder v.6.1 with EnergyPlus v.8.9. referring to:

- Building Thermal Envelope and Fabric Load Tests
- Space-Heating Equipment Performance Tests HE100 to HE230
- Space-Cooling Equipment Performance Comparative Tests CE300 to CE545
- Space-Cooling Equipment Performance Analytical Verification Tests AE101 to AE445
- Space-Cooling Equipment Performance Analytical Verification Tests CE100 to CE200.

The climatic data are taken from ASHRAE (American Society of Heating, Refrigerating and Air-Conditioning Engineers) [42].

The focus of this chapter is an energy, environmental, and technical-economic comparison between a GSHP and two common generators of thermal energy, i.e., an air source heat pump or a condensing boiler coupled to an air-cooled chiller.

Regarding the DesignBuilder software, the CTFM (Conduction Transfer Function Module) is selected based on the algorithm "conduction transfer function". Moreover, the algorithm DOE-2 [43] is set for the outside convection and the algorithm TARP [44] for the inside convection.

HVAC systems can be defined in DesignBuilder using 3 different levels of detail:

- Simple HVAC. The heating/cooling system is modelled using basic loads calculation algorithms. For convective heating systems and all cooling systems the EnergyPlus Zone HVAC: *Ideal Loads Air System* is used to calculate heating and cooling loads. This supplies hot/cold air to meet heating and cooling loads. Mechanical ventilation loads are calculated locally for each zone. When using the Radiant/convective heating system type the EnergyPlus Zone HVAC: *High Temperature Radiant System* type is used to calculate heating loads. With Simple HVAC, heat generator (typically a boiler or heat pump) and chiller fuel energy consumption are calculated from zone heating and cooling loads as a post-process using efficiency factors.
- Compact HVAC. The heating/cooling systems are defined in DesignBuilder using moderately basic HVAC descriptions which are expanded into detailed HVAC definitions and modelled in EnergyPlus including boiler, chiller and fan part-load characteristics.
- Detailed HVAC. The HVAC system is modelled in full detail using EnergyPlus air and water-side components linked together on a schematic layout drawing.

In this research the Detailed HVAC is set and the HVAC component hierarchy is shown in Figure 7.

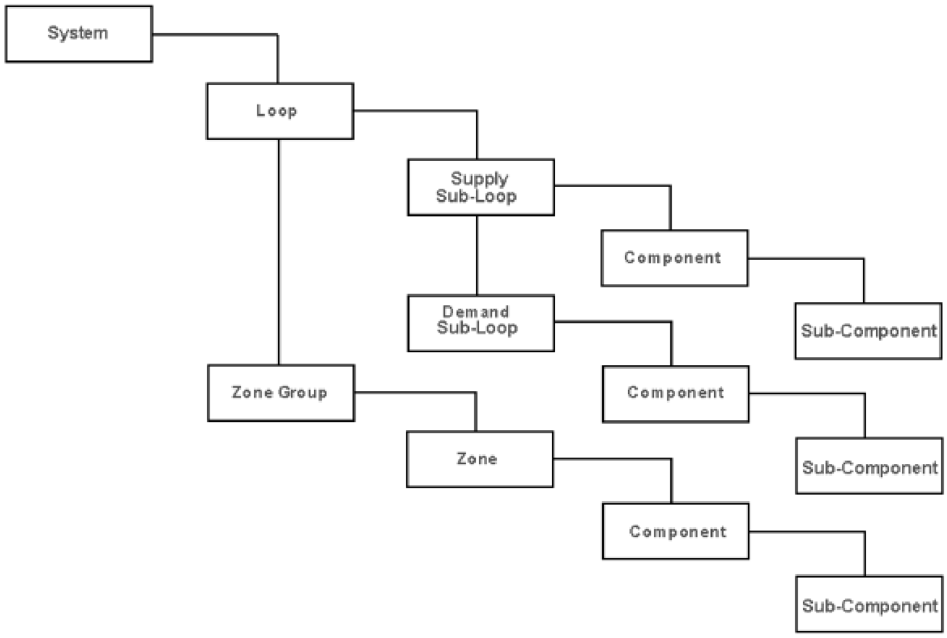

Figure 7. Detailed HVAC hierarchy in DesignBuilder simulation software [45].

The chiller model is an empirical model used in the DOE-2.1 building energy simulation program. In this case the performance information at reference conditions are found by using three curve fits for cooling capacity and efficiency to determine chiller operation at off-reference conditions. The performance curves can be generated by fitting the manufacturer's catalog data or measured data. For this data an EnergyPlus Reference Datasets (Chillers.idf) is available.

During the simulation the electric power of the compressor is calculated using:

$$Q_{compressor} = (Q_{ref} / COP_{ref}) * CAPFT * EIRFT * EIRPLR \qquad (1)$$

Where:

- CAPFT is the name of a bi-quadratic performance curve [46] that parameterizes the variation of the cooling capacity as a function of the leaving chilled water temperature and the entering condenser fluid temperature.

- EIRFT is the name of a bi-quadratic curve [46] that parameterizes the variation of the energy input to cooling output ratio (EIR) as a function of the leaving chilled water temperature and the entering condenser fluid temperature. The EIR is the inverse of the COP.
- EIRPLR is the name of a quadratic performance curve [47] that parameterizes the variation of the energy input ratio (EIR) as a function of the part-load ratio. The EIR is the inverse of the COP, and the part-load ratio is the actual cooling load divided by the chiller's available cooling capacity.

When the Detailed HVAC approach is set, the GSHP is made up of three loops (combined heating and cooling):

- HW loop (for heating applications) - Hot water loop (Water-to-water heat pump heating)
- CHW loop (for cooling applications) - Chilled water loop (Water-to-water heat pump cooling)
- Condenser loop - Ground heat exchanger loop (heat exchanges with the ground via either surface, pond or vertical borehole types).

Also in this case, the model used to simulate the performances of the heat pumps is based on different load curves. The equations implemented in DesignBuilder are of the type "fit-base model", i.e., four non-dimensional equations or curves to predict the heat pump performance [48], [49] .The equations (referring to both cooling and heating modes) are:

$$\frac{Q}{Q_{,ref}} = A_1 + A_2\frac{T_L}{T_{ref}} + A_3\frac{T_S}{T_{ref}} + A_4\frac{\dot{V}_L}{\dot{V}_{Lref}} + A_5\frac{\dot{V}_S}{\dot{V}_{Sref}} \qquad (2)$$

$$\frac{Power}{Power_{,ref}} = B_1 + B_2\frac{T_L}{T_{ref}} + B_3\frac{T_S}{T_{ref}} + B_4\frac{\dot{V}_L}{\dot{V}_{Lref}} + B_5\frac{\dot{V}_S}{\dot{V}_{Sref}} \qquad (3)$$

where:

- A_1–B_5 Equation fit coefficients for the cooling and heating mode;
- T_{ref} Reference temperature;
- T_L Load side entering water temperature, K;

- T_S Source side entering water temperature, K;
- $\dot{V}_L$ Load side volumetric flow rate, m^3/s;
- $\dot{V}_s$ Source side volumetric flow rate, m^3/s;
- $V_{L,ref}$ Reference load side volumetric flow rate, m^3/s;
- $V_{S,ref}$ Reference source side volumetric flow rate, m^3/s;
- Q Load side heat transfer rate (cooling mode and heating mode), W;
- $Q_{,ref}$ Reference load side heat transfer rate (cooling mode and heating mode), W;
- Power Power needed (cooling mode and heating mode), W;
- $Power_{,ref}$ Reference power needed (cooling mode and heating mode), W.

The coefficients A_1–B_5 (based on the data of the manufacturer) are inserted in the model to simulate the energy performances. They refer to the partial load performance of heat pumps in the database of DesignBuilder.

Also, the undisturbed temperature of the ground is needed in order to evaluate the seasonal efficiency of a GSHP. To this end, the equation of Kusuda [50] has been applied:

$$T_g(D,t) = T_{av} - A \cdot \exp\left[-D \cdot \sqrt{\frac{\pi}{365 \cdot \alpha_g}}\right] \cdot \cos\left[\frac{2\pi}{365} \cdot \left(t - t_{T_{min}} - \frac{D}{2} \cdot \sqrt{\frac{365}{\pi \cdot \alpha_g}}\right)\right] \quad (4)$$

where:

- T_g (D,t) is the ground temperature at a depth D after t days (starting from 1 January), °C;
- T_{av} [°C] is the yearly average temperature of the outdoor environment on the basis of statistical information;
- A [°C] is the amplitude of the temperature yearly oscillation;
- t is the sequential number of the day (1 refers to 1st of January);
- t_{Tmin} is the sequential number of the day corresponding to the minimum ground temperature, according to statistical data (1 refers to 1st of January);
- D [m] is thedepth of the ground;

- α_g [m²/day] is the daily equivalent thermal diffusion of the ground.

The seasonal energy performance indexes of the heat pumps and chiller (seasonal coefficient of performance (SCOP) for heating operation, seasonal energy efficiency ratio (SEER) for cooling) are calculated by means of Equations (5) and (6):

$$SCOP = \eta_{II} \frac{(\Theta_h + 273.2)}{(\Theta_h - \Theta_c)} \tag{5}$$

$$SEER = \eta_{II} \frac{(\Theta_c + 273.2)}{(\Theta_h - \Theta_c)} \tag{6}$$

where:

- θ_h is the absolute temperature of the hot source;
- θ_c is the absolute temperature of the cold source;
- η_{II} is the second law efficiency.

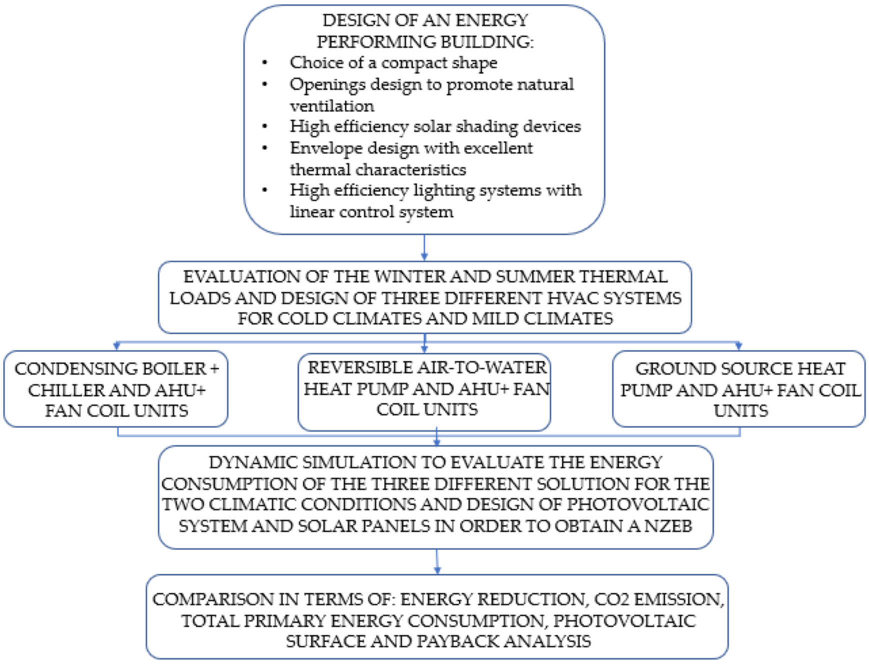

Figure 8. Flowchart of the methodology used.

For the evaluation of the correct size of the heat pump, the thermal power necessary for handling the treated ventilation external air (“primary air”) was also considered. In the examined case study, this is about 6 kW in summer; moreover, considering a ground that dissipates 50 W/m of thermal energy, the number of 4 vertical U-bend probes (80 m for each probe) was obtained for both Milan and Palermo.

To calculate the CO_2 emissions, the standard emission factors of greenhouse gases are taken from [51]. These values are equal to 0.202 $kgCO_2/kWh$ and 0.483 $kgCO_2/kWh$ for natural gas and electricity, respectively.

In Figure 8 a flowchart of the methodology of the application on a case study is shown.

2.2.1 Description of the case study

The case study is a new construction, i.e., a building used as a bed and breakfast and in order to investigate different scenarios, it is virtually located in two Italian cities with different climates (Table 1): Palermo (South Italy), with mild winters and very hot summers; Milan (North Italy), with cold winters and hot summers.

Table 1. Geographic and climatic conditions of the selected towns [52].

Town	Heating Degrees-Day	Climatic Zone for Heating	Latitude	Longitude	Outdoor Design Temperature	
					Summer	Winter
Milan	2404 K·day	E	45°28′38″28 N	9°10′53″40 E	33.1 °C	−4.9 °C
Palermo	751 K·day	B	38°6′43″56 N	13°20′11″76 E	33.8 °C	6.6 °C

The building has a square shape and stands up on two floors with a total heated area of 310 m^2 and a heated volume of 900 m^3.

Accurate design of the building and passive design rules are applied in order to achieve the NZEB target. Particularly, considering the sun position, the living zone is placed on the south side in order to maximize solar gains in winter, while the service rooms and sleeping zone are placed on the north side (Figure 9 and Figure 10). Moreover, the windows are designed to optimise natural ventilation. A compact form of the building is chosen, so the surface-to-volume ratio is equal to only 0.20 m^{-1}. Low values of unitary thermal transmittance of the building envelope components are used (Table 2), particularly for the coldest town (Milan), in order to minimise the thermal losses in winter.

Figure 9. Three-dimensional model of the case study building.

Table 2. Unitary thermal transmittance of the case study building envelope (W/m^2K).

Town	U_{Walls}	U_{Roof}	U_{Floor}	$U_{Windows}$
Milan	0.24	0.21	0.23	1.20
Palermo	0.31	0.30	0.35	1.69

Specifically, the vertical walls consist of (starting from inside):

- Cement plaster:
  thickness 1.5 cm;
  thermal conductivity 0.72 W/mK;
  density 1860 kg/m^3.
- Areated Brick:
  thickness 20 cm;

thermal conductivity 0.30 W/mK;
density 1000 kg/m^3.

- Insulation layer in exstruded polystyrene:
thickness 7 cm for Palermo and 10 cm for Milan;
thermal conductivity 0.034 W/mK;
density 35 kg/m^3.
- Areated Brick:
thickness 10 cm;
thermal conductivity 0.30 W/mK;
density 1000 kg/m^3.

The roof consists of (starting from inside):

- Cement plaster:
thickness 1 cm;
thermal conductivity 0.72 W/mK;
density 1860 kg/m^3.
- Reinforced concrete:
thickness 20 cm;
thermal conductivity 2.30 W/mK;
density 2300 kg/m^3.
- Vapor barrier
thickness 0.2 cm
thermal conductivity 0.23 W/mK
density 1100 kg/m^3.
- Insulation layer in exstruded polystyrene:
thickness 10 cm for Palermo and 15 cm for Milan;
thermal conductivity 0.034 W/mK.
density 35 kg/m^3.
- Areated concrete cast:
total thickness 3 cm;
equivalent thermal conductivity 0.23 W/mK;
density 700 kg/m^3.
- Asphalt and reflective material
total thickness 1 cm;
equivalent thermal conductivity 0.70 W/mK;
density 2100 kg/m^3.

The first floor rests on a ventilated crawl space and consists of:

- Reinforced concrete
  thickness 20 cm;
  thermal conductivity 2.30 W/mK;
  density 2300 kg/m^3.
- Insulation layer in espanded polystyrene:
  thickness 9 cm for Palermo and 14 cm for Milan;
  thermal conductivity 0.035 W/mK;
  density 25 kg/m^3.
- Floor screed:
  total thickness 5 cm;
  equivalent thermal conductivity 0.41 W/mK;
  density 1200 kg/m^3.
- Ceramic tiles:
  total thickness 1 cm;
  equivalent thermal conductivity 1.30 W/mK;
  density 2000 kg/m^3.

The windows consist of double glass with argon (Palermo) and triple glass with argon (Milan) and PVC frame.

The building is divided in different thermal zones, based on different numbers of people, occupancy schedules, internal gains and uses. The thermal zones are n°6 bedrooms with a bathroom (two persons for each room), a kitchen, a breakfast room and a laundry room.

The occupancy schedules for each thermal zone are the following:

- Hall (5 persons):
  from 7 A.M. to 12 A.M. (100% of the occupancy value);
  from 5 P.M. to 8 P.M. (100% of the occupancy value).
- Bedroom (2 persons):
  from 1 A.M. to 9 A.M. (100% of the occupancy value);
  from 9 A.M. to 10 A.M. (50% of the occupancy value);
  from 6 P.M. to 8 P.M. (50% of the occupancy value);
  from 10 P.M. to 11 P.M. (50% of the occupancy value);
  from 11 P.M. to 12 P.M. (100% of the occupancy value).
- Kitchen (3 persons):

from 7 A.M. to 3 P.M. (100% of the occupancy value).

- Breakfast room (10 persons):
  From 8 A.M. to 11 A.M. (100% of the occupancy value).
- Laundry room (3 persons):
  from 9 A.M. to 12 A.M. (100% of the occupancy value).

The lighting system is characterized by LED luminaires with linear control. The following lighting levels are guaranteed for each thermal zone:

- hall - 300 lux
- bedrooms - 100 lux;
- kitchen - 250 lux;
- breakfast room - 200 lux;
- laundry - 200 lux.

Finally a metabolic rate equal to 0.69 MET is set for the bedrooms and 1.7 MET is set for all the others thermal zone.

Table 3 reports the design thermal loads of the building (for both heating and cooling conditions), calculated by the software, while Table 4 shows the values of the seasonal average energy efficiency for the three compared systems.

The HVAC system used presents the fan-coil units located inside the rooms and an air handling unit (AHU) for primary air. The primary air assumes the value of 39.6 m^3/h per person for all thermal zones, with the exception of the kitchen and the breakfast room where the assumed value is 36 m^3/h per person. In this way, the total primary air value is equal to 1580 m^3/h.

The design thermo-hygrometric conditions are as follows:

- room conditions: temperature of 20 °C for winter and 26 °C for summer, relative humidity of 50% for both winter and summer;

- supply primary air conditions: temperature of 20 °C for winter and 12 °C for summer.

The fan-coils are entrusted with the task of balancing the sensible thermal load. The primary air is entrusted with the task of balancing the latent thermal load. For this reason the supply primary air is set at temperature equal to 20 °C (neutral air) in winter conditions.

Table 3. Design thermal loads of the case study building for both heating and cooling.

Town	Volume	Thermal (Heating and Cooling) Loads			
		Winter Conditions		Summer Conditions	
	m³	kW	W/m³	kW	W/m³
Palermo	900	10	12	22	24
Milan		12	13	21	23

Table 4. Seasonal average energy efficiency for the analysed solutions.

	Milan		Palermo	
	Boiler Efficiency or SCOP	SEER	Boiler Efficiency or SCOP	SEER
GSHP (ground-to-water heat pump)	4.80	7.00	6.20	5.60
Air source heat pump (air-to-water heat pump)	4.10	4.80	4.80	4.90
Condensing boiler + air-cooled chiller	0.90	4.80	0.90	4.90

Referring to the heating mode, different operation schedules are selected for the two analysed towns, according to DPR 74/2013 [53] and DPR 74/2013 pt. 10.1 [54] :

- Palermo (climatic zone: B): from 1 December to 31 March (6:00–9:00 A.M., 6:00–11:00 P.M.—8 hours per day);
- Milan (climatic zone: E): from 15 October to 15 April (5:00–9:00 A.M., 12:00 A.M.–3:00 P.M., 5:00–12:00 P.M.—14 hours per day).

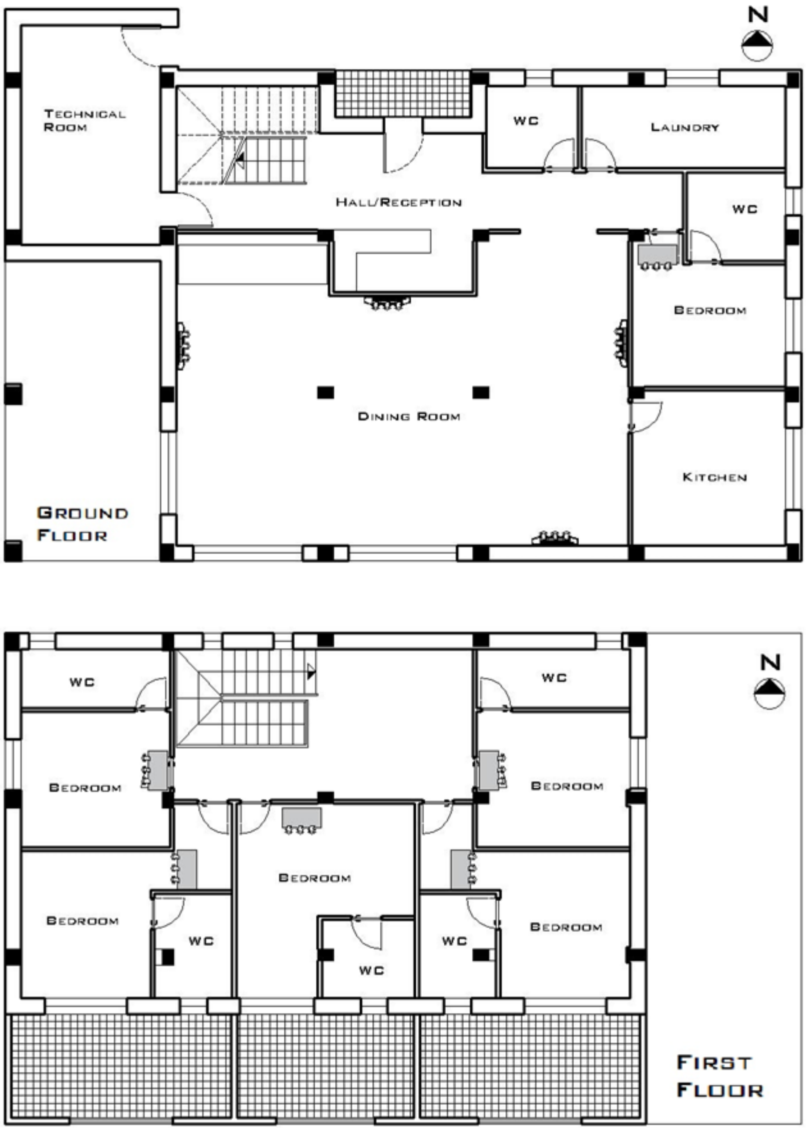

Figure 10. Plan of the ground floor and first floor of the case study building.

Referring to the cooling mode, no mandatory rules are in force and the operational programs are fixed as follows:

- Palermo: from 1 June 1 to 30 September (11:00 A.M.–4:00 P.M., 6:00–10:00 P.M.—9 hours per day);

- Milan: from 1 June to 30 September (11:00 A.M.–3:00 P.M., 6:00–10:00 P.M.—8 hours per day).

The production of domestic hot water (DHW) is entrusted to solar thermal collectors (5 in the case of Milan, 4 in the case of Palermo) and, in addition, to a dedicated air-to-water heat pump (COP = 2.5), while the consumption rate is 2.5 l/m^2day.

There is an intelligent artificial lighting system with LED devices and linear control system (2.5 W/m^2_100 lux). The design values of the illuminance are 300 lux in bedrooms and 500 lux in common spaces.

Few other electrical devices exist, so a range of only 1–4 W/m^2 is considered.

2.3 RESULTS AND DISCUSSION

The first important results concern the reduction of energy demands. These values are found for the various proposed solutions for the different energy uses and they are shown in Table 5 and Table 6, for Palermo and Milan, respectively.

When comparing the yearly primary energy consumption for all the energy uses, it is clear how it is necessary to reduce the energy needs for heating and cooling particularly in buildings located in cities with a continental climate. When comparing Figure 11 (Milan, continental climate) and Figure 12 (Palermo, mild climate), it is possible to notice that the energy requirements for a continental climate is higher and the need to achieve energy savings is more felt. Particularly, the primary energy consumption (Figure 11) for heating and cooling in the case of Milan is in the range of 50-22 kWh/m^2. The value of primary energy consumption for air conditioning in the case of the air source heat pump is 29 kWh/m^2. Instead, the ground source heat pump is more energy efficient. In fact, this value is lower and equal to 22 kWh/m^2.

Table 5. Energy consumption for different HVAC proposals for the building located in Palermo.

PALERMO										
	Air Source Heat Pump			**Ground Source Heat Pump**			**Boiler + Chiller**			
	Electricity	**Electricity**	**Primary Energy**	**Electricity**	**Electricity**	**Primary Energy**	**Electricity**	**Gas**	**Electricity**	**Primary Energy**
	[kWh]	*[kWh/m²]*	*[kWh/m²]*	*[kWh]*	*[kWh/m²]*	*[kWh/m²]*	*[kWh]*	*[kWh]*	*[kWh/m²]*	*[kWh/m²]*
El. devices	1015	3.3	7.9	1015	3.3	7.9	1015	-	3.3	7.9
Lighting	1597	5.2	12.5	1597	5.2	12.5	1597	-	5.2	12.5
Heating	590.0	1.9	4.6	456.8	1.5	3.6	-	3146	-	10.7
Cooling	1499	4.8	11.7	1312	4.2	10.2	1499	-	4.8	11.7
H+C	2089	6.7	16.3	1769	5.7	13.8	-	-	-	22.4
DHW	1429	4.6	11.2	1429	4.6	11.2	1429	-	4.6	11.2
Total	6131.3	19.8	47.9	5810	18.7	45.4	5541	3146	17.9	53.9

Table 6. Energy consumption for different HVAC proposals for the building located in Milan.

MILAN											
	Air Source Heat Pump			**Ground Source Heat Pump**			**Boiler + Chiller**				
	Electricity *[kWh]*	**Electricity** *[kWh/m²]*	**Primary Energy** *[kWh/m²]*	**Electricity** *[kWh]*	**Electricity** *[kWh/m²]*	**Primary Energy** *[kWh/m²]*	**Electricity** *[kWh]*	**Gas** *[kWh]*	**Electricity** *[kWh/m²]*	**Primary Energy** *[kWh/m²]*
El.devices	995	3.2	8	995	3.2	7.8	995	-	3.2	7.8
Lighting	1626	5.2	13	1626	5.2	12.7	1626	-	5.2	12.7
Heating	2740	8.8	21	2220	7.2	17.3	-	12488	-	42.3
Cooling	993	3.2	8	658	2.1	5.1	993	-	3.2	7.8
H+C	3733	12.0	29	2878	9.3	22.5	-	-	-	50.1
DHW	1817	5.9	14	1817	5.9	14.2	1817	-	5.9	14.2
Total	8171	26.4	64	7316	23.6	57.1	5431	12488	17.5	84.7

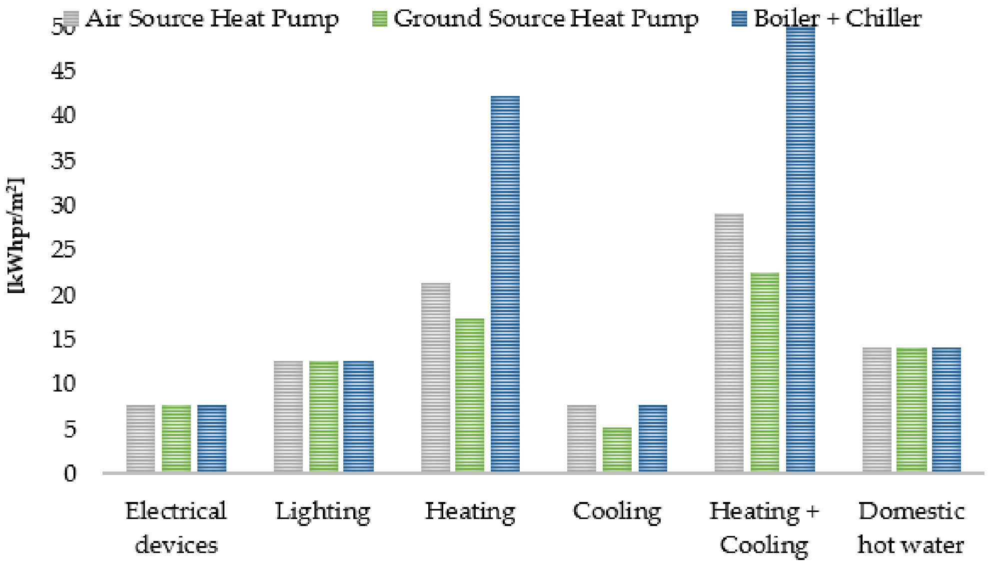

Figure 11. Primary energy consumption for different energy uses in the case of Milan.

When considering a city with mild climate (Figure 12), although the energy demand for air conditioning is lower than the continental climate, the geothermal heat pump allows almost zero energy demand for heating and for the total one there is a value of 14 kWh/m^2 for heating and cooling. In this case the use of a ground source heat pump instead of an air source heat pump is less convenient than in the continental climate. In fact, the primary energy spent on air conditioning using air source heat pump is slightly higher and equal to 16 kWh/m^2.

When considering the total yearly consumption of primary energy for Milan, Figure 13 shows that the ground source heat pump allows a 10% saving compared to the air source heat pump and 33% compared to the solution with the condensing boiler plus chiller. The yearly electric energy consumption varies from 8171 kWh/y (26.4 kWh/m^{2}y) related to the use of the air source heat pump, to 7316 kWh/y (23.6 kWh/m^{2}y, i.e., −10%) related to the use of the GSHP, as reported in Table 6.

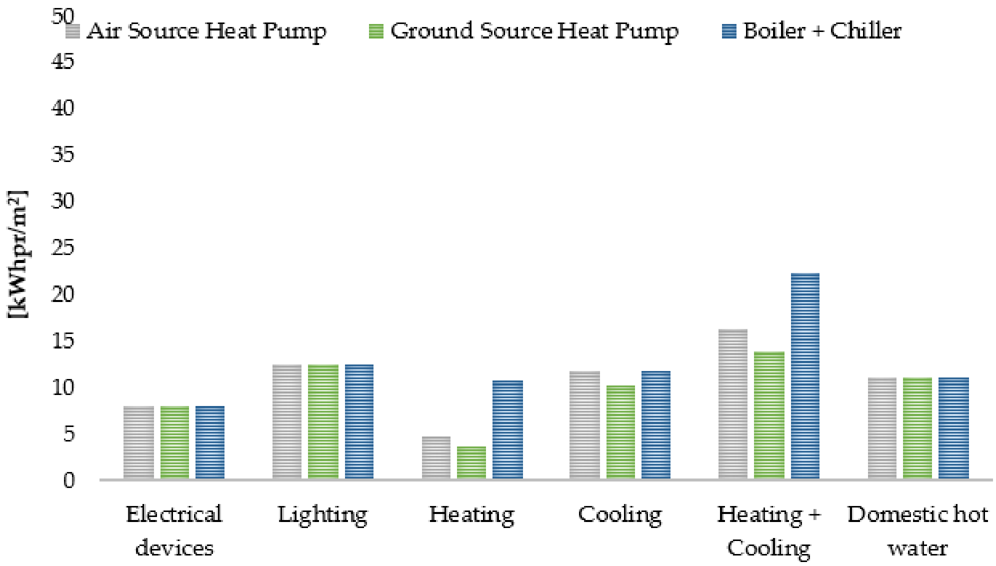

Figure 12.Primary energy consumption for different energy uses in the case of Palermo.

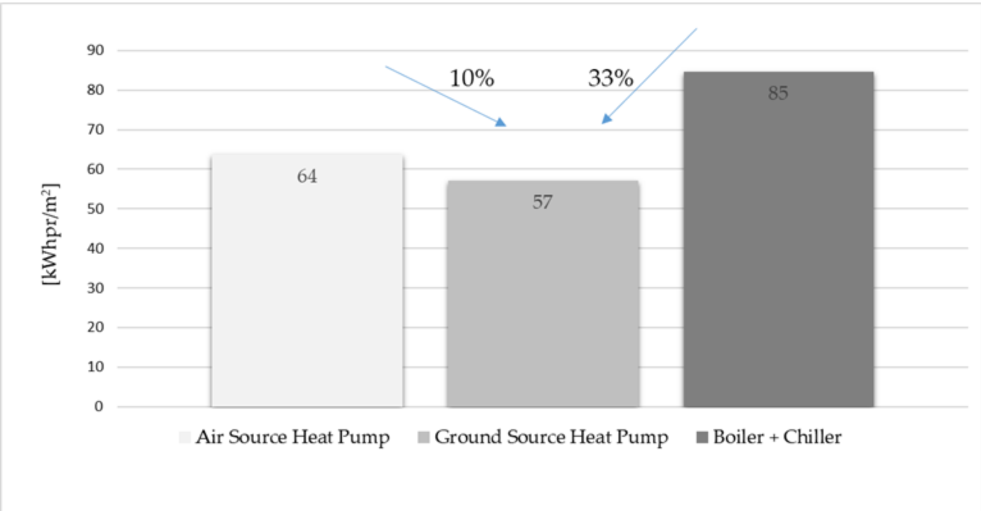

Figure 13. Total primary energy consumption in the case of Milan.

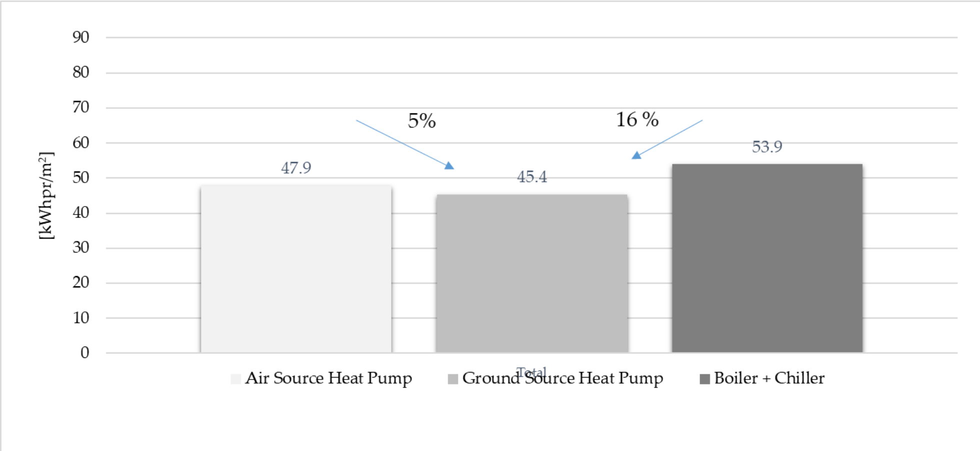

Figure 14. Total primary energy consumption in the case of Palermo.

In the case of Palermo (mild climate), the percentage of total primary energy savings can be obtained from Figure 14, the use of GSHP allows a total primary energy saving of 16% for heating plus cooling compared to the boiler plus chiller; the above mentioned saving is 5 % when compared to the case with air source heat pump. The yearly electric energy is 6131 kWh (19.8 kWh/m^2) in the case of Air-to-Water heat pump, and it is 5810 kWh (18.7 kWh/m^2) in the case of Ground-to-Air heat pump. Although the percentage saving of total primary energy between the GSHP and the air source heat pump seems to be small, it is useful to highlight that the total primary energy consumption is equal or lower of 57 kWh/m^{2}y when using a GSHP. According to the New Building Institute of the U.S. [39] that value identifies an NZEB, and this result in a cold climate such as Milan is reached only by using a GSHP as a thermal energy generator.

These results are compared with others presented in literature. Similar results are found in García-Céspedes et al. [55] where the authors evaluate the energy saving when a GSHP is present in the HVAC system instead of an air source heat pump. The results obtained are in line and reach percentages of 20%. Another comparison is made according to an ENEA report [56] when the electricity consumptions of hotels and bed and breakfast are monitored. The results are in line with those in this thesis.

Table 7. CO_2 emissions for heating and total energy consumption related to different scenarios.

	Energy Vector	**Heating**	**$CO_{2,heating}$ emissions**	**Energy Vector**	**Total consumption**	**$CO_{2,total}$ emissions**
MILAN	/	kWh	$KgCO_2$	/	kWh	$KgCO_2$
Condensing Boiler + Chiller	natural gas	12488	2649	natural gas	12488	5272
				electricity	5431	
Air Source Heat Pump	electricity	2740	1323	electricity	8171	3947
Ground Source Heat Pump	electricity	2220	1072	electricity	7316	3534
PALERMO						
Condensing Boiler + Chiller	natural gas	3147	667	natural gas	3147	3344
				electricity	5541	
Air Source Heat Pump	electricity	590	285	electricity	6131	2961
Ground Source Heat Pump	electricity	457	221	electricity	5811	2807

In fact, for B&B's located in Italian cities with mild climates, the electricity consumption is in the range of 30–60 kWh/m², while for B&B's located in Italian cities with continental climates the electricity consumption is in the range of 30–90 kWh/m² . Considering that the analysed building is designed in order to be an NZEB and the thermal characteristics of the building envelope are excellent, the electric consumption (24 and 26 kWh/m²) are in line with those of before mentioned report.

The subsequent results concern the CO_2 emissions reductions obtainable with the GSHP rather than with the condensing boiler or with an air source heat pump. The CO_2 emissions are related to the yearly energy use of the building and their reductions are assessed with reference to both heating only and global energy used during the year.

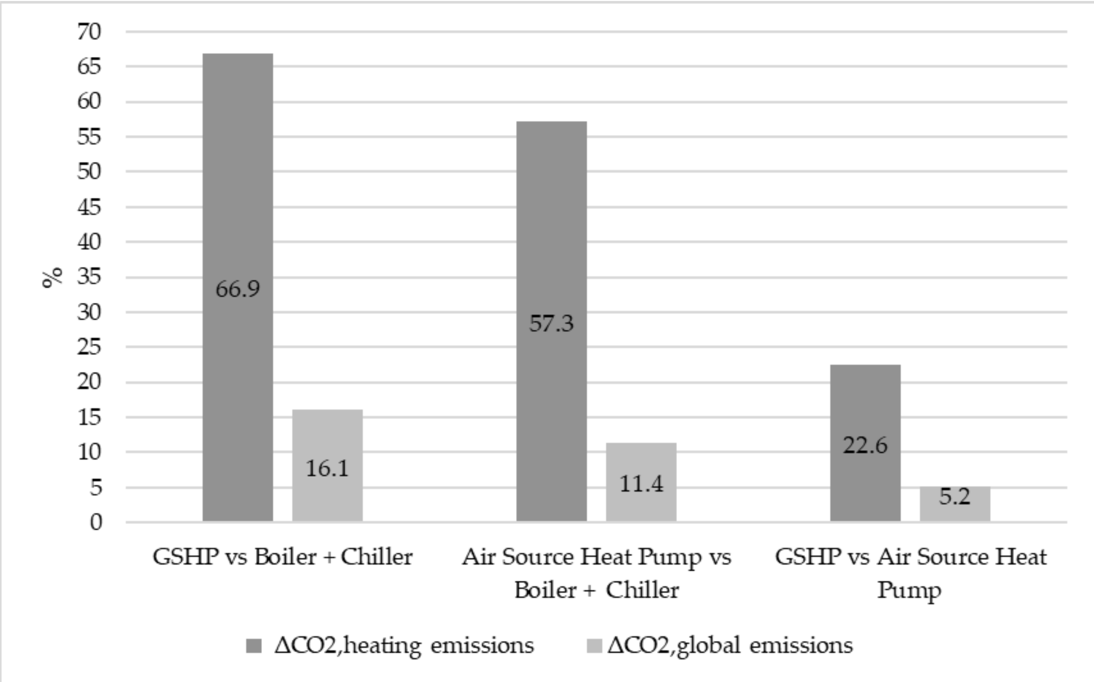

Figure 15. Percentage reduction of CO_2 emissions for different scenarios in the case of mild climate.

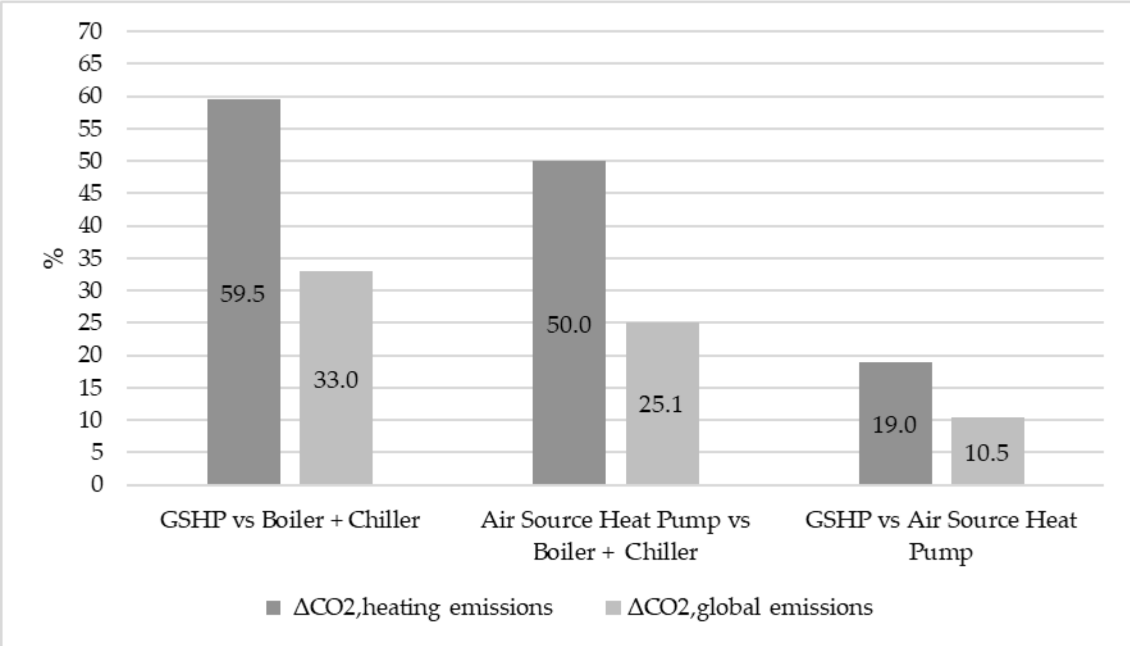

Figure 16. Percentage reduction of CO_2 emissions for different scenarios in the case of continental climate.

In Table 7 as it is well known, the most CO_2 emissions are related to the use of gas boilers and the reduction of these emissions are noticeable when a GSHP is used as a heating and cooling generator.

In a city with a mild climate, this reduction is equal to about 70% for heating when using a GSHP instead of a gas boiler and it is equal to 22.6 % for heating when using a GSHP instead of an air source heat pump (Figure 15) in a city with a mild climate.

These percentages of reductions referred to a city with a continental climate are shown in Figure 16 and are equal to 59.5 % and 19 % when using the GSHP as a heating generator instead of a condensing boiler or an air source heat pump, respectively.

The last step is to calculate the numbers of photovoltaic panels in order to satisfy the entire energy consumption of the building by using only renewable energy sources.

The monthly and yearly energy production is calculated using PVGIS tool [57] for its authoritativeness.

With reference to Table 8 (mild climate conditions), due to low energy consumption for heating and cooling, the target NZEB is always achieved. Of course, in the case of boiler plus chiller, the number of PV panels is higher when compared with the electric heat pumps for heating and cooling. The difference between the air source and the ground source is of only one panel.

Table 8. Net Zero Energy balance and number of PV modules for Palermo [58].

PALERMO										
PHOTOVOLTAIC PANELS(320 Wp per panel production 431 kWh/year per panel)										
	n° of solar thermal panels	**Yearly energy requirements**	**Primary energy conversion factor**	**n° of PV panels**	**Reduction of PV panel number**	**Yearly energy production**	**Required area for PV panels**	**Maximum vailable area for PV modules**	**NZEB balance**	**NZEB primary energy < 57kWh/m²**
	[-]	*[kWh]*	*[-]*	*[-]*	[%]	*[kWh]*	*[m²]*	*[m²]*	*[-]*	*[-]*
Boiler + chiller	4	3469 5541	*1.05* [-]	8.0 13	92	3469 5541	42	90	✔	✔
Air-to-water heat pump		6131	[-]	14	5	6131	28		✔	✔
Ground source heat pump		5811	[-]	13	–	5811	27		✔	✔

Instead, with reference to Table 9 (cold climate conditions), the target NZEB is achieved only when the electric heat pumps are installed. This is due to the too high number of PV panels required to satisfy the energy balance in the case of a condensing boiler plus a chiller. With reference to a common reference value of maximum yearly primary energy consumption for an NZEB [39] equal to 57 kWh/m², it is verified only in the case with ground source heat pumps. Despite this, the difference of number of PV panels to entirely balance the energy consumption is very small when comparing the air source heat pump and the ground source heat pump. Furthermore, it is important to highlight that the air source heat pump can be affected by malfunction when the external temperature is very low (cold climate). Instead, the ground source heat pump has the added advantage of being more reliable from this point of view.

Another result concerns the percentage of renewable energy exploits by the different HVAC configurations. Considering both the climatic conditions, 81% is related to the use of the GSHP, 75–76% for the air source heat pump, and 63–64% for the solution with boiler plus chiller.

Table 9. Net Zero Energy balance and number of PV modules for Milan [58].

MILAN										
PHOTOVOLTAIC PANELS (320 Wp per panel - production 352.2 kWh/year per panel)										
	n° of solar thermal panels	**Yearly energy requirements**	**Primary energy conversion factor**	**n° of PV panels**	**Reduction of PV panel number**	**Yearly energy production**	**Required area for PV panels**	**Maximum vailable area for PV modules**	**NZEB balance**	**NZEB primary energy < 57kWh/m²**
	[-]	*[kWh]*	*[-]*	*[-]*	[%]	*[kWh]*	*[m²]*	*[m²]*	*[-]*	*[-]*
Boiler + chiller		13113	1.05	37	61	13113	105		**x**	**x**
		5431	[-]	15		5431				
Air-to-water heat pump	5	8171	[-]	23	10	8171	46	90	✔	**x**
Ground source heat pump		7316	[-]	21	–	7316	42		✔	✔

The last result is an economic analysis in order to evaluate how the use of these different solutions can affect the energy bills. The comparison is made in terms of saved money and discounted payback period (DPB). To evaluate the money saved, the energy cost for different cases is referred to the values recommended by Eurostat's "Statistics Explained" [59], i.e., an average value of 0.225 €/kWh and of 0.100 €/kWh for electricity and for natural gas, respectively. The comparison is summarized in Table 10. Although the ground source heat pump is a perfect technology to achieve an NZEB from an energy and environmental point of view, when comparing the GSHP with the air source heat pump, the DPB the value is not acceptable, being more than a useful life of the technology. This is due to the highest cost of the GSHP compared to the cost of the condensing boiler and to the cost of the air source heat pump.

Table 10. Economic evaluation and SPB-DPB for the two different cities.

PALERMO				**MILAN**			
Boiler+chiller - Air to water heat pump							
Additional cost	**Saving**	**SPB**	**DPB**	**Additional cost**	**Saving**	**SPB**	**DPB**
[€]	*[€]*	*[years]*	*[years]*	*[€]*	*[€]*	*[years]*	*[years]*
0	182	-	-	0	632	-	-
Boiler+chiller - Ground source heat pump							
Additional cost	**Saving**	**SPB**	**DPB**	**Additional cost**	**Saving**	**SPB**	**DPB**
[€]	*[€]*	*[years]*	*[years]*	*[€]*	*[€]*	*[years]*	*[years]*
2273	254	9	14	2084	825	3	3
Air to water heat pump - Ground source heat pump							
Additional cost	**Saving**	**SPB**	**DPB**	**Additional cost**	**Saving**	**SPB**	**DPB**
[€]	*[€]*	*[years]*	*[years]*	*[€]*	*[€]*	*[years]*	*[years]*
3123	72	43	> 50	3684	192	19	50

2.4 CONCLUSIONS

This chapter investigates through an energy assessment the contribution that a geothermal heat pump can have on the reduction of CO_2 emissions, energy consumption and the consequent reduction of the surface to be used for photovoltaic panels in order to obtain an NZEB with only on-site renewable sources. These assessments are carried out by comparing the GSHP with a common system, i.e., a condensing boiler coupled to a chiller, or with a more energy efficient system such as an air to water heat pump. It was shown that when a GSHP is installed, in the comparison with other two HVAC proposed systems, the NZEB target is obtained by using a smaller photovoltaic surface. Furthermore, although the comparison is also carried out with a performing technology such as the air-to-water heat pump, the GSHP is the only system that allows yearly primary energy consumption equal to or lower than 57 kWh/m^2 to be obtained for both cold climates and mild climates. This is an important result since this value in the current scientific community is taken as a reference to define an NZEB. These are the main innovative aspects obtainable from this paper, that is, the optimal coupling of a GSHP with a photovoltaic system to obtain the NZEB target, minimizing the number of photovoltaic panels.

In more detail, it was found that the use of the GSHP, compared with the two other systems, allows considerable energy savings for heating and cooling (15–38% for Palermo and 23–55% for Milan).

Moreover, a significant reduction of CO_2 emissions is obtained when using a ground source heat pump instead of a condensing boiler (plus chiller). This reduction

- is 60 and 67% when considering only heating energy requirements for Milan and

Palermo, respectively;

- is instead 33% for Milan and 16% for Palermo in reference to global energy consumption.

The CO_2 emissions reduction comparing the GSHP, and the air source heat pump is also significant (19–23%) regarding only the heating consumption. Conversely, when considering the global energy consumption, this reduction is only 5–11%.

Regarding the photovoltaic surface necessary to entirely cover the energy need of the NZEB, the use of a GSHP instead of a condensing boiler coupled to a chiller leads to reductions of 92% for Palermo and 61% for Milan. These reductions are 5% for Palermo and 10% for Milan when comparing the GSHP with a more efficient technology such as the air source heat pump. The obtained results in the context of the NZEB is very important, as in highly urbanized contexts the space to allocate the production energy systems from renewable sources is often small and even 10% of surface savings can make

the difference to obtain the NZEB target. In fact, the results showed that in the case of a continental climate such as Milan, in which the winter energy demand is predominant, it is not always possible to satisfy the NZEB target due to insufficient roof surface.
Beyond satisfying the energy balance, an energy demand limit value was considered to classify a building as an NZEB: it is suggested by the New Building Institute of the U.S. and is equal to 57 kWh/m^2. If this limit value is considered, the building in question can be considered an NZEB for both climatic conditions only by using the GSHP.
Finally, referring to the energetic-economic analysis, the discounted payback (DPB) period for the GSHP is about 3 years for Milan and 14 years for Palermo when compared to the configuration with boiler plus chiller, while it is more than the useful life when compared to an air source heat pump. Therefore, the air source heat pump seems more convenient than the GSHP from an economic point of view. However, it should be noted that the air source heat pump, especially in cold climates (Milan), can be affected by malfunctions in the case of very low external temperatures, when it may sometimes not satisfy the user.
Clearly, for the analysed cases, in order to obtain an NZEB, the ground source heat pump (compared to the common configuration with a condensing boiler coupled to a chiller and to the solution with the air source heat pump) has the highest performance from an energy point of view, but is still too expensive. Therefore, from an economic point of view (discounted payback period), it is mainly convenient for continental climates (Milan) when compared to the solution with a condensing boiler coupled to a chiller.

The contents of this chapter are an extension of the following publication in which I am the corresponding author:

- D'Agostino, D., Mele, L., Minichiello, F., Renno, C. "The use of ground source heat pump to achieve a net zero energy building". *Energies*, 2020, 13(13), 3450.

3 EARTH-TO-AIR HEAT EXCHANGER (EAHX)

3.1 STATE OF THE ART

The Earth-to-Air Heat eXchanger is the second technology that exploits the low geothermal energy of the ground which is investigated in this thesis work. The EAHXs are systems based on several ducts, horizontally or vertically buried in the ground at a depth useful to exploit the ground property of exhibiting, under undisturbed conditions, almost constant temperature during the whole year. The heat transfer fluid to be used in EAHXs is typically air: in the most common configurations the EAHX is inserted in a mechanical ventilation system, more rarely in a primary air circuit. As the ground temperature, below about 10 m depth, is often higher in winter and lower in summer than air temperature [60], the EAHX gives rise to a pre-heating of the external ventilation air in winter and pre-cooling in summer (Figure 17).

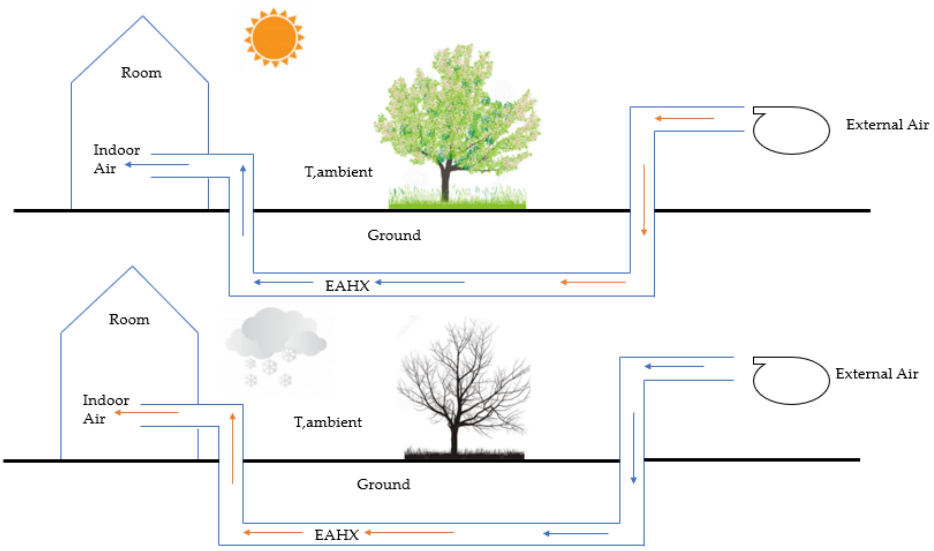

Figure 17. EAHX scheme as pre-cooling technology for summer and pre-heating technology in winter conditions.

The EAHXs should be adequately projected to let the air, during the ducts blowing, brings its temperature close to the undisturbed ground one.
Several different solutions are used with reference to: material of the air ducts (or pipes); layout and geometry of the plant; number of the ducts; etc. Based on the air circulation mechanism, EAHXs are classified into two macro categories: open loop and closed loop systems. In open loop systems the heat transfer fluid is the environmental external air that crosses the buried ducts where it is treated (heated or cooled). Subsequently the air is either sent directly to the building to be ventilated/air-conditioned or carried in a conventional Air Handling Unit (AHU) present in the HVAC system, to be further heated or cooled and then sent to the building. The open loop system provides that the air, after it has completed its "conditioning" task, would be expelled directly from the building into the atmosphere. In the closed loop systems, at the end of the air conditioning process (heat exchange with the ground through flowing in the ducts and heat transfer with the building to be conditioned) the air is fed back at inlet of the EAHX ducts to be recirculated. Therefore, in a closed loop EAHX system, after several circulations, the air needs to exchange a relatively lower amount of heat with the ground compared to an open loop system. In general, the closed loop configuration is energetically more efficient than the open loop one, also allowing to reduce the problem of undesired water condensation in the ducts due to the humidity rate of the external air introduced in the EAHX (a typically summer problem). However, the open loop system is often preferable because it also allows the air exchange in the building, which is not possible for the full air recirculation systems; moreover, the air recirculation could carry to the contamination of the HVAC systems by Coronavirus or other viruses.

EAHX systems can be characterized by vertical or horizontal air ducts. The arrangement of the pipes plays a fundamental role since the portion of the ground required for the installation of the EAHX systems in order to satisfy the heating/cooling demand depends on the design and layout of the pipes; indeed, the air conditioning potential of an EAHX system is strongly linked to its geometric configuration. Horizontally oriented pipes are generally used in EAHX systems, mainly because they present a simpler and cheaper type of installation than the vertical ducts, since the former requires a shallower excavation. De Carli and Zarrella in [61] fixed some useful parameters to dimension the EAHXs, below reported:

- The length should be at least 20 m.
- The diameter of the piping should be between 0.2. and 0. 3 m.
- The laying depth should be between 2 and 3 m.
- The air speed should be between 1 m/s and 3 m/s, which is a good compromise between heat exchange and pressure drops.
- Condensate collection:
    - when the depth increases in the direction of the air flow, the minimum slope is 2.5%;
    - if the depth increases in the opposite direction of the air flow, the minimum slope is 3.5%.
- Slope is also useful for periodic cleaning of the pipes.

A further classification in the EAHX system with horizontal ducts can be made between single-layer configuration, with all the ducts buried at a single depth level, and multi-layer configuration where the ducts, horizontally oriented, are buried one on the other at various depths in the ground and separated by vertical drops. Single layer configurations are by far the most used among the solutions proposed in literature [62] [63]. At the best of my knowledge, very few are the investigations performed on multilayer EAHX systems but worthy of attention is the work proposed by de Jesus Freire et al. [64] . They made a comparison in an EAHX between multilayer pipes and single layer configurations, on equal number of tubes and distance between one each other, as well as the same were the duct design parameters (diameter, length, air velocity) [64] . On equal amount of heat transfer surface, number of tubes and air velocity, they detected 3% and 6% decreasing in temperature span, respectively considering the two- and three-layer configurations compared to the single layer one. On the other side, the two- and three- layer configurations analysed required a reduction of the available flat surface for installation estimated, respectively, on 50% and 67%, if compared to the single-layer one. Indeed, despite of slight energy performances decreasing, the multi-layer configuration could prove very promising in urban contexts with limited installation surfaces.

Earth-to-air heat exchanger is a very promising technology but mandatory is the optimization of the system to the purpose of appropriately setting the design parameters (such as diameter, length and number of tubes, displacements of the tubes, air velocity), according to the installation specifics and limits as well as to the geographical zone, in order to let the EAHX system showing the highest energy performances [65]. To pursuit this goal, before the installation of the system, it is important to widely test the projected EAHX system. This crucial point could be addressed by means of the development of an accurate numerical model able to predict the energy performances under a wide number of working conditions.

Based on the literature analyses, it is therefore possible to briefly summarize the main advantages in using and investigating EAHX systems: i) the working fluid is air (unlimited and free available); ii) the energy consumptions of stand-alone EAHX or EAHX/HVAC-coupled systems are lower than the traditional HVAC systems, as well as higher are the coefficients of performances too; iii) the EAHX system is simple, therefore it requires few maintenance and operating costs; iv) the environmental impact deriving from the operation of the EAHX system is reduced with respect to the traditional ones, since the former is supplied by a renewable energy source and, furthermore, it requires less use of compressors and GWP (Global Warming Potential) refrigerants. However, it must be pointed out that the use of the EAHX is not yet widespread. This is due to both the space problems related to the installation of buried pipes, which can be problematic in widely urbanized contexts, and the excavation costs necessary for burying the pipes.

Many of the numerical models reported in the scientific literature for the analysis of the EAHX are herein reviewed and summarized. Bordoloi et al. [66] in their review paper classified and compared the energy performances of the main EAHX systems describing the most relevant analytical and experimental studies on the different combinations of EAHXs, up to the year 2018. Another very appropriate classification was proposed by Bisoniya et al. [67] in their review where, specifically, the numerical models of EAHX were categorized based on the method they are solved through and the dimensions of the geometry investigated. Anyhow, the common denominator of both the reviews is to propose an overview of the worldwide research scenario on this type of geothermal system; the emerging data is the really huge number of EAHX systems and models proposed. An accurate numerical model should be able of evaluating punctually both the conductive (from/to duct/ground) and the convective (related to the air flowing in the duct) heat transfer mechanisms acting in the EAHXs. Even if several commercial software like TRNSYS or EnergyPlus allow to easily model geothermal systems, providing qualitative data on their performances ("black-box approach"), they are not able to provide punctual (in space and time) indications on the heat transfer and temperature fields in the whole systems. Indeed, to perform accurate heat transfer investigations on the operation of earth-to-air heat exchangers, one of the most appropriate solutions is represented by Computational Fluid Dynamics (CFD)-based models, founded on the discretization of the domain in finite differences/volume/elements despite of the method adopted for solving the differential equations that govern the heat transfer problem.

In open literature, various 1-D, 2-D, and 3-D models of earth-to-air heat exchangers were presented and described.
Over the years, the beginning investigations on EAHXs founded on the development of one-dimensional models with simple balances were made to derive the inlet-outlet relations for the air parameters. In 2002 Kabashnikov et al. [68] introduced one of the first one-dimensional models of an earth-to-air heat exchanger; the mathematical model was very simple as well as few were the results collected: based on Fourier integral for evaluating the temperature in the system, a mathematical investigation was carried out, by varying length, diameter and depth of the ducts. As main result the model can provide an analytical expression giving the mathematical value of the length and the diameter that optimizes the heat exchange between the air and the ground. In 2003 De Paepe and Janssens [69] shared with the scientific community their one-dimensional analytical model where the convective heat exchange is accounted through the calculation of the convective coefficients by means of dimensionless numbers approach. They evaluated the influence of pressure drop as function of volumetric air-flow rate, of diameter and length of the duct. They noticed that smaller diameters provide higher thermal performance, but greater pressure drops. The solutions they suggested is to project EAHX with more ducts placed in parallel to counteract these contrasting trends. Through the one-dimensional mathematical model proposed in 2008 by Cucumo et al. [70] the effect of burial depth of the tubes on the energy performances of earth-to-air heat exchanger systems was evaluated. The model is able to provide the results following two methods: superposition principle, Green functions. They performed the investigation in

a sandy soil, and they asserted that optimal deepness belongs to the range 3-6 m. The effect of burial depth was also investigated by Sehli et al. [71] by means of a finite volume CFD model. The convective heat exchange of the fluid flowing under turbulent motions was evaluated through the k-ε method. They identified 4 m as optimal depth and they noticed that, as soon as Reynolds number increases, the inlet-outlet temperature span decreases due to the less time spent by the air in tube and, consequently, for the heat exchange with the ground.

An intense study is the one of Serageldin et al. [72] that, with their one-dimensional CFD transient model of EAHX experimentally validated, asserted that with reference to Egyptian weather: i) the larger are duct diameter, length and distance, the higher is the inlet-outlet temperature span; ii) greater air flow velocities reduce the inlet-outlet temperature span; iii) the duct material does not affect significantly the heat exchange between the air and the ground. Among the latest 1-D models proposed, worthy of note is the one of Cuny et al. [73] published in 2020, where, following the multi-criteria optimization based on genetic algorithms, the Pareto front for an EAHX systems was determined. Three were the criteria selected, two energy based and one economic, and they were applied to the operation of an EAHX with reference to French climates. The optimum combination suggests high duct length (97 m), whereas small should be duct diameter (0.15 m) and air flow velocity (0.7 m s^{-1}). A good compromise between performances and cost for burial depth could be 3.2 m. Furthermore, in 2020, a one-dimensional model was used by Lin et al. [74] to quantify the correlation between the moisture of the ground and the log-term energy performances of an earth-to-air heat exchanger. Three different cases were considered: partially and fully saturated, fully dry. The results show that the EAHX energy performance is not affected by the soil moisture when the air velocity is low (up to 1 ms^{-1}) but for higher velocity the effect of the moisture in the soil affects significantly the energy performances, since also basing on their operative condition the flow evolves in turbulent. The performances are higher the more is the soil saturation and a 40% difference in energy performances between the fully dry and fully saturated grounds was appreciated. Moreover, they asserted that the maximum air flow velocity in the tube should not overcome 4.0 ms^{-1}.

One-dimensional models show some limits: they cannot calculate the field of speed and temperature of the air into a transversal section of the duct, neither the temperature field of the soil when the depth varies. These limits can be overcome by the development of two-dimensional models. Most of the 2-D models of earth-to-air heat exchangers presented in literature are solved through finite element methods. Ahmed et al. [75] proposed an intense investigation on the optimization of the energy performances of a horizontal earth-to-air heat exchanger with reference to the most salient parameters of the system. The model is 2-D and CFD-based implemented through the software FLUENT 15.0. The Navier-Stokes and energy equations were solved through the finite element method and the effect of the turbulent flow in the above equations was accounted through the k-ε model. The impact of air velocity, as well as duct depth, diameter, length, and material on the energy performances was studied with reference to a hot subtropical Australian climate and the results revealed the length of the tube being the most influent factor. Furthermore, the analysis showed that there is not a univocal combination of design parameters to optimize all the energy performance at the same time: i.e., the air flowing with 1.5 ms^{-1} velocity in a clay duct (0.003 m thickness) with 8.0 m, 60 m, 0.062 m as respectively depth, length and diameter, optimizes the efficiency of the EAHX but not the energy saving. To maximize the latter parameter another combination of such parameters is required. A further important problem to be analysed by means of 2D models is represented by the soil thermal saturation caused by the presence of the EAHX. This aspect was studied by Niu et al. [76] in 2015 through a numerical model founded on the transient method of control volume. They observed that the effect of saturation of the soil becomes relevant in the degradation of the cooling capacity if the system operates in continuous mode, whereas an intermittent working mode during the day allows the soil thermal recovering and consequently it mitigates the degradation of the energy performances.

With 3-D models, some other investigations about the EAHX were performed, with reference to: energy performance of the plant for various layouts of horizontal air ducts (grid configuration, radial one, parallel one); thermal interaction between adjacent air ducts. On the other side, also due to the need of accounting the turbulence of the flow, the 3-D models result much more complex in resolution and onerous from computational costs point of view. Among the novel noteworthy numerical studies on 3D models, there is the

one of Zhao et al. [77] where, based on an experimental 1:20 scaled earth-to-air system, a corresponding 3D model is developed to study the influence of the different parameters on thermal performances (mainly the length and diameter of the tubes and the inlet air velocity). Authors noticed that the thermal extraction efficiency increases with the duct length and decreases for rising values of diameter and air velocity. The highest value (0.96) was detected when the EAHX operates in cooling mode, with air speed of 0.5 ms^{-1} and a duct diameter of 20 mm, whereas the largest cooling and heating capacities calculated are, in that order, 21.17 kW and 21.72 kW. Furthermore, they asserted that at burial depth below 4 m, the soil temperature is not so accurately determinable.
In 2015, Bisoniya et al. [78], through the development of a quasi-steady state CFD 3-D model, focused on the energy payback period, the yearly thermal performances and the seasonal efficiency ratio of an experimental EAHX system installed in Bhopal (Central India). They asserted that considering 50 years as lifetime, the EAHX system allows the reduction of 101.3 tons of CO_2 whereas the total carbon credit has estimated being around $ 2838. Always about considering the operation of the EAHX for many years of system life, interesting is the concept of "derating factor" introduced by Bansal et al. [79] , that accounts the degradation of the thermal performances over the time. It is defined as instantaneous inlet-outlet temperature span detected on the corresponding steady state one. Indeed, due to the saturation of the soil, the smaller is the ratio, the greater is the degradation of the thermal performances.

A well-designed EAHX system can be used independently but it can also be coupled to a traditional HVAC system to meet the heating/cooling requirements of the buildings. In the inherent scientific literature, a number of interesting works investigated the energy performances of HVAC plants coupled to/integrated with earth-to-air heat exchangers systems. Bansal et al. [80] analysed the energy saving and economic impact deriving from integrating the earth-to-air heat exchanger technology into an evaporative cooling system. Specifically, by means of a CFD tool, they considered four base cases of air-conditioning and electric heater systems characterized by three diverse blowers: energy efficient blower, standard blower, and inefficient blower. With reference to these cases, the energy saving, and the payback period related to the use of the EAHX were evaluated. They found that a payback period of 2 years for integrating EAHX with an efficient blower evaporative system is very convenient. On the other side, for inefficient blowers the integration of an earth-to-air heat exchanger would result in a financially unviable choice. The authors showed that the energy saving was hardly affected by the electricity tariff and the blower efficiency. In 2016 Ascione et al. [81] analysed the effects on energy efficiency and environmental impact of employing an earth- to-air heat exchanger in the air conditioning system enslaving a nearly Zero Energy Building (nZEB) through the software Energy Plus. The HVAC plant based on an air-to-water heat pump supplying fan-coil units plus mechanical ventilation: the EAHX was employed as pre-treating unit (pre-heating in winter and pre-cooling in summer), located upstream of the air handling unit. They observed that the EAHX integration carried up to a 29% energy saving in winter and, as well as, 36-46% in summer, for a global yearly saving rate of 24–38%.

In 2020, Li et al. [82] analysed, from energy, environmental and economic point of view, the integration of an EAHX in an air-to-air heat recovery unit based on mechanical ventilation compared with the case of coupling a heat pump to a primary air handling unit. The EAHX was tested in a parametric analysis with two parallel horizontal ducts buried at 2.5 m and 5 m with 2 m and 5 m as space between the tubes. The results showed that for severe cold climates, the EAHX-based solution carries to remarkable benefits with reference to all the three above aspects. The static and dynamic payback periods for the EAHX-based system were about 2.1 and 2.4 years (with return rate of 8%); a reduction of 17% in equivalent emissions of CO_2 was also calculated. The most promising results were obtained with 5 m distance between the two ducts. D'Agostino et al. [83] evaluated the thermal performances of an EAHX compared to air-to-air heat exchangers providing promising energy savings also for this configuration but with higher economic costs.

Indeed, the above state-of-the art on numerical models of EAHX systems revealed the limits shown by one-dimensional models, especially in the impossibility of drawing the temperature and velocity profiles of the air flowing in the pipes, as well as the temperature range established around the pipes. As a matter of fact, even if these limits could be overcome through the development of both two- or three-dimensional models, currently, the vast majority of the numerical EAHX tools is 2D because the latter represents a good compromise in accuracy and computational costs. Anyhow, for complex geometries or particular placements of the pipes, where is needed, the 3D model is used.

At the best of my knowledge, the scientific research up now lacks a worldwide comparison on the performances of a hybrid HVAC system where an EAHX is installed upstream of the Air Handling Unit (AHU). At this aim, a case study office building is analysed and virtually collocated in various climatic zones around the world. The HVAC system is based on fan-coil units and primary air, and the EAHX is installed upstream of the Air Handling Unit (AHU). For the above considerations on the model dimensions, a 2D mathematical model of the EAHX is developed to obtain the system performance under different outdoor air temperatures. The problem is solved through finite element method. The analysed EAHX is characterized by 5 horizontal circular ducts displaced in parallel at 2.5 m deep. The EAHX is considered to pre-cool/pre-heat the open-loop airflow (primary air) of the Air Handling Unit. To make a comparison, the office building is virtually placed in six cities of Italy, which belong to different climatic zones according to Italian regulation DPR 412/93. For a further comparison, the case study building is also virtually collocated in eight localities around the word, basing the choice on the climate classification proposed by Köppen. The EAHX is simulated and optimized as a function of the diameter and length of the air ducts. The following parameters are calculated: the variation of air temperature in the EAHX; the EAHX thermal efficiency; the decreasing of cooling and heating capacity of the coils into the AHU when comparing with the solution without EAHX. The analysis on the coils of the AHU is performed for winter, summer and for all the year.

After the state of the art have been analysed, the state of the art, it is evident that the thermal and energy performances of the EAHX are greatly influenced not only by the characteristics of the soil, but also by the boundary climatic conditions of the place where the exchanger is located. For these reasons, the main steps of this chapter are as follows:

- a worldwide comparison about the thermal performance of an EAHX, which, at the best author’s knowledge, lacks in the scientific literature;
- the proposed comparisons are not only based on cities with various climates, but also considering different classifications of climatic conditions in the world;

- the EAHX has been commonly investigated as a component added to a usual mechanical ventilation system, while this paper analyses a hybrid air conditioning system in which the EAHX is inserted upstream of the air handling unit to minimize the energy requirements;
- for various climatic zones around the world, the thermal efficiency of the EAHX and the decreasing of cooling and heating capacity of the coils into the AHU are evaluated.

3.2 METHODOLOGY AND APPLICATION

The methodology of this chapter is based on a 2D mathematical model of an EAHX to obtain the system performances under different outdoor air temperatures. The EAHX is considered not only as an air pre-treatment device placed inside a mechanical ventilation system, but also as a component to pre-treat the air to be conditioned into an air handling unit inside a HVAC system. In this way it can ensure a relevant energy saving.

The investigation is conducted on a HVAC system for an office building. The building is spread over two floors for a total area equal to 260 m^2 and a volume equal to 910 m^3. In Figure 18 the ground floor and first floor are shown.

The investigated HVAC system is based on fan-coil units and primary air, with an upstream-placed horizontal-ducts EAHX system. According to Italian technical standard UNI 10339 [84] , the design ventilation outdoor airflow has been set at $11 \cdot 10^{-3}$ m^3 s^{-1} per person, for a total amount of $3.61 \cdot 10^{-1}$ $m^3 s^{-1}$ (1300 m^3 h^{-1}).
The analysed EAHX is characterized by five buried horizontal air ducts, installed in parallel at 2.5 m depth. The section of the buried pipes is circular, and the analysis is carried out referring to a maximum length of 100 m and to three different diameters (0.2 m, 0.3 m, and 0.5 m).
The choice to fix a maximum length equal to 100 m is dictated by the fact that, analysing the trend of the air temperature inside the EAHX after 80-100 m, this tends to an asymptotic value and the temperature variation is negligible.

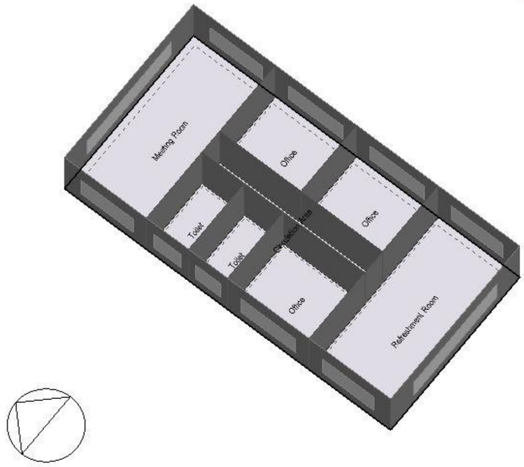

(a) (b)

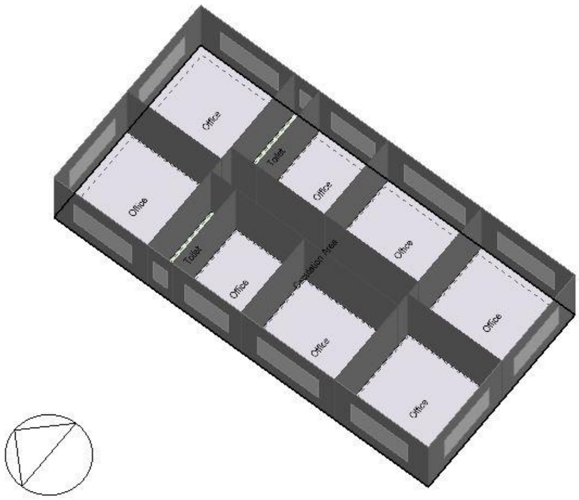

Figure 18. Office building object of the present analysis:(a) ground floor; (b) first floor.

By way of example, Figure 19 shows the temperature trend for the city of Naples and similar results are obtained for the rest of the cities analysed. Furthermore, similar results are in agreement with results found by Chiesa et al. in [85] and from Ascione et al. in [86].

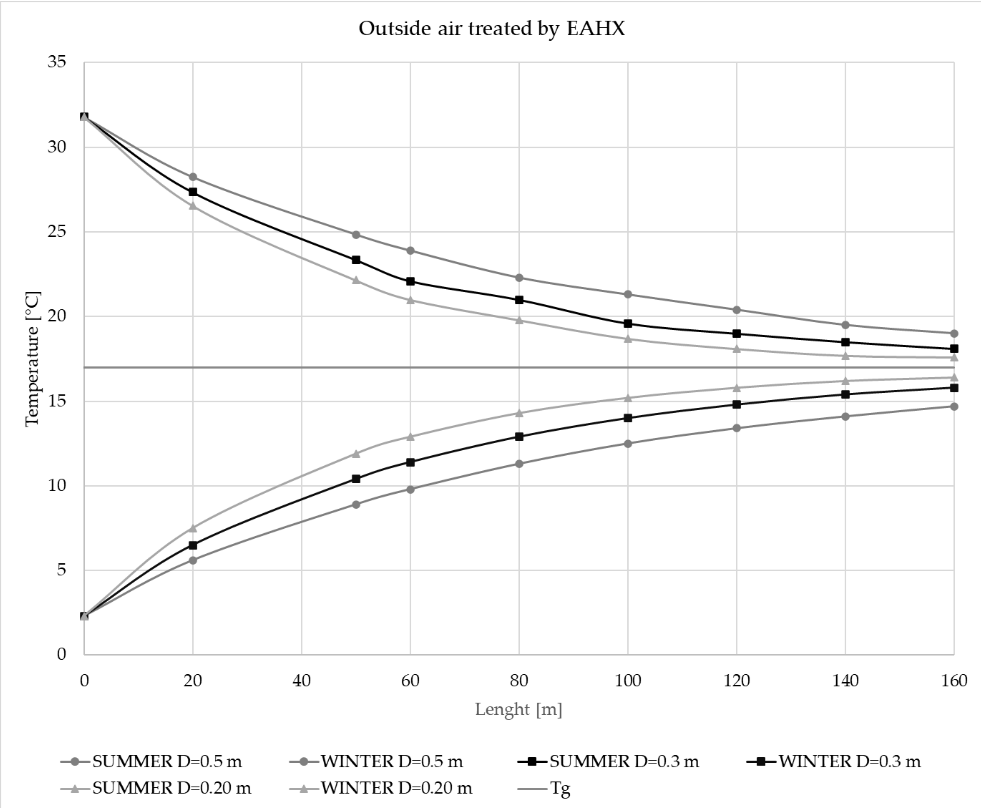

Figure 19. Trend of the external air temperature in the EAHX as the length of the pipe varies for different diameters.

Two adjacent ducts are spaced 2.5 m apart, then the system will extend over a rectangular surface with a maximum size of 12.5 m x 100 m.

The model considers only one of the ducts. The finite element method is used to solve the mathematical model formed by the equation of the mass conservation for fluid, the equations of momentum conservation of fluid, and the energy equations for the fluid and for the solid. The heat transfer processes between the fluid (humid air) and the solid (ground) are conjugated. The equations are solved with appropriate boundary and initial conditions. Specifically, at the bottom of the soil domain, a 1st type condition is used to fix the undisturbed temperature of the ground, identified through the Kusuda relation [50]. The sun-air temperature is forced as 1st type condition on upper boundary of the volume. The model is then validated by means of experimental data reported in the scientific literature.

The climatic conditions of the localities, where the system is installed, affect the EAHX thermal performance. Therefore, to make a comparison, the office building is virtually placed in six different cities of Italy, chosen to belong to six different climatic zones identified by D.P.R. 412/93 [53]. For a further comparison, the building is subsequently placed in eight cities of the world following the Köppen climate classification [87] (the Italian cities are also included).

During the analysis on the EAHX, the diameter of the air ducts is varied to optimize the system, but the airflow rate necessary for the building must remain constant, so the speed of the air varies consequently. The temperature of the air at the exit of the EAHX is evaluated; this air is then sent to the air handling unit before it is supplied to the building. The following parameters are evaluated: the variation of air temperature in the EAHX; its thermal efficiency; the decreasing of cooling and heating capacity of the coils into the AHU when comparing with the solution without EAHX. The analysis on the coils of the AHU is performed for winter, summer and for the whole year.

3.2.1 Italian climatic zones

According to D.P.R. 412/93 [53], as shown in Figure 20, the Italian territory is divided into six (A-F) climatic areas based on the heating degree-days of the localities. For each climatic zone, over one year, the period and the maximum number of hours per day where heating may be switched on are fixed. The heating degree-days are the unit used to assign a climatic zone to each municipality: they are the sum, extended to all days in a conventional yearly heating period, of only positive differences between indoor temperature (conventionally fixed at 20 °C) and the mean daily outdoor temperature. The coldest climatic zones in winter correspond to the greatest values of the degree-days. The degree-days vary from a minimum of 600 (for zone A) to over 3000 (for zone F).

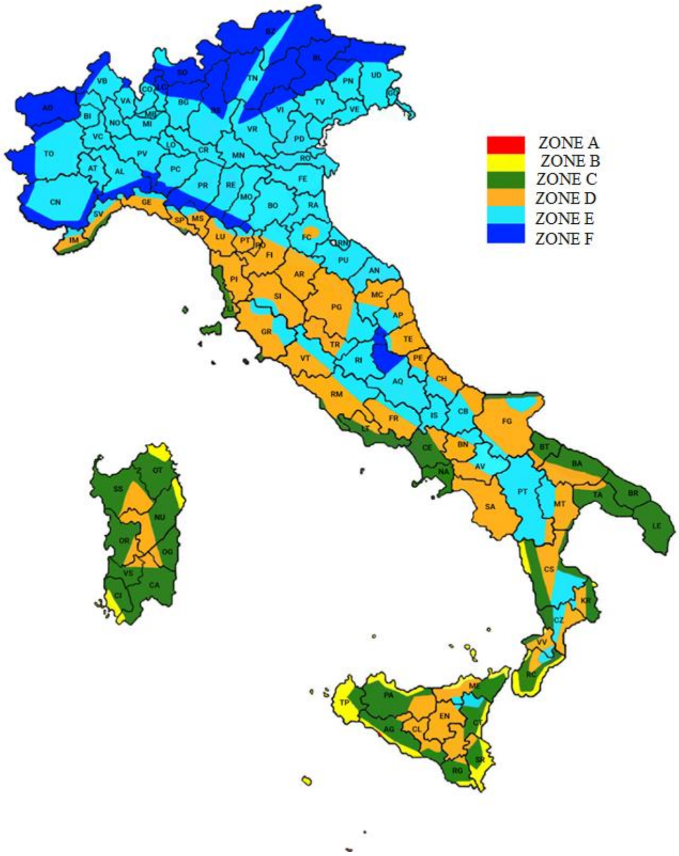

Figure 20. The different Italian climatic zones according to D.P.R. n. 412 of 1993.

To make a comparison, six Italian localities have been considered in this analysis (Lampedusa, Catania, Naples, Rome, Milan, Pian Rosa) belonging to the different six climatic zones. The weather data considered were identified through ASHRAE climatic data [52].

Table 11 shows, for each of the six localities, the design values of the outside air temperature, the relative humidity and the solar incident radiation in winter and summer.

Table 11. Winter and summer design outdoor parameters for the six localities chosen.

Climatic Zone - locality	**Geographic coordinates**	**Winter design parameters**			**Summer design parameters**		
		T [°C]	**RH** [%]	**G** [Wm^{-2}]	**T** [°C]	**RH** [%]	**G** [Wm^{-2}]
A-Lampedusa (AG)	Lat. 35° 30′ 05″ N Long. 12 °36′34″ W	9.80	54.60	874	31.00	65.80	831
B - Catania	Lat. 37° 30' 4"68 N Long. 15° 4' 27" W	2.90	71.20	824	32.80	44.10	819
C – Naples	Lat. 40° 51' 22" N Long. 14° 14' 47" W	1.90	52.00	808	31.90	48.60	825
D – Rome	Lat. 41° 90' 27" N Long. 12° 49' 23" W	0.10	60.40	783	32.60	37.80	829
E – Milan	Lat. 45° 46' 46" N Long. 9° 18' 85" W	-3.20	65.10	743	32.00	44.70	805
F - Pian Rosa (AO)	Lat. 45° 93' 33" N Long. 7° 70' 00" W	-22.20	44.60	1026	8.10	51.70	994

3.2.2 Climatic zones according to Köppen climate classification

The Köppen climate classification [87] is based on the evaluation of the local vegetation in each zone, since in a certain region the concentration of the vegetation depends on both the temperature and precipitation. The Köppen classification subdivides the Earth area into five main climatic zones based on temperature criteria, apart from the second zone (B) in which it is assumed that the dryness of the zone is the main key factor for vegetation's concentration.

The principal zones are identified with a capital letter as follows :

- Zone A: equatorial or tropical climates (the minimum monthly temperature value during the year is equal to or greater than 18 °C). This zone includes the warmest climates.
- Zone B: dry climates (yearly mean value of precipitation is less than a specific limit). This zone includes deserts and steppes.
- Zone C: mild temperate climates (monthly average temperature of the warmest month is equal or greater than 10°C, monthly average temperature of the coldest month ranging from -3°C to 18°C).
- Zone D: continental climates (monthly average temperature of the warmest month is equal or greater than 10°C, monthly average temperature of the coldest month is equal or lower than -3°C).
- Zone E: polar climates (monthly average temperature of the warmest month is less than 10°C).

Each climatic area can be also divided in subareas by means of a second letter to take into account precipitations; in some cases, also another sub-criterion (based on temperature) is considered, by adding a third letter.
Figure 21 shows the Italian map according to Köppen classification. Based on this classification, the Italian localities belong to the climatic zones reported in Table 12. Pian Rosa was omitted since it is characterized by extreme and not very generalizable climatic conditions. Furthermore, in the summer season it does not require a cooling system.

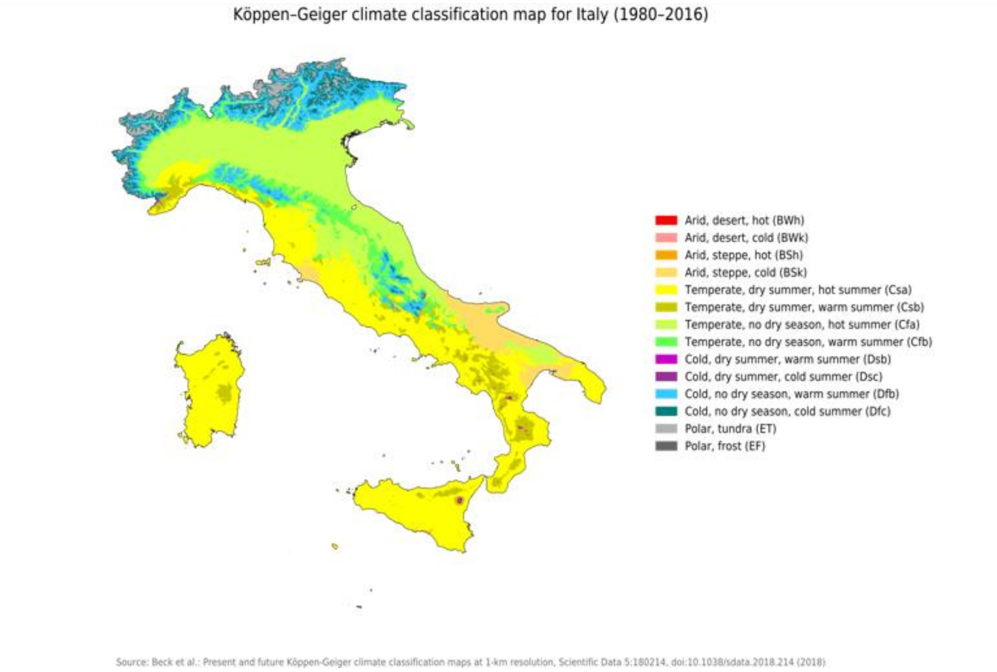

Figure 21.Köppen climate classification map for Italy.

Table 12. Classification of the chosen Italian cities according to Köppen climatic zones.

City	Climatic zone based on DPR 412/93 [53]	Climatic zone based on Köppen classification [87]
Lampedusa	A	Bsh
Catania	B	Csa
Naples	C	Csa
Rome	D	Csa
Milan	E	Cfb

As Table 12 shows, Lampedusa can be classified according to Köppen classification as Bsh (hot semi-arid climate); Catania, Naples and Rome as Csa (hot-summer Mediterranean climate); Milan as Cfb (temperate oceanic climate). Moreover, three further localities (Rio de Janeiro, Dubai, Ottawa) are analysed. They belong to the A, B and D zones, respectively, based on the classification proposed by Köppen, whereas zone E (polar area) is not considered. Table 13 shows, for these three towns, the design values of outside air temperature, relative humidity and solar incident radiation in winter and summer.

Table 13. Winter and summer design outdoor parameters for Rio de Janeiro, Dubai, and Ottawa.

Climatic Zone Locality	Geographic Coordinates	Winter design parameters			Summer design parameters		
		T [°C]	RH [%]	G [Wm-2]	T [°C]	RH [%]	G [Wm-2]
Aw Rio de Janeiro	Lat. 22° 54' 29.9988"S Long. 43° 11' 46.9968" W	17.1	76.8	826	32.8	47.5	923
Bwh Dubai	Lat. 25° 16' 37.1532" N Long. 55° 17' 46.4964" E	14.2	43.9	795	41.8	21.9	661
Dfb Ottawa	Lat. 45° 25' 28.9956" N Long. 75° 41' 42.0000" W	-20.8	64.9	858	29	50.1	846

According to this classification, Rio de Janeiro belongs to Aw (tropical wet and dry climate) climate zone; Dubai to Bwh (hot desert climate) and Ottawa to Dfb (warm-summer humid continental climate).

3.2.3 The HVAC system description

The air conditioning system is characterized by fan coils and primary air. A reversible (invertible) heat pump provides hot and cold water for both the coils of an air handling unit, in order to treat the primary air, and the fan-coil units located in each room of the building. The design external (or outdoor) air flow has been set at $11\cdot10^{-3}$ m^3 s^{-1} per person, for a total of 1300 m^3 h^{-1}. The design thermo-hygrometric conditions to be guaranteed inside each room are:

- indoor air: temperature of 20 °C for winter and 26 °C for summer, relative humidity (RH) of 50% for both winter and summer;
- supply primary air: temperature of 20°C and RH of 50% for winter, 15°C and RH of 85.2 % for summer (this value of RH is calculated after evaluating the specific humidity ω by means of a mass balance for each room, referred to water).

Two air conditioning systems are analysed: Figure 22 shows the traditional one characterized by only the AHU for primary air (without EAHX), whereas Figure 23 shows the system where the EAHX is placed upstream of the AHU. The first one is a usual HVAC system with only the AHU (without EAHX) and fan-coil units: the air treated in the AHU is outdoor air. The second air conditioning system is instead characterized by the EAHX which pre-heats or pre-cools the outside air before being handled into the AHU.

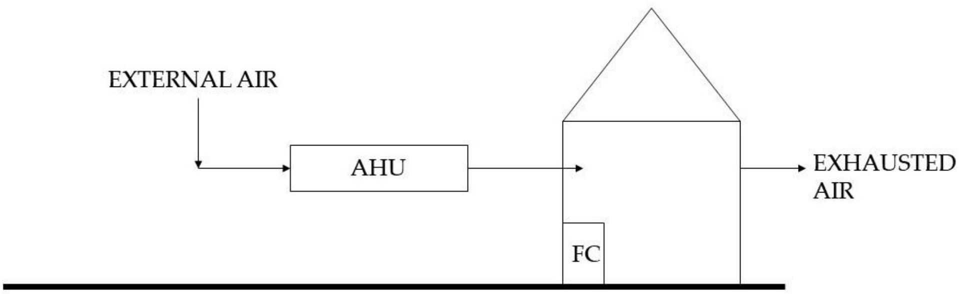

Figure 22. HVAC system without EAHX.

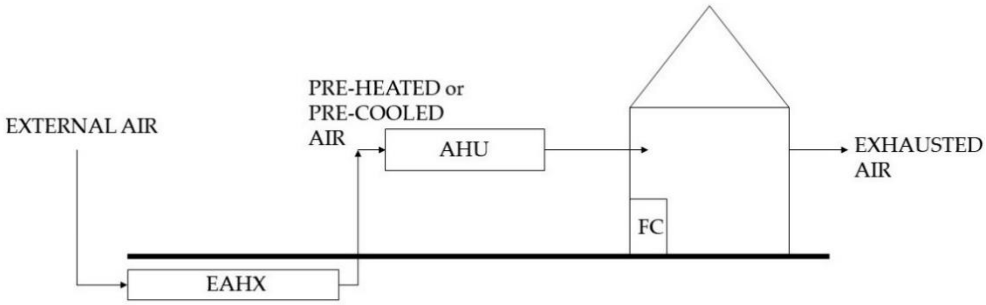

Figure 23. HVAC system with EAHX.

The AHU is composed of the following main components:

- filters;
- pre-heating water coil;
- cooling and dehumidifying water coil;
- humidifying section;
- re-heating coil;
- supply fan.

In the Figure 24 (a) for summer and Figure 24 (b) for winter the transformations in the AHU are reported on the psychometric chart. During the summer (Figure 24 (a)) the processes that the humid air undergoes are: cooling and dehumidification from point "o" (outdoor air conditions) to point "A" and subsequent re-heating from point "A" to point "s" (supply air conditions). The cooling coil is supposed to be ideal with a by-pass factor equal to 0% (i.e., RH_A=100%). During the winter (Figure 24 (b)) the processes are: pre-heating from point "o" to point "A", humidification with liquid water from point "A" to point "B" and re-heating from point "B" to point "s" which coincides with the thermohygrometric conditions to be maintained in the room (point "r"). The humidifier is supposed to be ideal (with saturation efficiency of 100%). When the EAHX is used for pre-cooling/pre-heating the air flow, the point "o" (outside air) is substituted with the point EAHX (air conditions at the exit of the EAHX, individuated through the 2D model below described).

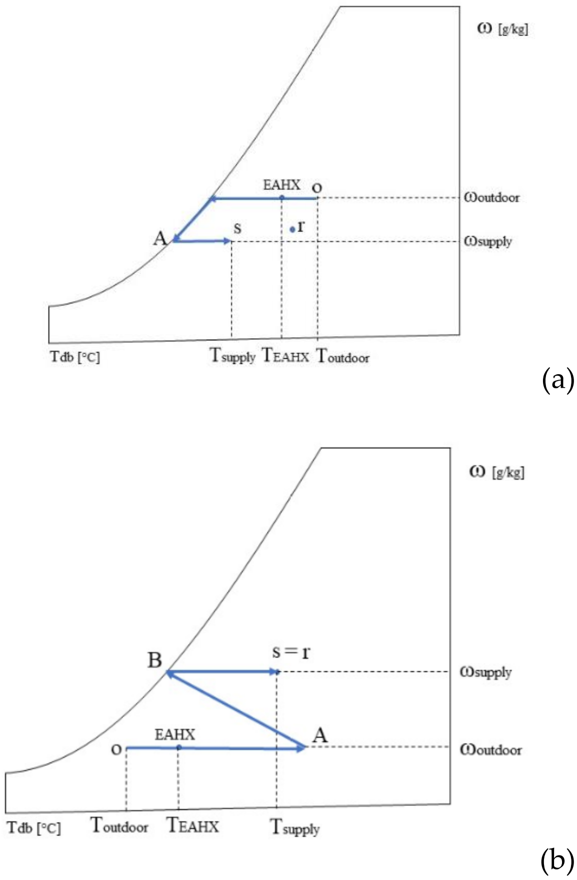

Figure 24. Processes of the humid air into the AHU reported on the psychometric chart during: (a) summer and (b) winter.

To evaluate the coils capacity, the mass and energy balances are carried out on the control volumes shown in Figure 25(a) and Figure 25(b). During the summer (Figure 25(a)) the running components of the AHU are: the cooling coil and the re-heating coil.

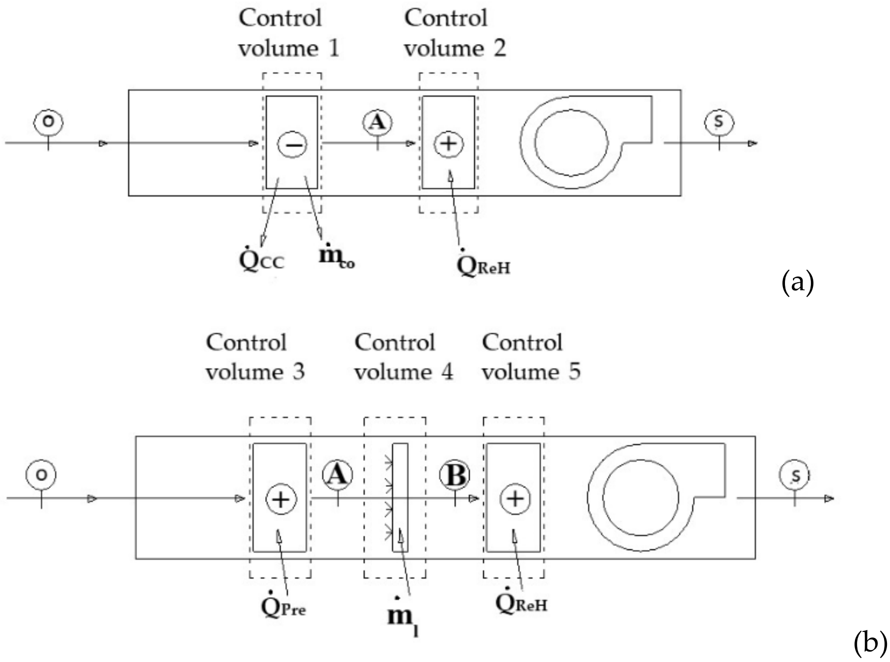

Figure 25. Schematic of active components in the AHU for primary air in: (a) summer and (b) winter.

The energy balance equation for calculating the cooling capacity (with reference to control volume 1 of Figure 25(a)) is:

$$\dot{Q}_{CC} = \dot{m}(h_o - h_A) - \dot{m}_{co}h_{co}, \qquad (7)$$

The re-heating coil capacity (control volume 2 of Figure 7 a) can be evaluated as:

$$\dot{Q}_{ReH} = \dot{m}c_p(T_s - T_A), \qquad (8)$$

During the winter, as shown in Figure 25 (b), the active components are: the pre-heating coil, the humidifier with liquid water and the re-heating coil. The pre-heating coil capacity (control volume 3 of Figure 25(b)) can be evaluated as:

$$\dot{Q}_{PRE} = \dot{m}c_p(T_A - T_o), \qquad (9)$$

The mass flowrate of humidification water (control volume 4 of Figure 25(b)) can be evaluated as:

$$\dot{m}_w = \dot{m}(\omega_B - \omega_A), \qquad (10)$$

The re-heating coil capacity (control volume 5 of Figure 25(b)) is obtained from the equation:

$$\dot{Q}_{ReH} = \dot{m}c_p(T_s - T_B), \qquad (11)$$

When the EAHX is in use, the reduced capacity of the AHU coils both for summer and winter has been evaluated. Consequently, the reduction of the coils' capacity obtained by the introduction of the EAHX technology compared to the AHU without this heat exchanger is calculated, considering the coils operating in winter season, summer season and all over the year.

3.2.4 Mathematical model of EAHX

In this research, the open-loop earth-to-air heat exchanger was 2D modelled through a finite element method software. The EAHX was made of five horizontal ducts. The horizontal disposition was chosen since vertical one usually involves with higher installation and maintenance costs. The number of tubes has been chosen to obtain, at fixed air volumetric flowrate, a range of air velocity between 0.4 and 2.5 m s^{-1} that is a good compromise between effectiveness of heat transfer and pressure drops. 2.5 m is the distance d stemming between two adjacent ducts: this value is chosen to avoid thermal interaction between the two air ducts. The computational domain of the model consists of one circular buried duct (for air flowing) surrounded by a ground volume of 20 m deep. This value of deepness was chosen to consider the ground as undisturbed [22] [88].

The buried duct is installed at 2.5 m deep from the soil surface because, in agreement with other studies [60], for deepness more than 2 m, the soil temperature is about undisturbed and close to the yearly mean values of the outdoor air. Burying the pipe between 2 m and 3 m is a good compromise [81] [89] between yearly temperature excursion and excavation costs.

The mass flowrate of the air entering each pipe is evaluated as:

$$\dot{m}_{pipe} = \frac{\dot{m}}{5}, \qquad (12)$$

Various values of the length and diameter of the air ducts are considered:

$$L = [20; 50; 60; 80; 100]\ m,$$

$$D = [0.2; 0.3; 0.5]\ m,$$

The outside airflow of 1300 m^3 h^{-1} must be provided to the building, so the modification of the duct diameter leads to a modification in the air speed. In Table 14 for each diameter the air velocity and the Reynolds number are reported. The table clearly shows that the airflow rate can be always considered in fully turbulent developed regime.

Table 14. Reynolds numbers evaluated for each couple of diameter and inlet velocity for each air duct.

D [m]	**u [m s^{-1}]**	**Re [10^4]**
0.2	2.3	2.83
0.3	1.0	1.85
0.5	0.37	1.14

In Figure 26 the computational domain and the used mesh with a triangular shape are reported. The model is solved through finite element method and the domain was divided into 70625 free-triangular elements: a higher concentration of elements can be found inside and surrounding the duct where more marked is the temperature gradient. The diameter and the length of the ducts are indicated with D and L, respectively. The air entering the tube has temperature and relative humidity proper of the external air.

The following assumptions are used in the present study:

- two-dimensional model;
- no thermal interaction between the buried ducts;
- a longitudinal section of the domain (composed by the ground and the duct) is modeled for symmetry;
- the air flow velocity ensures the full turbulent regime;
- the thermal resistance of the tube is neglected;
- the study is time-dependent and the model runs until reaching the steady-state;
- temperature in soil undisturbed at 20 m depth;
- constant properties of the soil in the whole domain;
- constant properties of the air flow in the ducts;
- the soil considered as an isotropic medium.

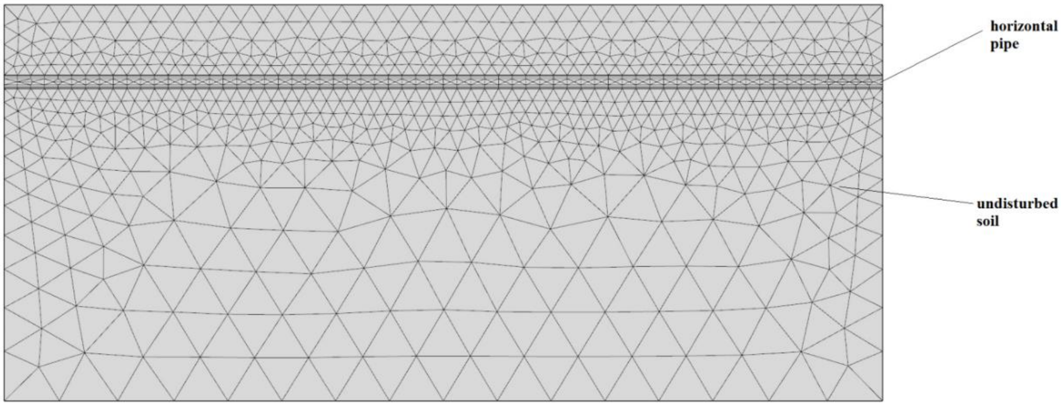

Figure 26. Computational mesh domain of the investigation on a single buried duct of the EAHX.

The air entering the ducts is humid air. The thermodynamic properties of humid air (dry bulb temperature; relative and specific humidity) can be punctually evaluated, in time and space, through the model. Therefore, the condensed water flow rate can be also evaluated. For the fluid domain the following differential equations can be numerically solved:

- the mass conservation of the humid air:

$$\frac{\partial \rho}{\partial t} + \nabla(\rho \vec{\boldsymbol{v}}) = \dot{S}_m, \tag{13}$$

  where $\dot{S}_m$ is a negative term that represents the mass of water vapor condensed;
- the momentum conservation of the air flow is guaranteed by the Navier-Stokes equations for turbulent flow:

$$\rho \frac{\partial \vec{v}}{\partial t} + \rho(\vec{\boldsymbol{v}} \cdot \boldsymbol{\nabla})\vec{\boldsymbol{v}} = \boldsymbol{\nabla} \cdot \left[-p\vec{\boldsymbol{I}} + (\mu + \mu_T)[\nabla\vec{\boldsymbol{v}} + (\nabla\vec{\boldsymbol{v}})^T]\right], \tag{14}$$

  where μ_T is the turbulent viscosity defined as:

$$\mu_T = \rho C_\mu \frac{K}{\hat{\varepsilon}}, \tag{15}$$

with C_μ, that is one of the constants of the K-$\hat{\varepsilon}$ model for turbulent flow [76];

- the energy equation for the air flow:

$$\frac{\partial(\rho E)}{\partial t} + \nabla \cdot [\vec{\boldsymbol{v}}(\rho E + p)] = \boldsymbol{\nabla} \cdot \left[k_{eff}\nabla \mathrm{T} - \textstyle\sum_j \mathrm{h_j}\vec{\mathrm{J}}_j + (\tau_{\mathrm{eff}} \cdot \vec{\boldsymbol{v}})\right], \tag{16}$$

where k_{eff} is the effective conductivity defined as the sum of the conventional thermal conductivity of the fluid (k_f) and the thermal conductivity of the turbulent flow (k_T) and thus modeled as:

$$k_{eff} = k_f + k_T, \tag{17}$$

- Using the K-$\hat{\varepsilon}$ model for turbulent flow, the turbulence kinetic energy equation is:

$$\frac{\partial(\rho k)}{\partial t} + \rho\vec{\boldsymbol{v}} \cdot \nabla K = \nabla \cdot \left(\left(\mu + \frac{\mu_T}{\sigma_K}\right)\nabla K\right) + P_K - \rho\varepsilon \tag{18}$$

(14)

where P_K can be evaluated as:

$$P_K = \mu_T\left(\nabla\vec{\boldsymbol{v}}: (\nabla\vec{\boldsymbol{v}} + (\nabla\vec{\boldsymbol{v}})^{\boldsymbol{T}}) - \frac{2}{3}(\nabla \cdot \vec{\boldsymbol{v}})^2\right) - \frac{2}{3}\rho K \nabla \cdot \vec{\boldsymbol{v}} \tag{19}$$

The specific dissipation rate equation is:

$$\frac{\partial(\rho\varepsilon)}{\partial t} + \rho\vec{\boldsymbol{v}} \cdot \nabla\varepsilon = \nabla \cdot \left(\left(\mu + \frac{\mu_T}{\sigma_\varepsilon}\right)\nabla\varepsilon\right) + C_{\varepsilon 1}\frac{\varepsilon}{K} P_K - C_{\varepsilon 2}\rho\frac{\varepsilon^2}{K} \tag{20}$$

The experimental constants of the K-$\hat{\varepsilon}$ model are reported in Table 15.

Table 15. Experimental constants of the K-ε ˆmodel

Constant	Value
C_μ	0.09
$C_{\varepsilon 1}$	1.44
$C_{\varepsilon 2}$	1.92
σ_k	1.0
σ_ε	1.3

The differential equation of conduction in solid domain numerically solved is:

$$\frac{\partial(\rho_{soil} c_{soil} T_{soil})}{\partial t} = \boldsymbol{\nabla} \cdot (k_{soil} \nabla T_{soil}), \tag{21}$$

The soil humidity is considered balancing water and solid properties throughout the porosity (Y) with the following equation:

$$z_{soil} = \psi z_{liquid} + (1 - \psi) z_{solid}, \tag{22}$$

For each locality of the analysis the thermal properties of the soil are evaluated and reported in Table 16.

Table 16. Thermal properties of the soil.

City	**k** [W m^{-1} k^{-1}]	**ϱ** [kg m^{-3}]	**c** [J kg^{-1} K^{-1}]	**α** [10^{-6} m^2 s^{-1}]	**Ref**
Rio de Janeiro	3.67	850	1800	2.33	[54]
Dubai	0.26	1538	1270	0.133	[55]
Italian localities	2.20	2500	900	0.980	[56]
Ottawa	2.1	1620	800	1.62	[57]

For all the Italian localities, the mean value of the soil thermal properties is considered corresponding to a porosity of 37%.
The associated thermal boundary conditions for the domain are:

- at the side boundaries of the soil domain, adiabatic (2nd type) conditions are used disregarding any thermal influence from the ground beyond these boundaries;
- at the bottom of the soil domain, since the ground temperature remains constant beyond this boundary (deep 20 m), a 1st type condition is imposed, following the undisturbed temperature evaluated with the Kusuda equation [50] already reported in the paragraph 2.1 (equation 4).

Table 17 reports the weather data used in the Kusuda relation and the resulting undisturbed ground temperature for each locality of the present analysis.

Table 17. Temperature of the undisturbed soil obtained by Kusuda equation.

City	**T_m [°C]**	**A [°C]**	**Depth [m]**	**a [m^2 day^{-1}]**	**t [day]**	**t_{min} [day]**	**T_{ground} [°C]**
Lampedusa	20	5.4	100	0.0821	365	15	**20.00**
Catania	17.6	7.8	100	0.0821	365	15	**17.60**
Naples	17.0	8.5	100	0.0821	365	15	**17.0**
Rome	15.9	8.9	100	0.0821	365	15	**15.90**
Milan	12.3	9.4	100	0.0821	365	15	**12.30**
Pian Rosa	-5.0	6.95	100	0.0821	365	15	**-5.10**
Rio de Janeiro	25.1	-2.8	100	1.028	365	15	**25.0**
Dubai	29.3	7.9	100	0.795	365	15	**29.0**
Ottawa	12.1	-1.2	100	0.064	365	15	**12.0**

- at the top of the soil domain (the surface), a 1st type boundary condition is assumed: the sun-air temperature. This temperature takes into account both the incident solar radiation on the ground surface and the convective heat exchange with the external air, and is expressed with the following equation:

$$T_{sa}(x, 0, t) = T_{air,ext}(t) + \frac{\alpha G(t)}{h_c}, \tag{23}$$

- the air temperature at the inlet of the duct is fixed according to the values of external air reported in Table 11 and Table 13 for the different localities in summer and winter season;

- inlet air velocity (in x direction) depends on the tube diameter.

After the calculation of the outside air at the exit of the EAHX (by means of the described mathematical model), the thermal efficiency of the EAHX is calculated through the typical equation (24) for heat exchangers (as the ratio between the EAHX temperature span and the ideal temperature difference):

$$\varepsilon = \frac{T_{outlet} - T_{inlet}}{T_{ground} - T_{inlet}}, \tag{24}$$

A time dependent solver is used to solve the mathematical model, while the implicit BDF (Backward Differentiation Formula) is used as time step procedure. The implicit BDF procedure utilizes backward differentiation equations that present accuracy from one (named as the backward Euler method, too) to five. BDF procedures were often utilized due to their stability characteristics. On the other hand, they could show some damping effects, mainly when considering the lowest order methods (some high frequencies are often damped). Although one could expect a solution with sharp gradient, a frequently smooth solution is obtained due to the above-mentioned damping effects. The use of BDF could be characterized by high order if possible, and lower order when it is indispensable to reach stability. The strategy of the solver selected for the model used in this work is BDF with "Free time stepping": in this way, the solver can set greater or smaller time steps to satisfy the required tolerances. In fact, the solver tries to calculate with the largest possible time step, but, when the solution starts to rapidly vary and therefore the (relative and absolute) tolerances are not verified, it decreases the timestep size until it is indispensable. The values of the absolute and relative tolerances fixed for the solver of the introduced model are $5 \cdot 10^{-4}$ and $1 \cdot 10^{-2}$, respectively.

The independence of the spatial grid is evaluated after the model was simulated on equal initial boundary, and operative conditions with three different meshing geometries: the system is evaluated with the domain divided into 11124, 15827, 70625 triangular elements, following free triangular meshing.

The average temperature profiles at the outlet of the buried ducts for different mesh size are reported in Figure 27 as a function of time. The small box reported in the figure represents a zoom of the end of the time interval to better highlight the spacing of the curves at different meshes.

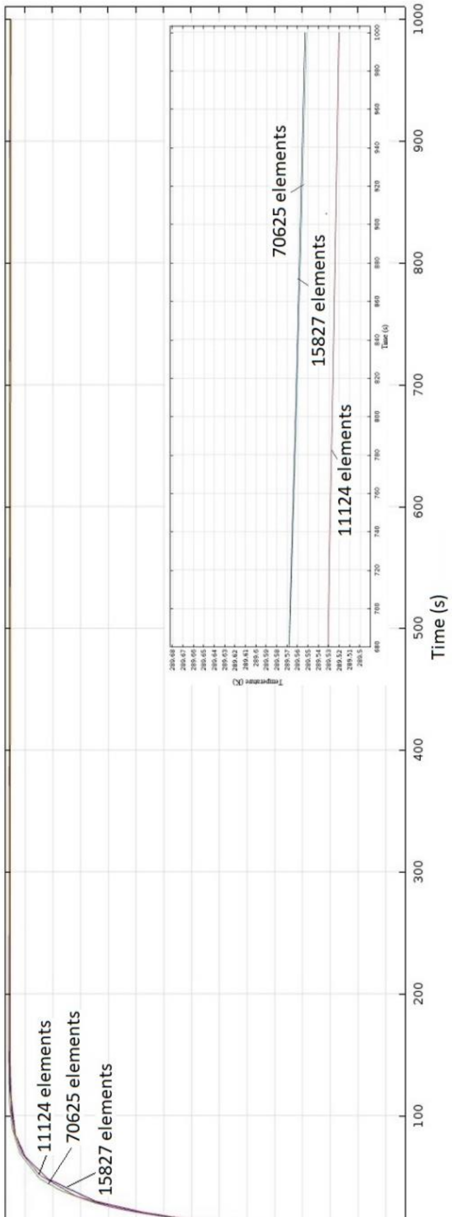

Figure 27. Average air temperature at the outlet of the buried pipes as a function of time for three different meshing (11124, 15827, 70625 elements).

As clearly visible from the figure we found a substantial overlapping between the temperature profiles with 15827 and 70625 elements and a good agreement between the solution with 11124 elements (maximum difference lower than 0.04 K). Since the computational time for elaborating the solution does not differ appreciably if we simulate with 15827 and 70625 elements, we opted for the finer meshing (70625 elements).

3.2.5 Model validation

To ensure the reliability of the results obtained with the numerical code, the model is validated by comparing it with experimental data available in open literature. Specifically, three case studies of horizontal EAHX installed in three different countries (Algeria, Morocco, Egypt) are chosen for validation.
The experimental data published by Hatraf et al. [90] have been obtained for an EAHX installed at the University of Biskra, Algeria (Longitude 5° 44'E, Latitude 34° 48 'N), a location characterized by a hot and dry summer, typical of the Saharan climate. The experimental facility consists of four horizontal ducts buried at a depth of 3 m; each duct is 60 m long with an inner diameter of 0.11 m. The external air at the inlet of the EAHX was at a temperature of 36 ° C with two different volumetric air flowrates (135 m^3h^{-1} and 156 m^3h^{-1}). The corresponding Reynolds numbers ($2.63 \cdot 10^4$ and $3.03 \cdot 10^4$) ensure for the air flow in the ducts a fully developed turbulent regime. Figure 28 shows a comparison between the experimental and the numerical values of air temperature at different location along the tube length for both the volumetric flowrates considering the same geometrical parameters and boundary conditions.
In Table 18 is reported the absolute and relative error on the outlet air temperature: the maximum relative deviation between the experimental and the numerical data is 3.5% (at 17 m of tube length). That is, the maximum difference between the predicted and the experimental air temperature at the outlet of the EAHX is 1°C.

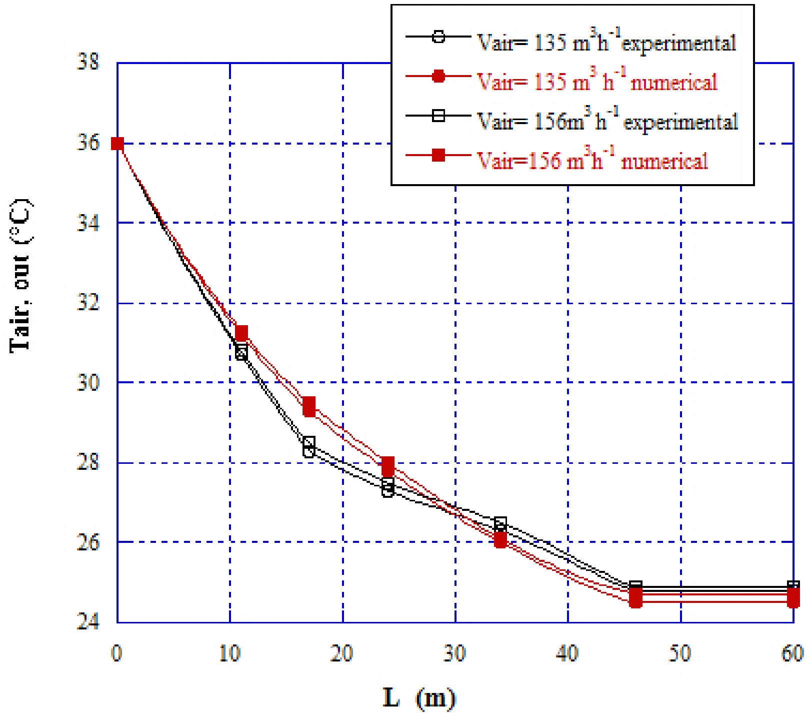

Figure 28. Experimental and numerical values of air temperature alongside one pipe of the EAHX with two inlet volumetric flow rates (135 m^3 h^{-1} and 156 m^3 h^{-1}).

Table 18. Absolute and relative error on air outlet temperature [90].

L [m]	ε_{135} [°C]	$\varepsilon_{135\%}$ [%]	ε_{156} [°C]	$\varepsilon_{156\%}$ [%]
11	0.5	1.6	0.5	1.6
17	1	3.5	0.99	3.5
24	0.5	1.8	0.5	1.8
34	0.3	1.5	0.4	1.5
46	0.3	1.20	0.2	0.80
60	0.3	1.20	0.2	0.80

In addition, the EAHX model has also been validated by means of some of the experimental results provided by Khabbaz et al. [91], related to an Earth-to-Air Heat Exchanger system located in Marrakech (Morocco) (Latitude 31°38′02″ N, Longitude -7°59′59″ E), location characterized by hot semi-arid climate. The experimental EAHX is constituted of three horizontal parallel ducts (length: 77.7 m; inner diameter: 0.15 m), buried at 2.2 m and 3.5 m depth; the air enters the ducts with a velocity of 5 ms^{-1} (corresponding to a Reynolds number of $4.55 \cdot 10^4$ that ensures a turbulent flow regime). Measure uncertainties on temperature is + 0.5°C. The experimental tests have been carried out at the air inlet temperature of 34.5 and 35.9 °C. In Figure 29 the numerical and experimental values of air temperature values are reported alongside the buried pipes.

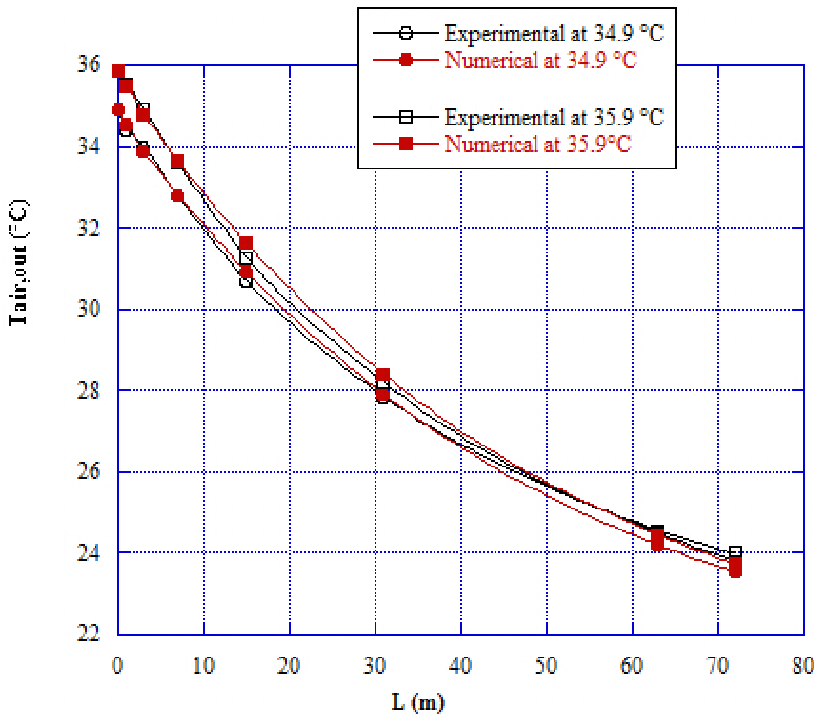

Figure 29. Experimental and numerical values of air temperature alongside one pipe of the earth-to-air heat exchanger at an external inlet temperature of 34.9 and 35.9 °C

In Table 19 the absolute and relative error on the outlet air temperature are reported. It can be noted that the maximum relative deviation between the experimental and the numerical data is 1.2% (at 63 m of tube length). The maximum difference between the predicted and the experimental values of air temperature at the outlet of the EAHX is 0.3 °C (lower than the experimental uncertainty on the measured temperature).

Table 19. Absolute and relative error on air outlet temperature [91].

L [m]	$\varepsilon_{34.9}$ [°C]	$\varepsilon_{34.9\%}$ [%]	$\varepsilon_{35.9}$ [°C]	$\varepsilon_{35.9\%}$ [%]
1	0.14	0.41	0.03	0.084
3	0.12	0.35	0.13	0.37
7	0.030	0.091	0.06	0.18
15	0.22	0.72	0.35	1.12
31	0.07	0.25	0.20	0.71
63	0.3	1.2	0.11	0.45
72	0.26	1.1	0.25	1.04

A further validation of the model is presented with experimental data of Serageldin et al. [72]. The experimental system is an EAHX installed at the University of Science and Technology of Borg El Arab (Egypt) (Latitude 3° 55 'N Longitude 29° 42' E), a location characterized by a desert climate, generally hot, sunny and dry throughout the year. The experimental heat exchanger is a horizontal PVC duct of 5.5 m long, with an inner diameter of 0.0508 m, buried at a depth of 2 m. The comparison refers to the summer operating mode, with an inlet air temperature at 30.2 °C and a volumetric flow rate of 11 $m^3 h^{-1}$ (the corresponding Reynolds number is $5.05 \cdot 10^3$). The Reynolds number follows in the transition between laminar and turbulent flow. In this range the numerical model uses the laminar solution. The experimental temperature was detected with T-type calibrated thermocouples, with an error following in the normal range with deviations between the thermocouples reading and that of a standard one (beta Calibrator TC-100) of + 0.1-0.5 °C. In Figure 30 is reported a comparison between experimental and numerical values of air temperature as a function of the tube length: the figure clearly shows that the numerical model always overpredicts the experimental data.

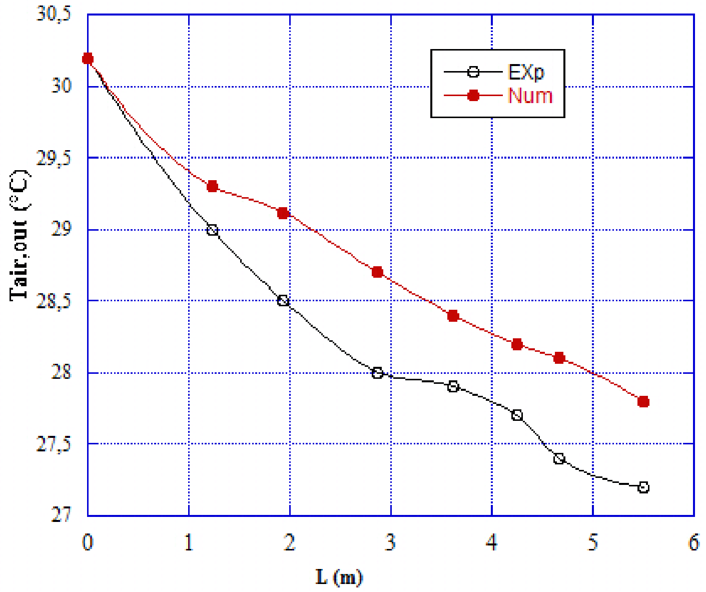

Figure 30. Experimental and numerical values of air temperature alongside the pipe of the earth-to-air heat exchanger.

Table 20. Absolute and relative error on air outlet temperature [72].

L [m]	ε [°C]	$\varepsilon_{\%}$ [%]
1.23	0.30	1.03
1.94	0.62	2.17
2.88	0.70	2.50
3.62	0.50	1.79
4.25	0.50	1.81
4.67	0.70	2.55
5.50	0.60	2.21

In Table 20 the absolute and relative error on the outlet air temperature is reported. It can be noted that the maximum relative deviation between the experimental and the numerical data is 2.55 % (at 4.67 m of tube length). The maximum difference between the predicted and the experimental values of air temperature at the outlet of the EAHX is 0.70°C.

All these analyses have demonstrated that the presented model is able to predict the thermal performance on a horizontal EAHX not only in fully developed turbulent flow but also in laminar or transition regime.

3.3 RESULTS AND DISCUSSION

In this chapter the thermal and energy performances of an EAHX pre-treating unit coupled to an AHU are evaluated. The thermal behaviour of an EAHX is not the same on the Earth but depends on the climatic context, the soil temperature, and the configuration of the EAHX. The soil temperature is very similar to the yearly mean temperature of the place in which the EAHX is installed; therefore, it is often higher than air temperature in winter and lower in summer. In this regard the performances of the EAHX are compared in: i) six localities of Italy belonging to different climatic zones according to the Italian D.P.R. 412/93 classification; ii) nine cities with different climatic conditions based on the classification proposed by Köppen. The described EAHX is tested by means of a mathematical model; each simulation is carried out until the steady state regime is obtained. At this point, all the parameters are calculated.

3.3.1 Comparison among the six different Italian localities

In Figure 31 the temperature variation along the tube length in winter and in summer varying the inner tube diameter for the six localities is reported. Figure 31 (f) represents the temperature profile for Pian Rosa; for this locality only the winter conditions are reported since the cold temperatures of the area do not require summer operation of HVAC system. On the Figure 31 the dew point temperatures (only for summer) and the ground temperature are also reported for each locality. Note that in Milan and in Lampedusa, in summer, the air temperature at the exit of the EAHX is minor than the dew point, and this means that the air specific humidity is reduced, and the air is dehumidified. The maximum value of the condensed water mass flow rate is achieved with the lower inner diameter (0.2 m) and the highest tube length (100 m) and is 1.16 g s^{-1} for Lampedusa and 1.51 g s^{-1} for Milano. The tube length corresponding to the beginning of vapour condensation decreases with the reduction of the inner tube diameter. Indeed, with a diameter of 0.2 m, the condensation begins at a lower length (50 m) compared to higher diameters. For all the figures a similar trend can be observed: the air flow temperature

increases/decreases through the tube length in winter/summer. This increment/decrement is faster for the initial length of EAHX (the first 20-30 m) and then becomes moderate. A temperature of the air close to undisturbed ground temperature (Knee point) is obtained at a duct length of about 80 m for all the localities.
The Knee point represents the length of the tube at which more than 90% of the global increase or decrease of the air temperature has been obtained.

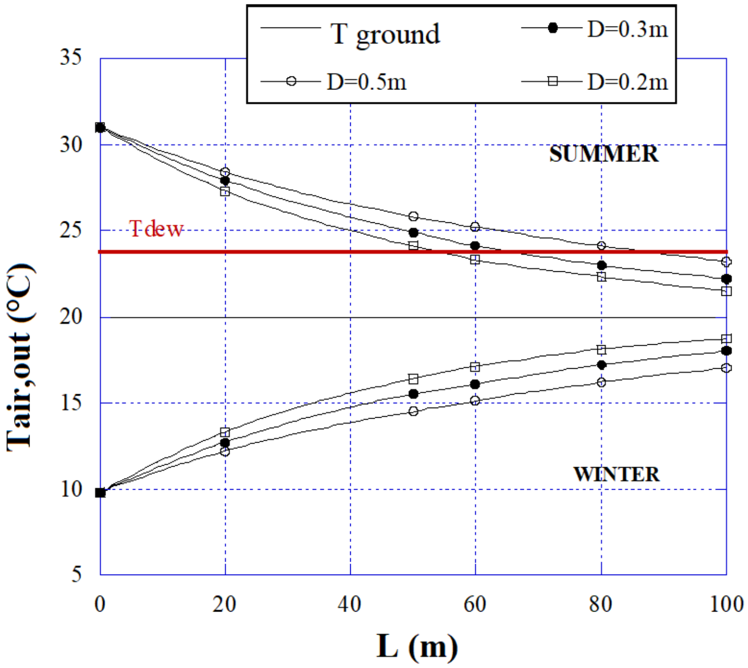

(a)

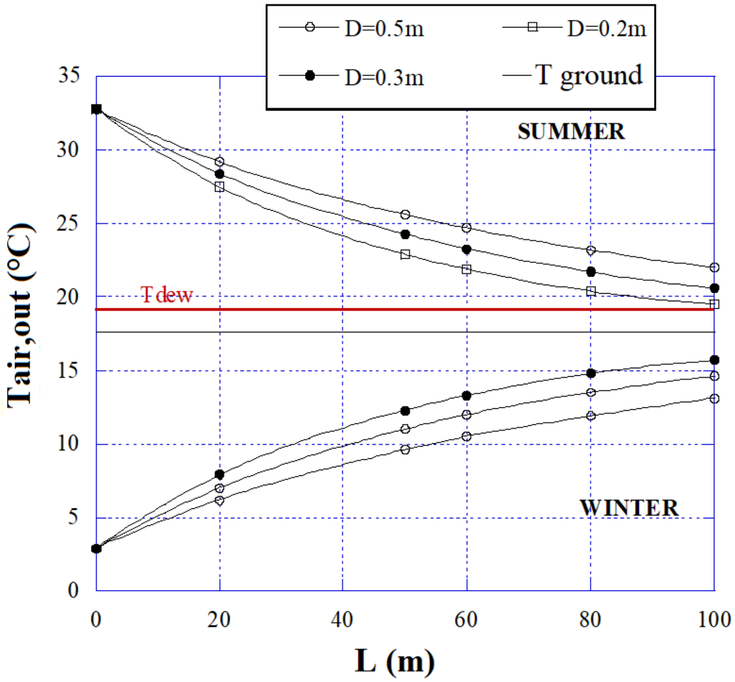
D=0.5m
D=0.2m
D=0.3m
T ground
SUMMER
WINTER
Tdew
Tair,out (°C)
L (m)
35
30
25
20
15
10
5
0
0
20
40
60
80
100

(b)

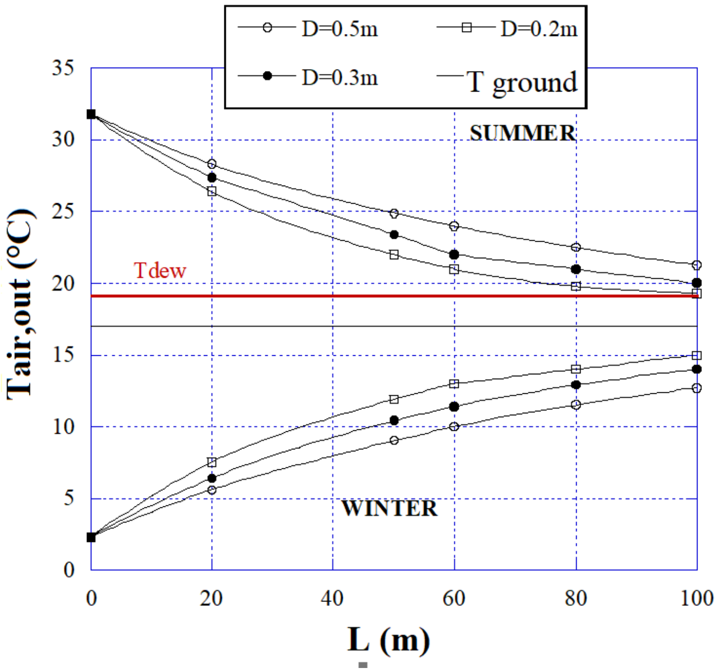
D=0.5m
D=0.2m
D=0.3m
T ground
SUMMER
WINTER
Tdew
Tair,out (°C)
L (m)
35
30
25
20
15
10
5
0
0
20
40
60
80
100

(c)

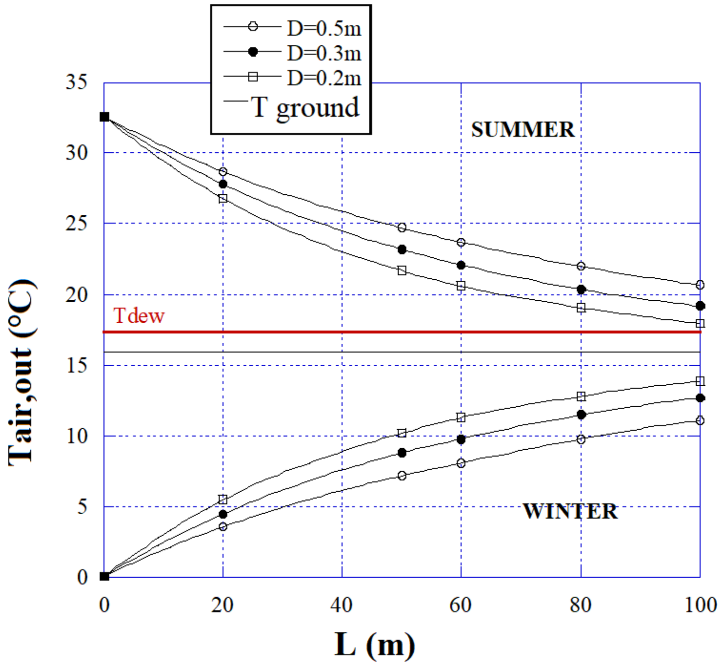
D=0.5m
D=0.3m
D=0.2m
T ground
SUMMER
WINTER
Tdew
Tair,out (°C)
L (m)
35
30
25
20
15
10
5
0
0
20
40
60
80
100

(d)

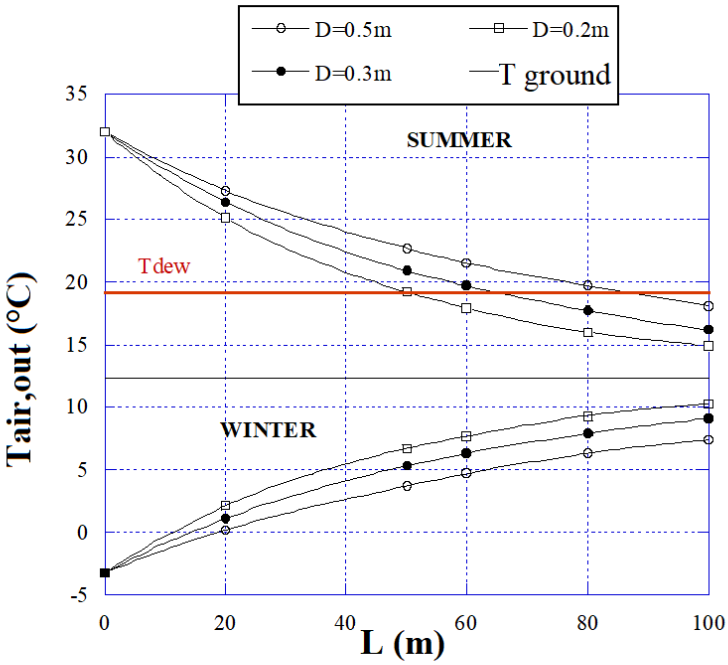
D=0.5m
D=0.2m
D=0.3m
T ground
SUMMER
WINTER
Tdew
Tair,out (°C)
L (m)
35
30
25
20
15
10
5
0
-5
0
20
40
60
80
100

(e)

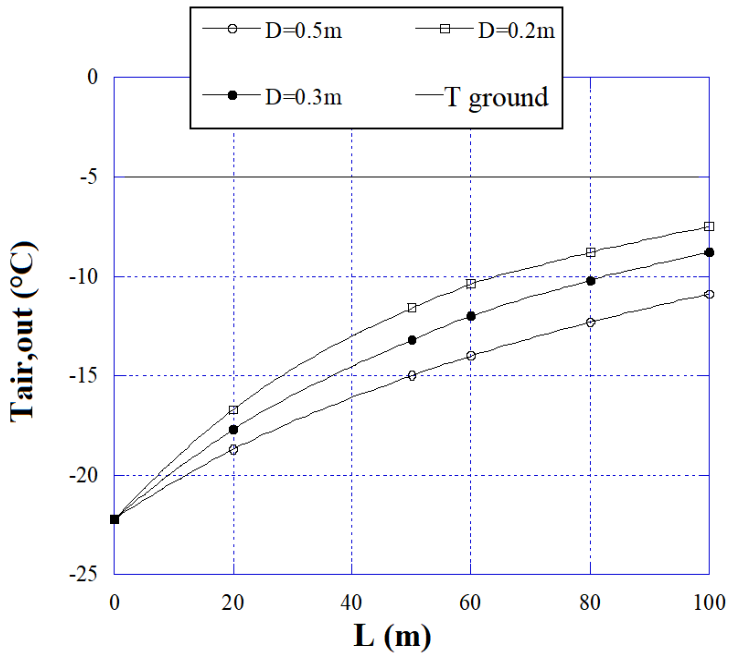

(f)

Figure 31. Air temperature along the tube length at different inner tube diameters for: (a) Lampedusa; (b) Catania; (c) Naples; (d) Rome; (e) Milan; (f) Pian Rosa.

Moreover, note that the air speed rises with the reduction of the duct diameter, and this implies the rising of the heat transfer coefficient for convection and, finally, the improvement of the heat exchange. Therefore, with the lowest value of the inner tube diameter (D = 0.2 m corresponding to an inlet air velocity of 2.3 m s^{-1}) a greater temperature variation can be obtained in the EAHX.

Figure 32 shows the air temperature span in summer between the inlet and the exit of the EAHX, for a duct diameter of 0.2 m, when varying the length of the air duct, considering the six analysed localities.

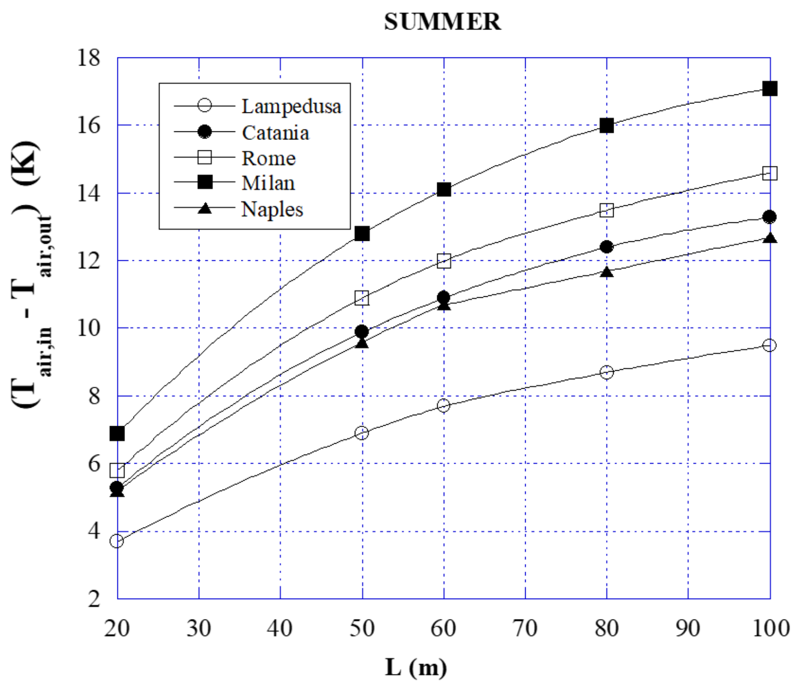

Figure 32. Air temperature variation in the EAHX as a function of the tube length for an inner tube diameter of 0.2 m in summer.

The Figure 32 clearly shows that temperature variation is more marked for Milan, a city characterized by cold winter and hot summer (with a maximum value greater than 17 K). The lowest values are those pertaining to Lampedusa, a locality characterized by very mild climate (maximum value lower than 10 K).

Figure 33 shows the variation between the outlet and the inlet temperature of the EAHX for the six localities in winter season.

It could be noted that the greatest temperature variation can be obtained for Pian Rosa, a locality characterized by very cold winters (maximum value of 14.7 K), whereas the lowest is for Lampedusa (maximum value of 8.9 K).

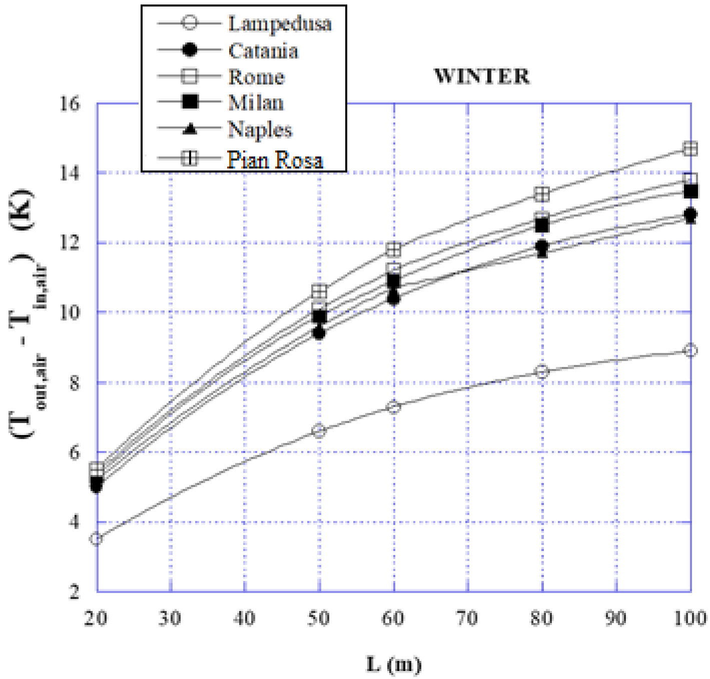

Figure 33. Air temperature variation in the EAHX as a function of the tube length for an inner tube diameter of 0.2 m in winter.

From the data plotted in Figure 32 and Figure 33 the following considerations can be drawn:

- the temperature variation that can be obtained with an EAHX at fixed tube length is always greater in the summer than in the winter season. This is due to the greater temperature difference between the external air and the soil during the summer for each of the tested localities;
- the temperature of the undisturbed ground is almost constant and very similar to the yearly average value for the outside air. So, the lowest temperature of the ground is for zone F, while the highest occurs for the zone A. The temperature difference between the ground and the outside air represents the principal driving force in the heat exchange process. Where the difference between the air temperature at the inlet of the heat exchanger (corresponding at L=0 in Figure 31) and the undisturbed soil is more marked, the more efficient is the heat transfer process. The greatest values of driving force can be obtained

in the localities with greater temperature excursions between summer and winter (Pian Rosa, Milan).

- Lampedusa shows the lowest temperature span because it has very mild winters with moderate rainfall and hot, dry summers. So, the temperature span along the EAHX is minor than 10 °C, although a relevant length of 100 m is considered for the air duct (ΔT belongs to 3.7÷9.5 K in summer and to 3.5÷8.9 K in winter).

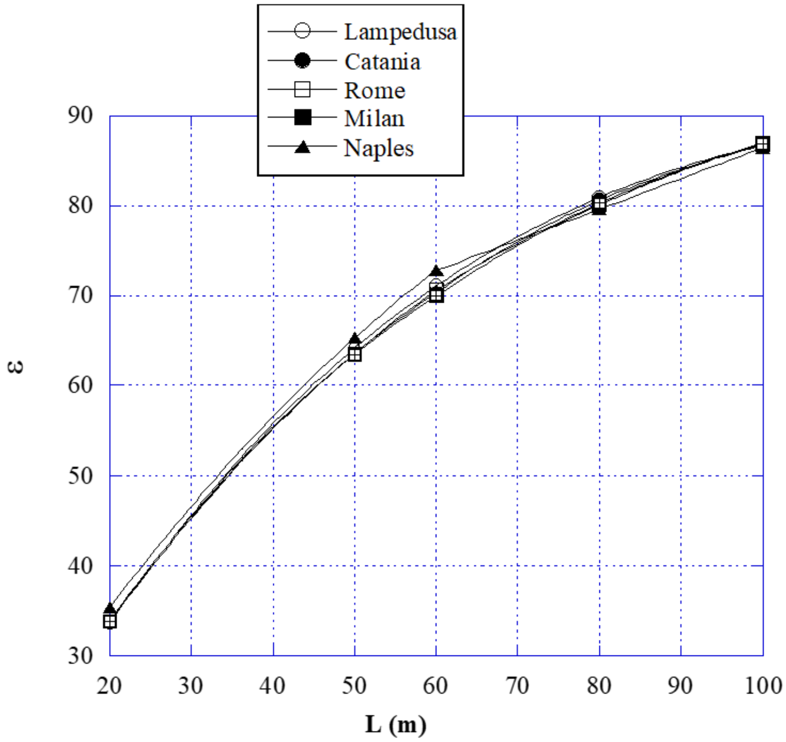

Figure 34. EAHX efficiency as a function of tube length for an inner tube diameter of 0.2 m.

Figure 34 shows the efficiency of the EAHX as a function of the tube length for the six localities for an inner tube diameter of 0.2 m. From the results obtained, the efficiency in winter and summer is almost the same, this is the reason why there is only one graph that can be used for both seasons. The graph also shows that at fixed tube length the efficiency is independent on the climatic zone where the EAHX is installed. Indeed, the effectiveness of the

heat exchange mainly depends on the convective heat transfer coefficient that at fixed inner tube diameter is almost constant for the different localities (because constant is the air flow velocity too).
Furthermore, the Figure 34 clearly shows that the increase of the efficiency is very pronounced up to about 80 m: for longer lengths, the increase becomes moderate. An optimal efficiency value of about 86% is ensured with a length duct of 100 m. This result is also relevant in the possible comparison between the analysed EAHX and an air-to-air heat recovery unit. In fact, the latter is characterized by a mean efficiency of about 65%- 80% [85], [92], [93] . Moreover, air-to-air heat exchangers are usually more dangerous due to the risk of spreading SARS-CoV-2 or other viruses.
The efficiency is a strong function of the inner tube diameter (and of the consequent fluid velocity). As an example, in Figure 35 is reported the efficiency for the different tube diameter for the city of Milan during summer. Similar results can be obtained in winter and for the other examined Italian localities.
We can observe the rising of the EAHX efficiency when the inner diameter of the air duct reduces (with a constant value of the duct length). In fact, when the duct diameter is reduced the air speed rises improving the heat transfer coefficient for convection (the air speed rises from 0.37 to 2.3 m s^{-1} when the duct diameter rises from 0.5 m to 0.2 m).
The EAHX also implies a relevant decreasing of the heating and cooling capacity of the coils inside the air handling unit.

Figure 36 reports the heating and cooling capacity of the operating coils during winter (i.e., preheating coil and reheating coil) (a), during summer (i.e., cooling coil and reheating coil) (b), all over the year (c), as a function of the tube length for an inner tube diameter of 0.5 m for the different localities.

Figure 36 also shows the heating and cooling capacity values for the system without the EAHX. Finally, the figure also reports the decreasing (in percentage) of these capacity values when the EAHX is considered, for various lengths of the air ducts.

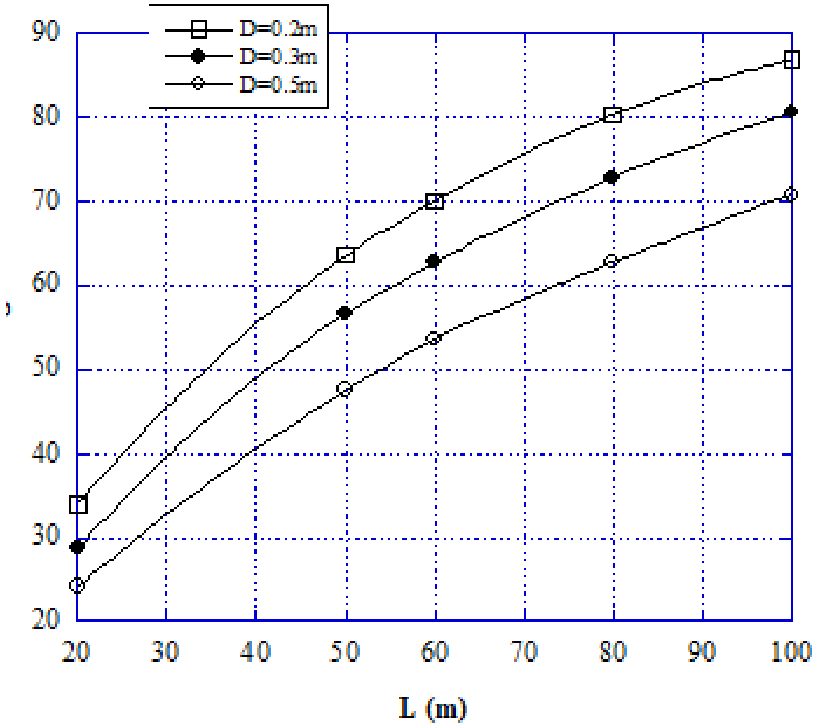

Figure 35. EAHX efficiency as a function of tube length varying the inner tube diameter in summer for Milan.

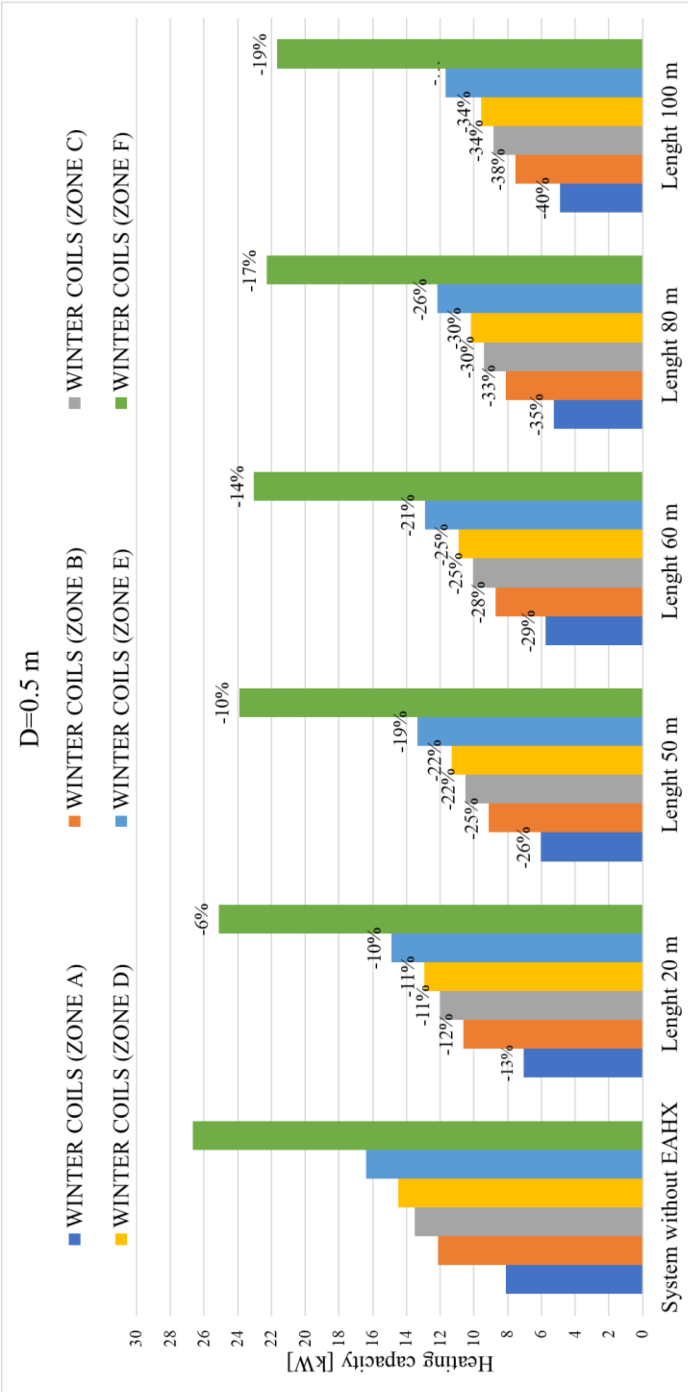
D=0.5 m
WINTER COILS (ZONE A)
WINTER COILS (ZONE B)
WINTER COILS (ZONE C)
WINTER COILS (ZONE D)
WINTER COILS (ZONE E)
WINTER COILS (ZONE F)
Heating capacity [kW]
System without EAHX
Lenght 20 m
Lenght 50 m
Lenght 60 m
Lenght 80 m
Lenght 100 m

(a)

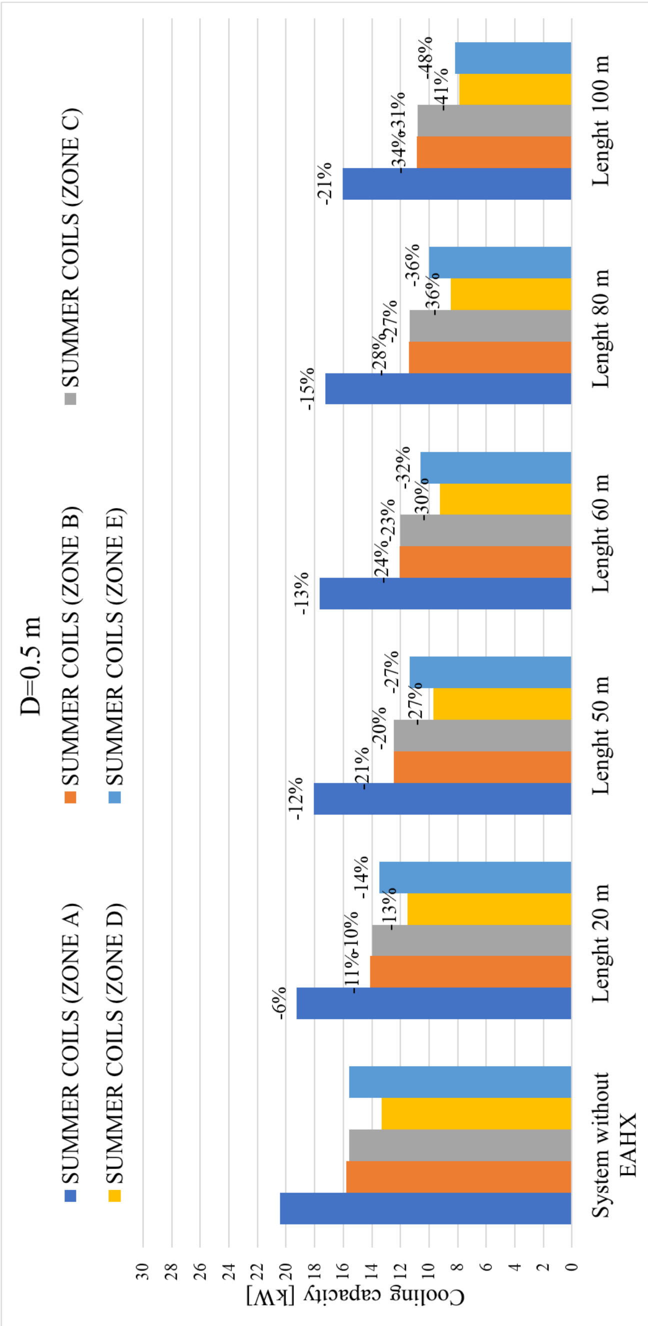
D=0.5 m
SUMMER COILS (ZONE A)
SUMMER COILS (ZONE B)
SUMMER COILS (ZONE C)
SUMMER COILS (ZONE D)
SUMMER COILS (ZONE E)
Cooling capacity [kW]
0
2
4
6
8
10
12
14
16
18
20
22
24
26
28
30
System without EAHX
Lenght 20 m
-6%
-11%
-10%
-13%
-14%
Lenght 50 m
-12%
-21%
-20%
-27%
-27%
Lenght 60 m
-13%
-24%
-23%
-30%
-32%
Lenght 80 m
-15%
-28%
-27%
-36%
-36%
Lenght 100 m
-21%
-34%
-31%
-41%
-48%
(b)

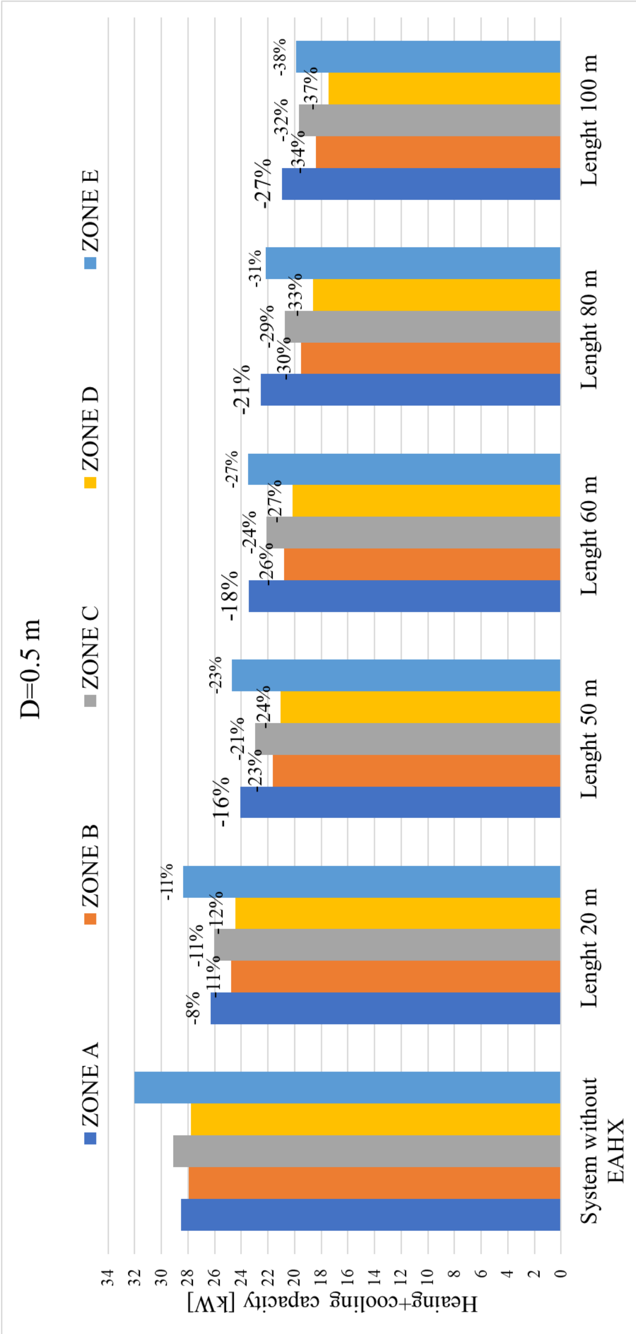

(c)

Figure 36. Capacity of the operating coils as a function of tube length for an inner tube diameter of 0.5 m: (a) during winter, (b) during summer, (c) all over the year.

From the Figure 36 the following considerations can be drawn:

- increasing the tube length carries to an augmentation of the capacity reduction, too. Therefore, the best results can be obtained with the duct 100 m long; during the winter (Figure 36 (a)) the capacity reduction using the EAHX to pre-heat the air flow is more marked in zone A (maximum value of 40%) than in zone F (maximum value of 19%). Indeed, in Lampedusa, the southernmost point of Italy with a very mild winter and hot, dry summer, the capacity reduction is greater than in Pian Rosa (with a short and cool summer and a long, freezing, and snowy winter);

- an opposite trend is observed during the summer (Figure 36 (b)) the capacity reduction using the EAHX to pre-cool air flow is more marked in zone E (maximum value of 48%) than in zone A (maximum value of 21%);

- with reference to winter and summer (Figure 36 (c)) the highest total decrease in capacity of the coils occurs for zone E (Milan – decrease of 38% for a duct length of 100 m), while the lowest value occurs for zone A (Lampedusa - maximum decrease of capacity equal to 27%). So, in Italy the yearly utilization of the EAHX linked to an air handling unit is useful in all the national territory, even if preferable in zone E (i.e. in the climatic areas showing a high temperature excursion between winter and summer) compared to zone A.

Similar trends are observed for the other inner tube diameters that are reported in the following figures.
In Figure 37 shows the winter (a), summer (b), global (c) coil capacities as a function of the tube length for an inner tube diameter of 0.3 m.

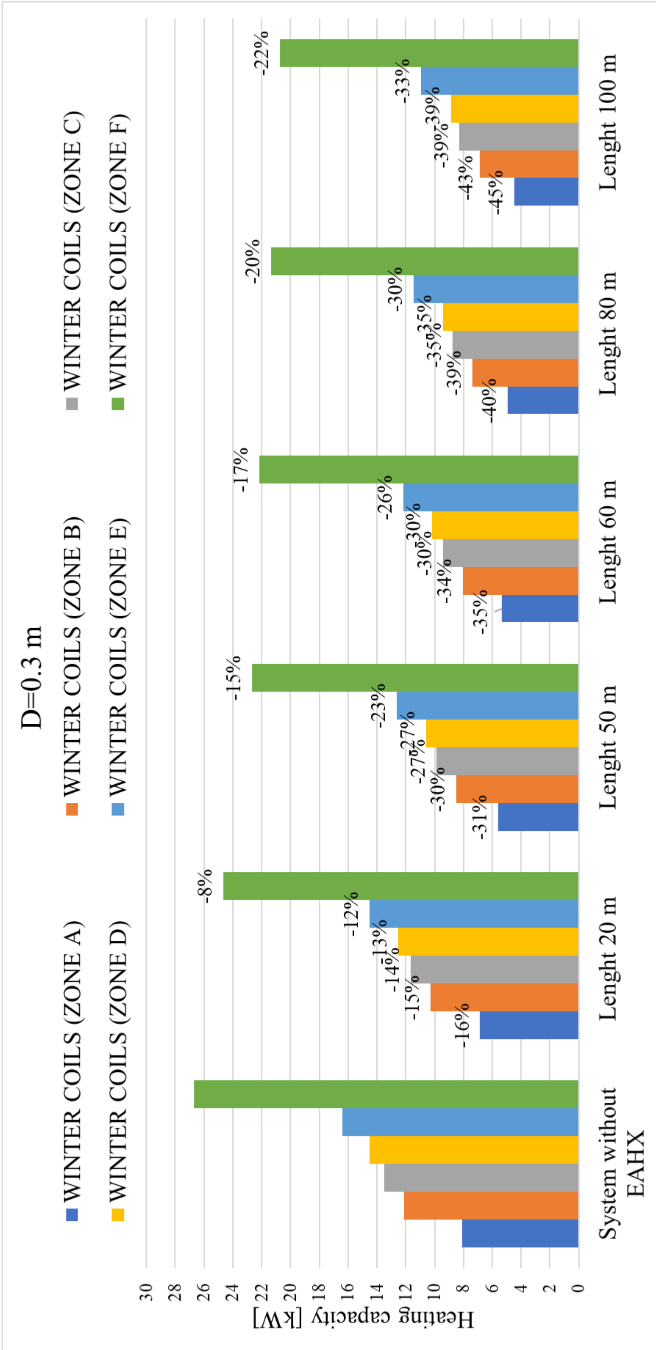
D=0.3 m
WINTER COILS (ZONE A)
WINTER COILS (ZONE B)
WINTER COILS (ZONE C)
WINTER COILS (ZONE D)
WINTER COILS (ZONE E)
WINTER COILS (ZONE F)
Heating capacity [kW]
30
28
26
24
22
20
18
16
14
12
10
8
6
4
2
0
System without EAHX
Lenght 20 m
Lenght 50 m
Lenght 60 m
Lenght 80 m
Lenght 100 m
-16%
-15%
-14%
-13%
-12%
-8%
-31%
-30%
-27%
-27%
-23%
-15%
-35%
-34%
-30%
-30%
-26%
-17%
-40%
-39%
-35%
-35%
-30%
-20%
-45%
-43%
-39%
-39%
-33%
-22%

(a)

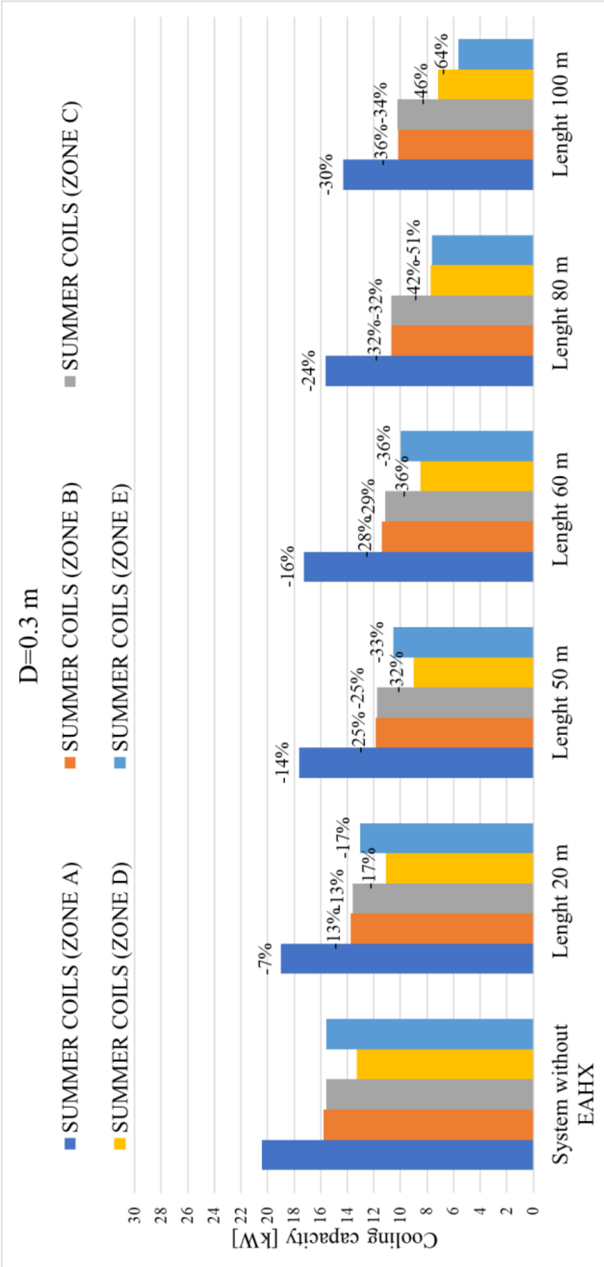
D=0.3 m
SUMMER COILS (ZONE A)
SUMMER COILS (ZONE B)
SUMMER COILS (ZONE C)
SUMMER COILS (ZONE D)
SUMMER COILS (ZONE E)
Cooling capacity [kW]
System without EAHX
Lenght 20 m
Lenght 50 m
Lenght 60 m
Lenght 80 m
Lenght 100 m
-7%
-13%
-13%
-17%
-17%
-14%
-25%
-25%
-32%
-33%
-16%
-28%
-29%
-36%
-36%
-24%
-32%
-32%
-42%
-51%
-30%
-36%
-34%
-46%
-64%

(b)

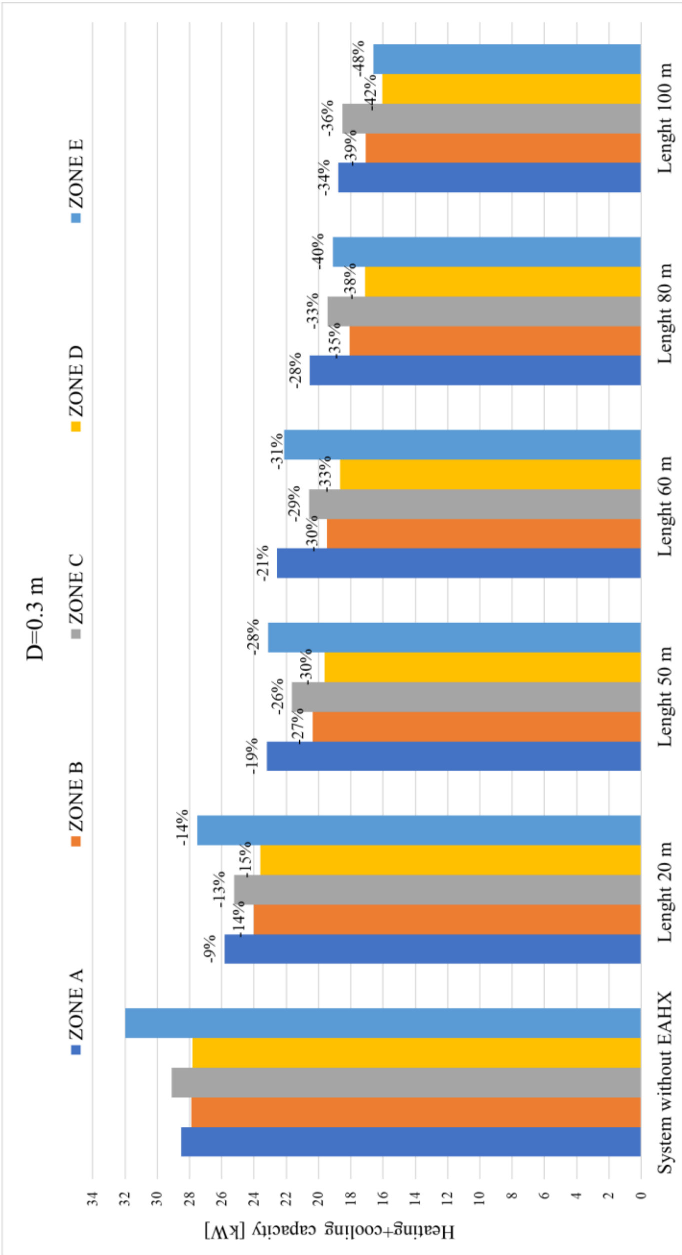

(c)

Figure 37. Capacity of the operating coils as a function of tube length for an inner tube diameter of 0.3 m: (a) during winter, (b) during summer, (c) all over the year.

In Figure 38 are shown the winter (a), summer (b), global (c) coil capacities as a function of the tube length for an inner tube diameter of 0.2 m for the different localities.

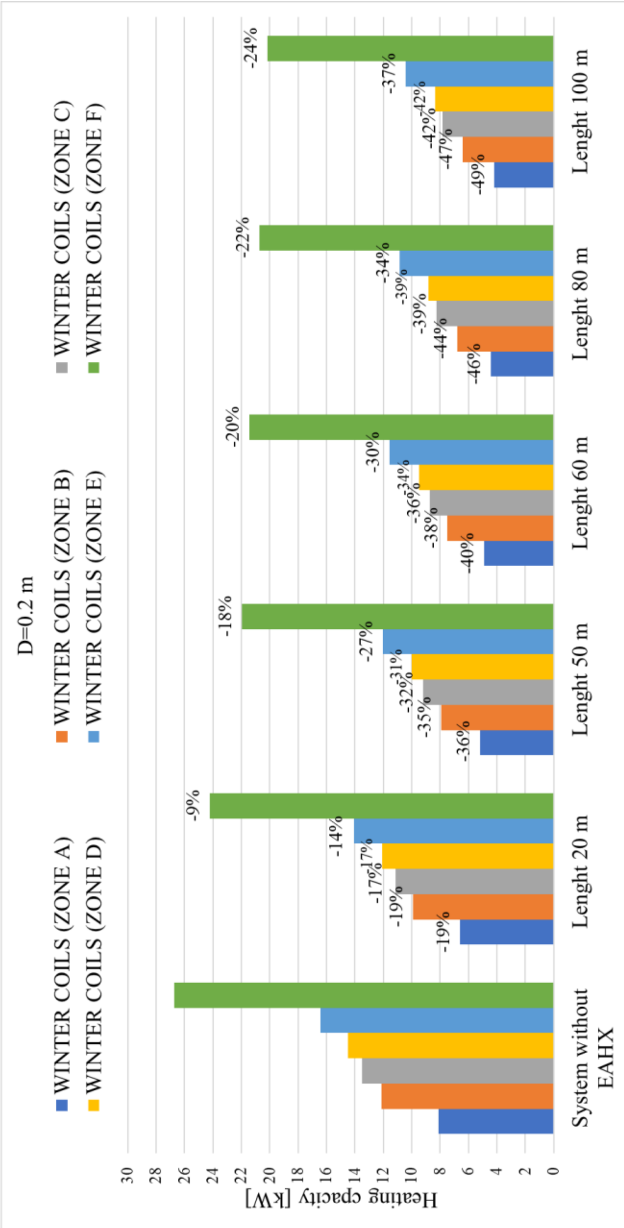

(a)

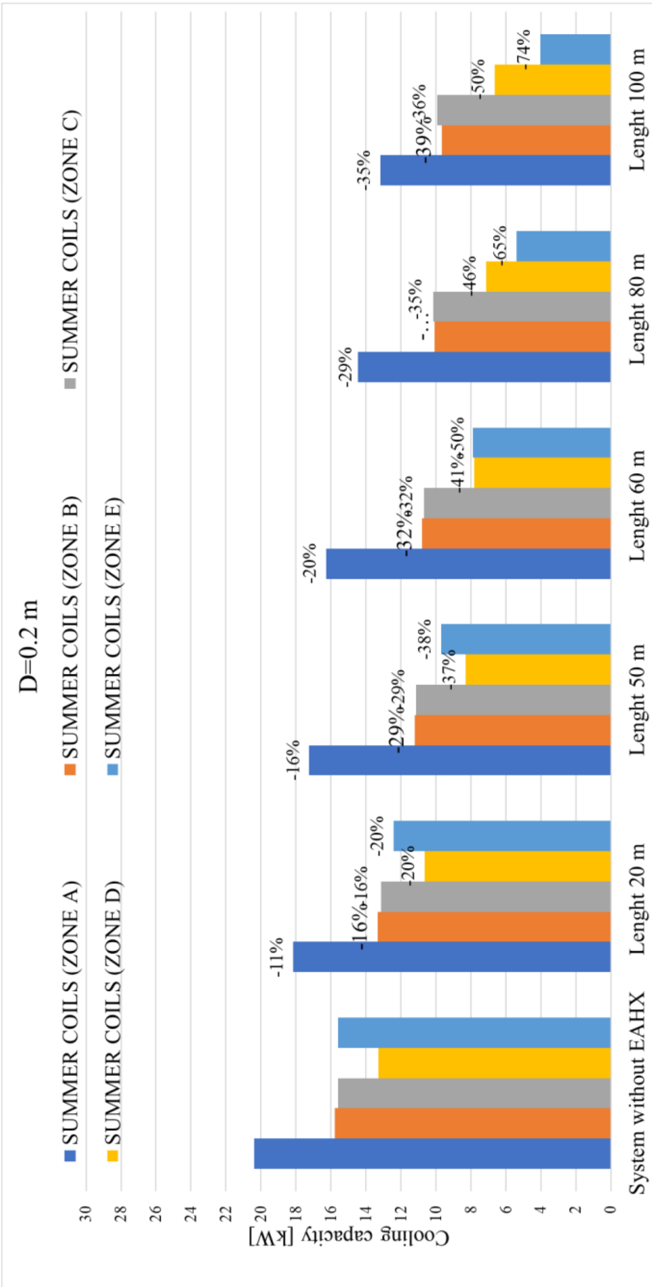
D=0.2 m
SUMMER COILS (ZONE A)
SUMMER COILS (ZONE B)
SUMMER COILS (ZONE C)
SUMMER COILS (ZONE D)
SUMMER COILS (ZONE E)
Cooling capacity [kW]
0
2
4
6
8
10
12
14
16
18
20
22
24
26
28
30
System without EAHX
Lenght 20 m
Lenght 50 m
Lenght 60 m
Lenght 80 m
Lenght 100 m
-11%
-16%
-20%
-20%
-16%
-29%
-37%
-38%
-20%
-41%
-50%
-29%
-35%
-46%
-65%
-35%
-50%
-74%
(b)

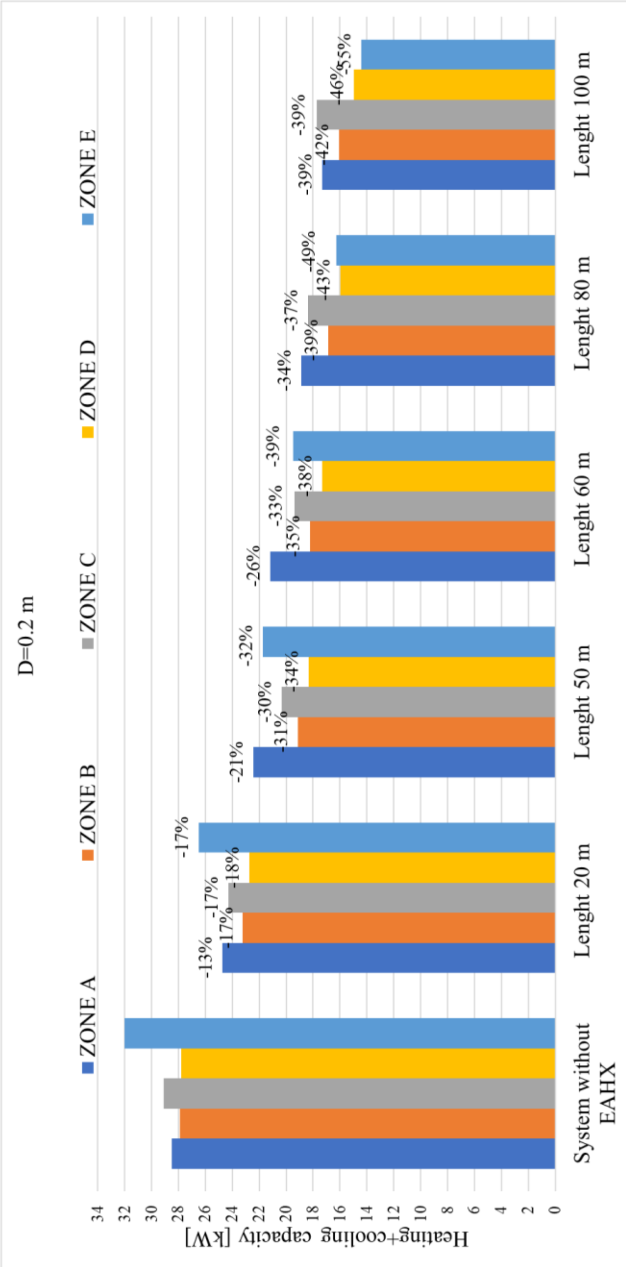

(c)

Figure 38. Coils capacity of the operating coils as a function of tube length for an inner tube diameter of 0.2 m: (a) during winter, (b) during summer, (c) all over the year.

From a comparison among Figure 36,Figure 37 and Figure 38 the emerging data is the greatest coils capacity reduction that can be achieved considering the smallest diameter of 0.2 m (maximum global power reduction of 55% in Milano).

3.3.2 Comparison among the different Köppen climatic areas

The previous analysis has shown that the best results can be obtained with the smaller inner tube diameter considered (0.2 m). Therefore, in this analysis the tube diameter is fixed at 0.2 m.
In Figure 39 reports the temperature variation in EAHX as a function of the tube length in summer (a) and in winter (b) season.
According to the Köppen classification, the analysed Italian localities belong to the zone C (mild temperature climates) except Lampedusa that belongs to the zone B (dry climates).
The figures clearly show that:

- the temperature span between the inlet and the exit of the EAHX, in the Italian localities, is lower in winter than in summer, while an opposite result is obtained for Ottawa, Dubai and Rio de Janeiro. This depends on the temperature span between the soil and the outside air. This difference in Italy is not so dissimilar between summer and winter and slightly greater in summer. Instead, the contrary is found for Dubai, Rio de Janeiro and Ottawa (in this last case there is a strong variation between summer (14.5 K) and winter (27.4 K);

- in summer conditions, the maximum EAHX temperature difference between the inlet and the exit is obtained for Milan (higher than 17 °C), while the minimum temperature difference is obtained for Rio de Janeiro (maximum value lower than 7 °C);

- during winter Ottawa shows the greatest temperature variation in the EAHX (maximum value of 27.4 °C), on the contrary Rio shows the lowest (maximum value 6.8 °C);

- the temperature of the undisturbed ground is almost constant and very similar to the yearly average temperature of the outside air, in all the considered climatic areas. The temperature difference between ground and outside air is the principal driving force in the heat transfer process related to the EAHX: its highest values occur in the climatic areas with higher temperature excursion between winter and summer. So, the most relevant results occur for zones C and D (mild temperate climatic areas and continental climatic areas, respectively), while the less relevant results occur for equatorial or tropical climatic areas (zone A).

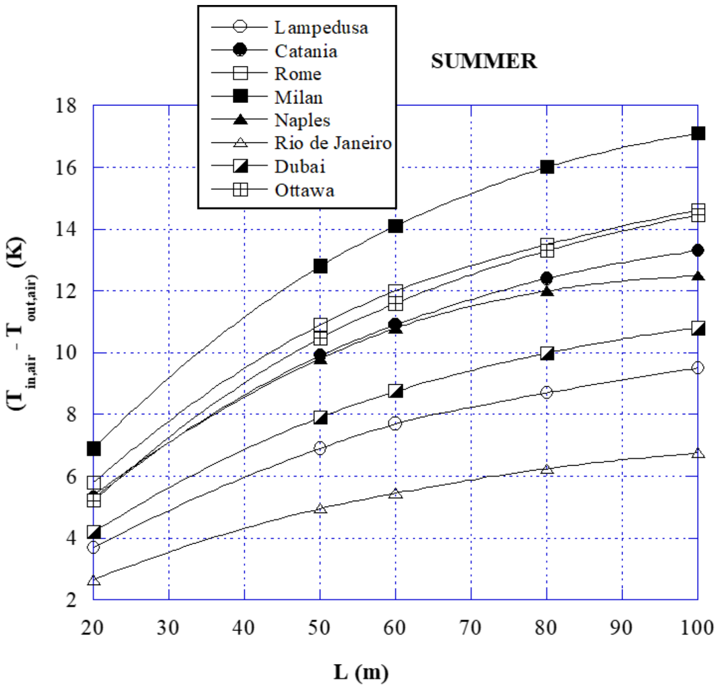

(a)

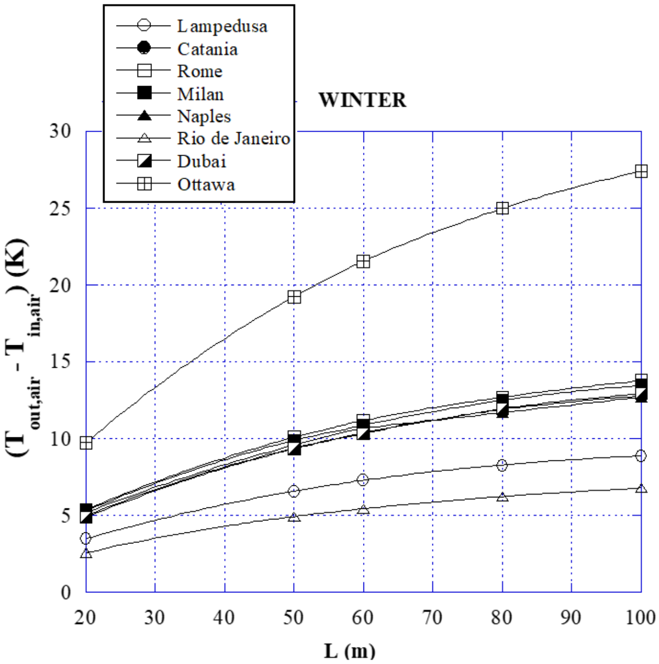

(b)

Figure 39. Air temperature variation in the EAHX as a function of the tube length for an inner tube diameter of 0.2 m in: (a) summer; (b) winter.

Figure 40 shows the EAHX efficiency in summer, when varying the air duct length, for the eight analysed towns. Indeed, in winter the results are almost the same. It can be shown that the efficiency depends slightly on the climatic and soil characteristics of the area in which the exchanger is installed. For all the climatic areas the efficiency exceeds 80% at 100 m tube length.

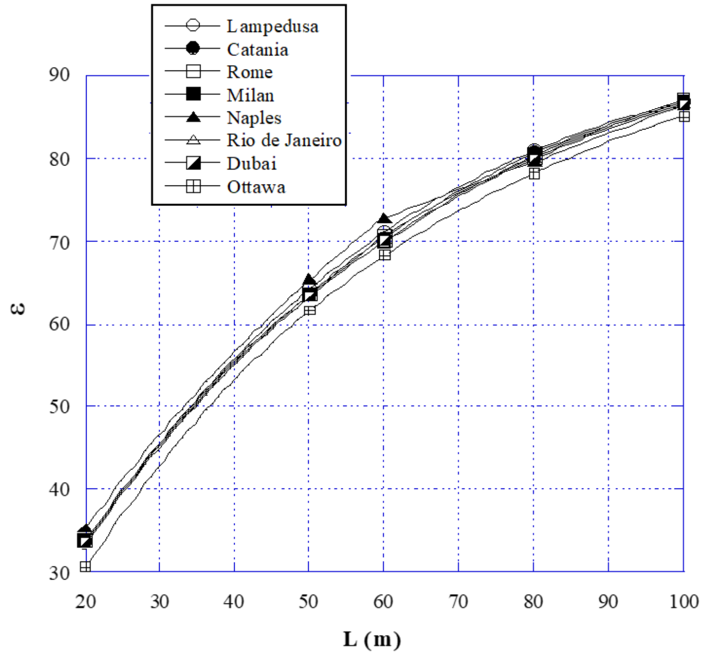

Figure 40. Efficiency of the EAHX as a function of the tube length for summer season.

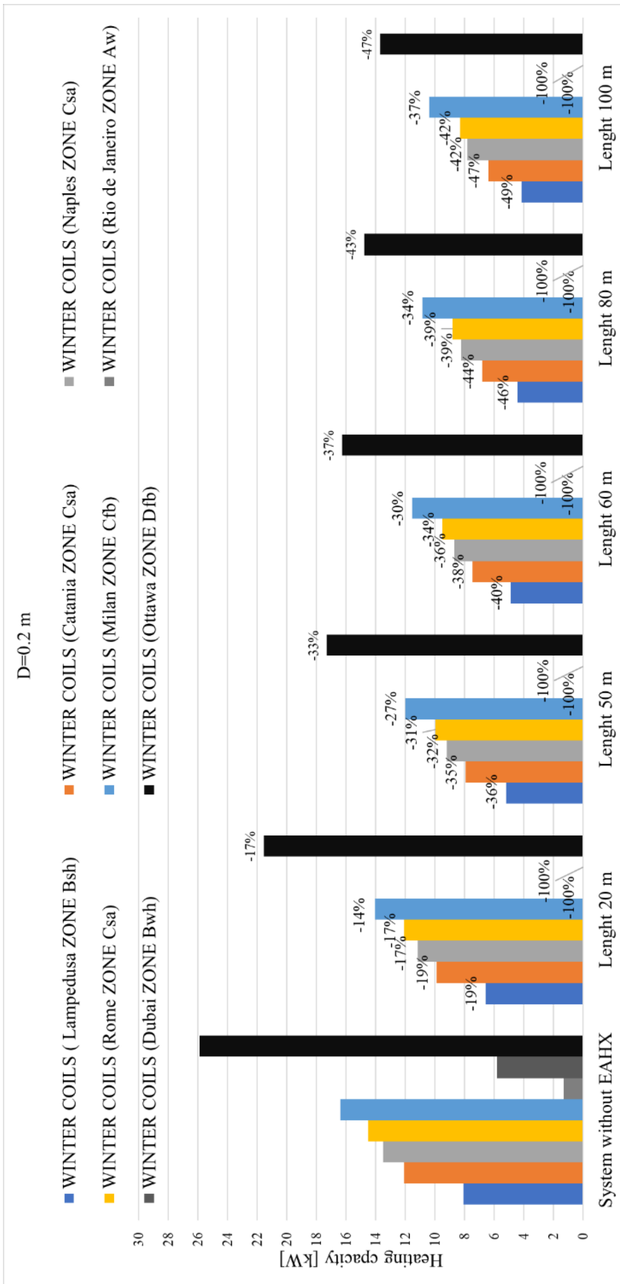
D=0.2 m
WINTER COILS (Lampedusa ZONE Bsh)
WINTER COILS (Catania ZONE Csa)
WINTER COILS (Naples ZONE Csa)
WINTER COILS (Rome ZONE Csa)
WINTER COILS (Milan ZONE Cfb)
WINTER COILS (Rio de Janeiro ZONE Aw)
WINTER COILS (Dubai ZONE Bwh)
WINTER COILS (Ottawa ZONE Dfb)
Heating cpacity [kW]
0
2
4
6
8
10
12
14
16
18
20
22
24
26
28
30
System without EAHX
Lenght 20 m
Lenght 50 m
Lenght 60 m
Lenght 80 m
Lenght 100 m

(a)

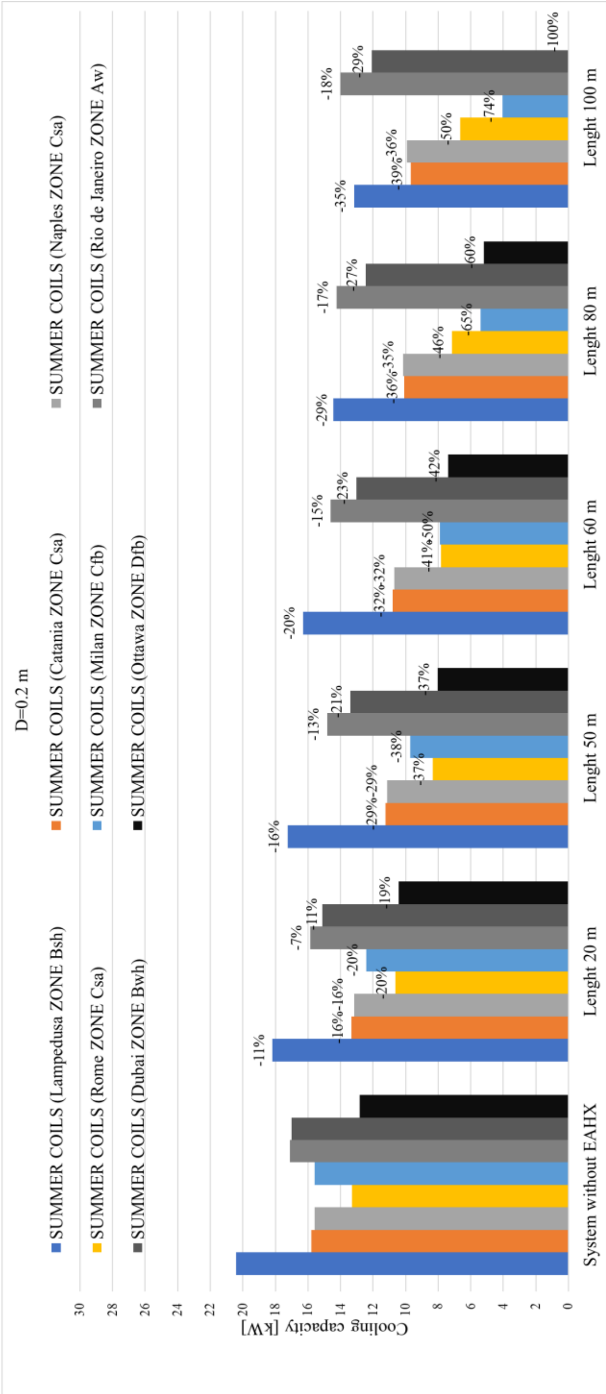
D=0.2 m
SUMMER COILS (Lampedusa ZONE Bsh)
SUMMER COILS (Catania ZONE Csa)
SUMMER COILS (Naples ZONE Csa)
SUMMER COILS (Rome ZONE Csa)
SUMMER COILS (Milan ZONE Cfb)
SUMMER COILS (Rio de Janeiro ZONE Aw)
SUMMER COILS (Dubai ZONE Bwh)
SUMMER COILS (Ottawa ZONE Dfb)
Cooling capacity [kW]
0
2
4
6
8
10
12
14
16
18
20
22
24
26
28
30
System without EAHX
Lenght 20 m
Lenght 50 m
Lenght 60 m
Lenght 80 m
Lenght 100 m
-11%
-16%
-16%
-20%
-20%
-7%
-11%
-19%
-16%
-29%
-29%
-37%
-38%
-13%
-21%
-37%
-20%
-32%
-32%
-41%
-50%
-15%
-23%
-42%
-29%
-36%
-35%
-46%
-65%
-17%
-27%
-60%
-35%
-39%
-36%
-50%
-74%
-18%
-29%
-100%
(b)

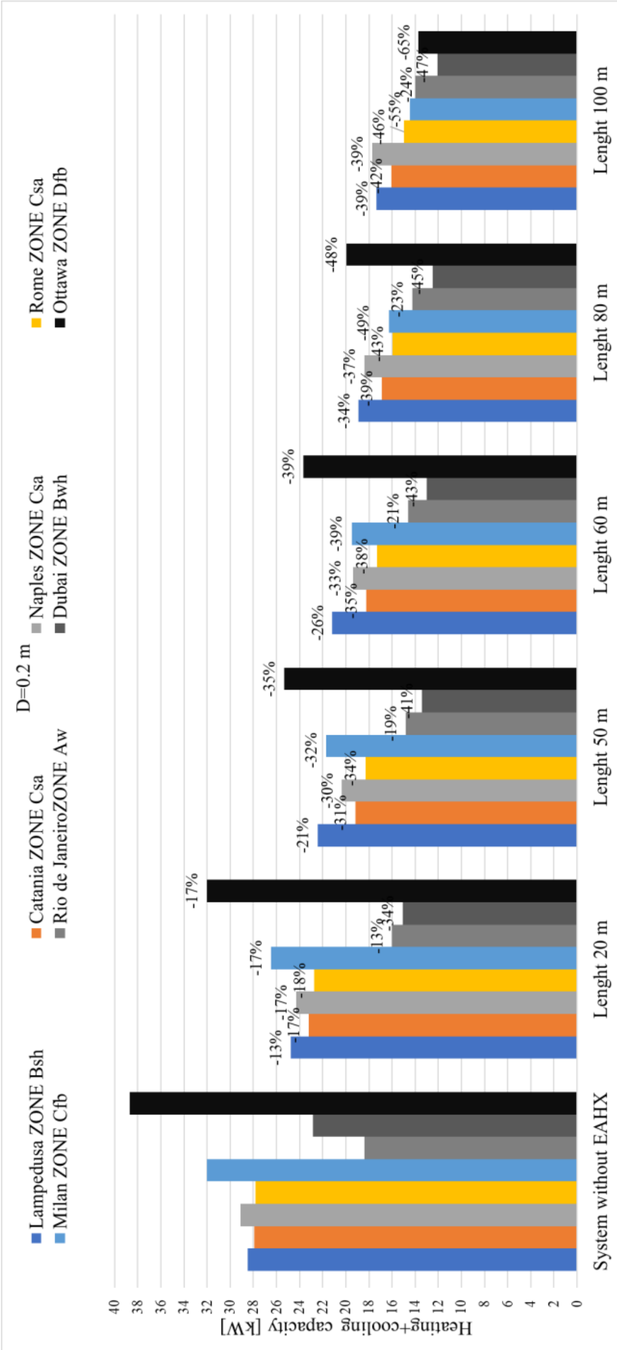

(c)

Figure 41.Coils capacity of the operating coils as a function of tube length for an inner tube diameter of 0.2 m: (a) during winter, (b) during summer, (c) all over the year.

Figure 41 reports the heating and cooling capacity of the operating coils during winter (a), summer (b), and all over the year (c), varying the tube length for an inner tube diameter of 0.2 m for the different localities. At the top of each histogram bar, the percentage reduction of coils capacity with the use of EAHX at each tube length is also reported.

From Figure 41 (a) the following considerations can be drawn about the percentage capacity reduction calculated for the winter season:

- in Dubai and Rio de Janeiro, the temperature of the air at the exit of the air duct is higher than 20 °C, even when the duct length is only 20 m. Moreover, the couple dry bulb temperature - specific humidity of the air at the exit of the air duct is very similar to those required for comfort conditions in winter. So, the air exiting the EAHX can be supplied to the building without any HVAC system (only a suitable filtration of the air is obviously required). Therefore, in these cases the decreasing of the heating capacity of the coils rises 100 % for the air handling unit working in heating operating conditions;

- the heating capacity reduction using the EAHX to pre-heat the air flow is more marked in A and B zones (maximum value of 100%) than in C or D zones (maximum value of 47%).

From Figure 41 (b) referred to summer, one can notice that:

- in Ottawa, with a tube length of 100 m the air flow reaches temperature and relative humidity values such that the air can be directly conveyed in the building without using the air conditioning plant. Therefore, the percentage cooling capacity reduction in cooling mode is 100%;

- the capacity reduction using the EAHX to pre-cooling the air is more marked in D and C zones (maximum value 100% for Ottawa) than for A and B zones (maximum value of 18% for Rio de Janeiro).

Figure 41 (c) highlights that the highest decreasing of cooling plus heating capacity for the coils occurs for Dubai while low values of the length of the air duct are considered (up to 60 m), whereas for higher lengths of the air ducts the best results occur for Ottawa. Therefore, one can conclude that the best results can be obtained for tube length of 100 m in the city of Ottawa (reduction of 65% of heating + cooling capacity using the EAHX) that belongs to the Dfb zone according to the Köppen classification. This city is characterized by the greatest temperature span between winter and summer season, with a very cold winter (with frequent snowfalls) and a hot-humid summer.

It is also important to highlight that the air temperature in the duct decreases below the dew point temperature (17.6 °C) in Ottawa, for duct lengths higher than 50 m; it means that the air has been dehumidified. The related mass flowrate values of the condensed water vapor ($\dot{m}_{co}$) at the EAHX exit are [0.06; 0.63; 0.99] g s^{-1} at [60;80;100] m length.

3.4 CONCLUSIONS

In this chapter the thermal and energy performance of an earth-to-air heat exchanger are investigated.

A two-dimensional unsteady numerical model of a horizontal EAHX has been developed. Five horizontal circular ducts have been considered, displaced in parallel at 2.5 m depth. Two adjacent ducts are 2.5 m spaced apart. The 2D model represents one of the five circular horizontal buried ducts of the EAHX surrounded by a ground volume 20 m deep; the problem is solved through finite element method. The model has been validated with experimental results found in literature: the maximum relative deviation between the experimental and the numerical data is 3.5 %, the absolute deviation is always lower than 1°C.

The EAHX is considered as a component of an air conditioning system for an office building. The air pre-heated or pre-cooled in the EAHX is not directly supplied to the building, but it is successively treated into the air handling unit. Since the thermal performance of the EAHX depends on the climatic conditions of the place where it is installed, the office building was firstly virtually placed in six different localities of Italy (Lampedusa, Catania, Naples, Rome, Milan, Pian Rosa), which belong to different climatic zones according to

the Italian law D.P.R. 412/93, based on heating degree-days. For a further comparison, the building was subsequently virtually placed in eight cities of the world according to Köppen climate classification (Dubai, Rio de Janeiro, Ottawa, plus five of the abovementioned Italian localities).
The EAHX is simulated and optimized as a function of the diameter and length of the air ducts. The following parameters are calculated: the variation of air temperature in the EAHX; the EAHX thermal efficiency; the decreasing of cooling and heating capacity of the coils into the AHU when comparing with the solution without EAHX. The analysis on the coils of the AHU is performed for winter, summer and for all the year. The following main conclusions are obtained.

- At the EAHX outlet, a temperature of the air close to the undisturbed ground temperature (Knee point) is obtained for tube length of about 80 m for all the localities. Therefore, a duct length of 80 m represents an acceptable compromise considering thermal performances, pressure drops and EAHX costs.

- Decreasing the tube diameter, the air velocity increases enhancing the convection heat transfer coefficient and, as a result, the heat exchange becomes more efficient. Therefore, with the lowest value of the inner tube diameter (0.2 m) a greater air temperature variation can be obtained in the EAHX.

- For all the analysed climatic zones, the undisturbed soil temperature is about constant and close to the yearly mean values of the external air. Temperature gradient between ambient air and soil is the main driving force for the heat transfer in the EAHX. The greatest values of driving force can be obtained in the locality with the greatest temperature excursions between summer and winter. Therefore, the worst results in terms of temperature variation in the EAHX can be obtained in zone A (according to Köppen climate classification, it refers to tropical or equatorial climates) and the best ones in zones D (continental climates) and C (mild temperate climates).

- Among the Italian localities, Lampedusa shows the lowest temperature span between the inlet and outlet of the EAHX, always smaller than 10 K even with a tube length of 100 m (ΔT belongs to

3.7÷9.5 K in summer and to 3.5÷8.9 K in winter). Milan (with a maximum value greater than 17 K) and Pian Rosa in winter (whose maximum temperature span is 14.7 K) show the highest temperature spans.

- According to the climate classification of Köppen, during summer the best results can be obtained in Milan (maximum value greater than 17 K), whereas the worst results are registered in Rio de Janeiro (maximum value lower than 7 K). During winter Ottawa shows the greatest temperature variation in the EAHX (maximum value of 27.4 K), on the contrary Rio de Janeiro shows the lowest (maximum value of 6.8 K).

- The efficiency of the EAHX is almost independent on the climatic zone where the EAHX is installed and its increase is pronounced up to about 80 m: for longer lengths, the increase becomes moderate. Indeed, 100 m as the length of each duct ensures the achievement of an optimal efficiency value, around 86%.

- Considering the reduction of heating and cooling capacity of the coils inside the AHU (deriving from the placement of EAHX upstream of the AHU) for the whole year, the best case is for Milan (zone E) with a heating + cooling capacity reduction of 55% for a tube length of 100 m, whereas the worst case is for Lampedusa (zone A) with a maximum value of reduction equal to 39%. Therefore, when the yearly operation period of the AHU coupled to an EAHX is considered, in Italy the use of an EAHX is recommended in all the climatic zones, but more in an E than in an A zone. The best results can be obtained in the localities with a great temperature excursion between summer and winter.

- Considering the reduction of heating and cooling capacity of the coils inside the AHU based on Köppen climatic zones, one can conclude that the best results can be obtained for tube length of 100 m in the city of Ottawa (reduction of 65% when using the EAHX) that belongs to the Dfb zone. This city is characterized by the greatest temperature excursion between winter and summer season, with a very cold winter (with frequent snowfalls) and a hot-humid summer. On the contrary, the worst results can be obtained in Rio de Janeiro (Aw zone) with a maximum value of reduction of 24%.

The contents of this chapter are an extension of the following publication in which I am the corresponding author:

- D'Agostino, D., Greco, A., Masselli, C. and Minichiello, F. "The employment of an earth-to-air heat exchanger as pre-treating unit of an air conditioning system for energy saving: A comparison among different worldwide climatic zones". *Energy and Building*, 2020, 229, 110517.

4 OPTIMIZATION OF A NET ZERO ENERGY BUILDING (NZEB) USING LOW ENTHALPY GEOTHERMAL SYSTEMS

In this chapter the two technologies analysed in the previous chapters, i.e., the Ground Source Heat Pump (GSHP) and the Earth-to-Air Heat Exchanger (EAHX) are implemented in retrofit strategies in order to obtain Net Zero Energy Buildings. These two plants are compared from an energy, environmental and economic point of view. A dynamic simulation software (DesignBuilder) based on EnergyPlus calculation engine is used. The results are very interesting and demonstrate how, by using a low enthalpy geothermal plant, a very low value of primary energy requirement can be obtained for the analysed building. Moreover, substantial savings on annual energy bills and reduction of CO_2 emissions are obtained. To the best of my knowledge, in the current literature panorama there is no energy comparison between the two plants analysed, although the state-of-the art shows the significant energy savings of buildings using low enthalpy geothermal energy systems.

4.1 METHODOLOGY AND APPLICATION

The case study is a real building located in Naples, a city of South Italy. The energy consumption of the existing building and the energy retrofit scenario are evaluated through dynamic simulation by referring to the detailed HVAC mode. The methodology used is the same illustrated in chapter 2, paragraph 2.2, in order to simulate the thermal behaviour of the building envelope and the energy consumption for different retrofit proposals.

DesignBuilder allows models of simple earth tubes that can be controlled by a schedule and through the specification of minimum and maximum, values of indoor temperature. As with infiltration and ventilation, the actual flow rate of air through the earth tubes, if not fixed on the basis of common standards regarding indoor air quality, can be calculated as a function of the difference between the inside and outside environment temperature and the wind speed. To overcome this simplified analysis, a pre-analysis was made,

based on the results obtained in chapter 3 regarding the optimal characteristics of the EAHX.
The external air flow was set to the minimum renewal air flow to be guaranteed per person (UNI 10339) equal to 0.011 m^3/s per person = 39.6 m^3/h per person. For each area of the building, the minimum amount of air was considered according to the number of people present for a total of outdoor air equal to 460.8 m^3/h.
The properties of the soil also affected the sizing, so from the Geological Map of Italy (Sheet No. 184) and the geological map of the Piana Campana (Figure 42), it was possible to ascertain the presence of pyroclastic deposits for the city of Naples.

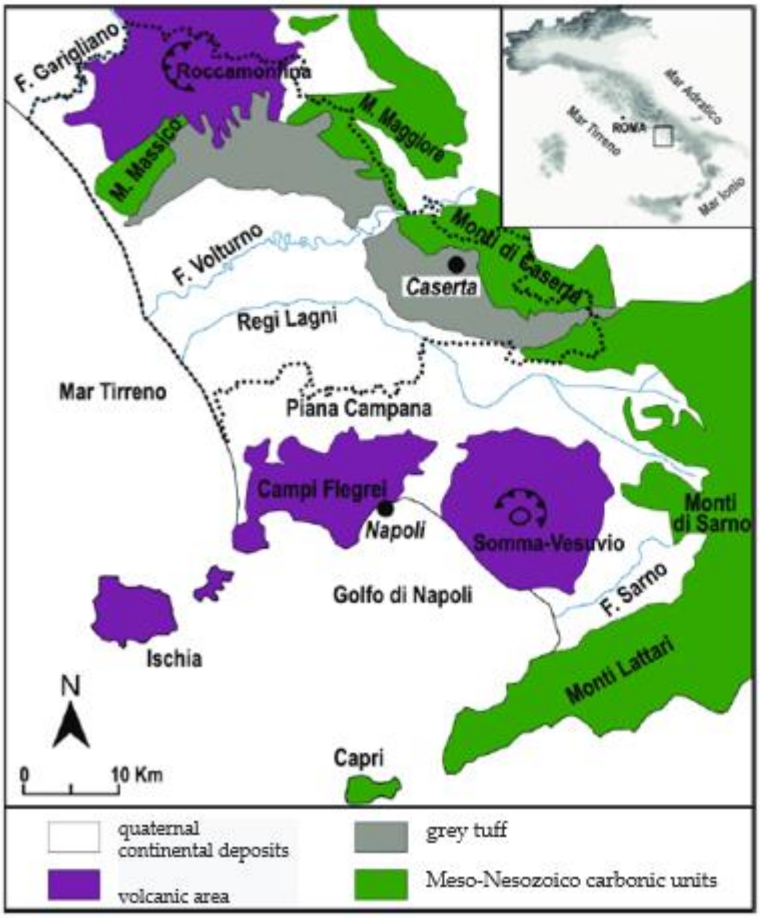

Figure 42. Geological map of Piana Campana, region of South Italy.

In function of this, the following properties have been considered for the soil, i.e., unitary thermal capacity equal to 2 MJ/ m^3K and thermal conductivity equal to 1.5 W/mK. The laying depth of the pipeline is 3 m. Based on the yearly trend of the soil temperature for the city of Naples and considered the afore mentioned parameters, using a spreadsheet made available by Prof. Zarrella AtGCalc [61] and an exchanger with an external diameter of 200 mm, thickness of 6 mm, a length of 80 m and a thermal conductivity of 0.28 W/mK was chosen.

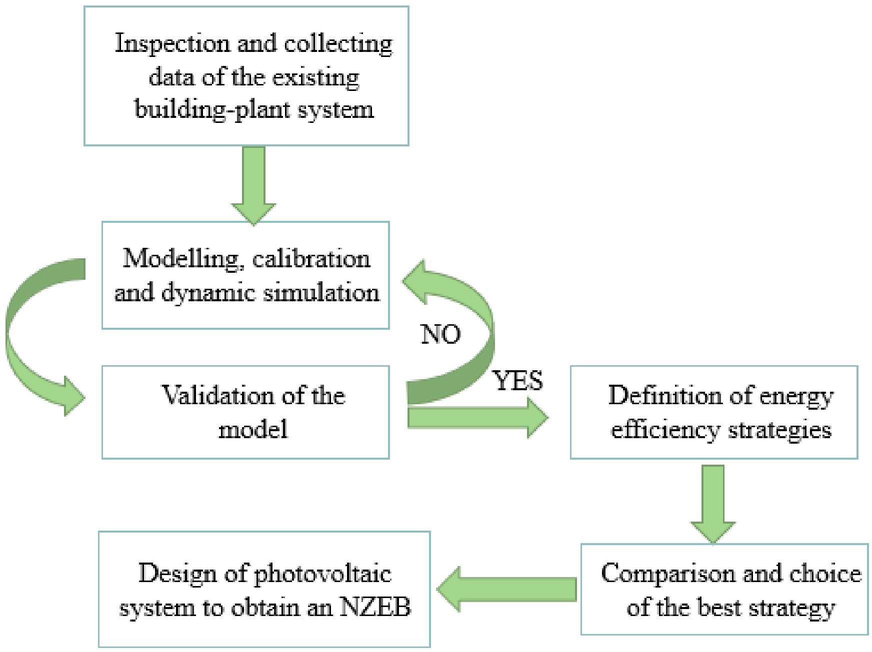

Figure 43. Workflow of the methodology used.

In Figure 43 a workflow of the methodology used is shown. The building is an existing building for which energy consumption bills are available. In this way the model implemented in DesignBuilder has been validated using the Mean Bias Error MBE [94] based on the annual gas consumption available from the energy bills. The equation of MBE (%) is:

$$\mathrm{MBE} = \frac{\sum_{time}(M-S)}{M}, \qquad (25)$$

where:

- M is the measured energy consumption, kWh;
- S is the simulated energy consumption, kWh.

The available data concern the gas bill of only one year, for the heating system and domestic hot water (DHW). Considering the measured data, the gas demand is 6330 kWh, while the value obtained through the simulation is 6489 kWh, with a 3% difference. Thus, even if calculated coarsely on one year, the MBE results equal to 1.20%, decidedly lower than the limit value considered by the U.S. DOE and ASHRAE guidelines [95] [94] for calibrated models (±5%). The validation procedure would have been more accurate if data from a longer period (i.e., three or five years) had been used. Unfortunately, the consumptions in the bills referring to a greater number of years were not available. However, downstream of the simulations, the results obtained were compared and considered consistent with others found in the international literature.

A simplified relation has been used to evaluate the global length of the geothermal probes of the GSHP, considering the heat extraction for the unit of length of probes and the evaporator/condenser capacity. The following conditions have been chosen: a typical soil with solid rock, with a specific heat extraction of 50 W/m by means of probes; the number of operating hours of the plant equal to 2400 (Table 21 [96]).

Table 21. Useful parameters to dimension the probes of GSHP.

Hours of plant operation	2400 h
Soil	solid rock and water saturated sediments
Specific heat extraction based on length of probes	50 W/m

After knowing the evaporator/condenser capacity and the specific heat extraction, the following equation allows to calculate the length of the geothermal probes:

$$L_P = max(\frac{C_{EV}}{q};\ \frac{C_{CO}}{q}) \qquad (26)$$

where:

- L_p is the length of the geothermal probes, m;
- q is the value of heat extraction for unit of length of probes, W/m.
- C_{EV} is the evaporator capacity in heating mode, W;
- C_{COND} is the condenser capacity in cooling mode, W.

After designing the HVAC system and the energy improvement interventions, the different scenarios have been compared to find the best solution from an energy point of view.

For each of the different scenarios, primary energy saving ΔPE [%] is evaluated with this equation:

$$\Delta\text{PE} = \left[\left(PE_{SC,0} - PE_{SC,n}\right)/PE_{SC,0}\right] \cdot 100 \qquad (27)$$

where PE is the primary energy in kWh/m^2 referred to the existing building (SC,0) and to the proposed scenario (SC,n). The total yearly primary energy is evaluated as the sum of the total electrical energy, E_e [kWh/m^2], multiplied by the primary energy conversion factor for electrical energy f_{el}, and the primary energy from natural gas E_{ng} [kWh/m^2]. The primary energy conversion factors, taken from [51], are equal to 2.42 and 1.05 for electricity and natural gas, respectively.

$$PE = \left[\left(\sum E_{el} \cdot f_{el}\right) + \left(\sum E_{ng} \cdot f_{ng}\right)\right] \qquad (28)$$

Finally, the integration of a photovoltaic plant is designed using PVGIS tool that allows information to be gathered on the performance of PV systems located in Europe and Africa, based on several irradiance maps obtained by satellite data collection. Satellite measurements are considered the most accurate source of information for PV production prediction, as demonstrated in studies that investigated the sources of uncertainty in yearly global horizontal radiation data [97], and are employed in several studies in very different climatic conditions [98].

To size the PV system, the energy balance of the NZEB is performed by using a control volume that coincides with the physical boundaries of the building, and therefore the building-systems energy demand and the energy produced by renewable sources (kWh) are considered in the yearly energy balance. The PV surface is obtained by considering the equation 29.

$$(E_{el,demand} - E_{el,renewable})_{year} = 0 \qquad (29)$$

4.1.1 Description of the case study

The case study refers to an existing building i.e., a single-family house (4 occupants), located in Naples (South Italy), a city characterized by mild winters and hot summers. In Figure 44 and Figure 45 an aerial photogrammetry of the intervention area and a plan drawing of the existing building are shown. The total net area of the single-level building is 85 m^2 with a height of 4.5 m. The thermal zones of the building are shown in Figure 46.

Figure 44. Aerial photogrammetry of the existing building.

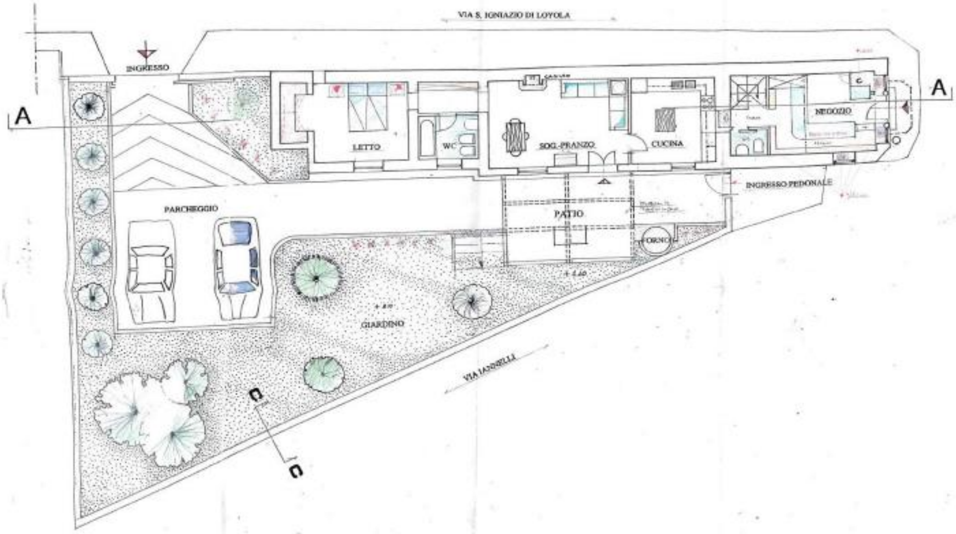

Figure 45. Plan drawing of the existing building.

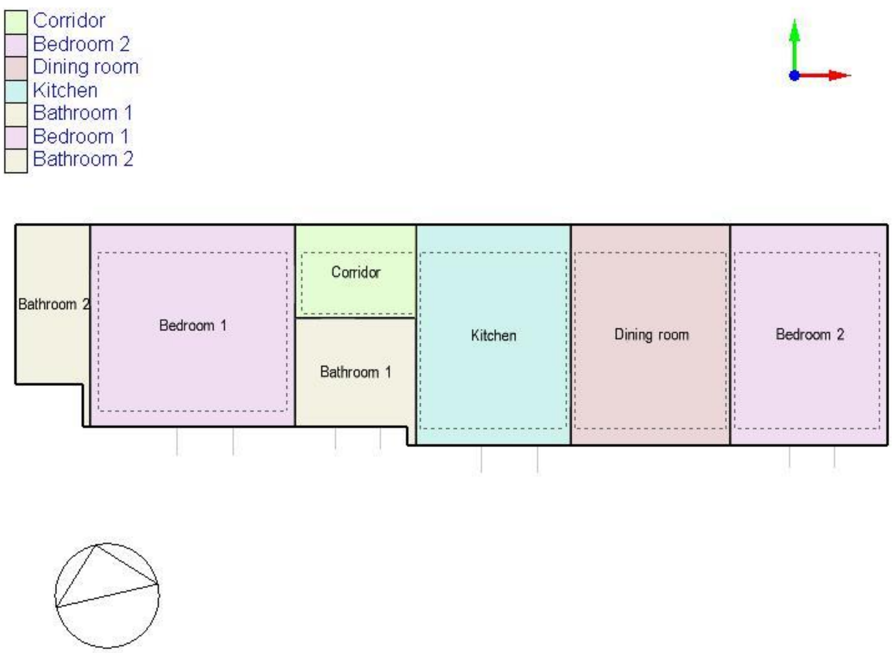

Figure 46. Thermal zones of the existing building.

The building envelope is composed of a masonry typical of the volcanic area (i.e., Neapolitan yellow tuff). The thickness of the walls is 35 cm for the south side and 60 cm for the north side. There is no thermal insulation. The windows are obsolete, and they are made of single glass and PVC frame. For this reason, the thermal transmittances do not respect the limit value dictated by the Italian legislation [38]. The existing building envelope has the thermal transmittances indicated in

Table 22.

Table 22. Unitary thermal transmittance of building envelope components in the current state.

	Thermal transmittance [W/m²K]		**Limit value of thermal transmittance for climatic Zone C** [38] [W/m²K]
Floor	0.29	<	0.38
Roof	0.93	>	0.33
Wall 35 cm	0.88	>	0.34
Wall 60 cm	0.54	>	0.34
Window	3.14	>	2.2

The heating plant is characterized by an obsolete gas boiler with radiators as terminals and dedicated split systems (2,7 kW and EER 2.2) in each room of the apartment for cooling. The gas boiler has a capacity of 24 kW and a nominal efficiency of 0.86. The boiler for heating is also the same for producing domestic hot water.

Based on DPR 412/93 [53] and DPR 74/2013 pt. 10.1 [54] Naples is characterised by 1034 Heating Degree Days and belongs to climatic zone C, for which the heating system can be turned on only from 15th of November to 31st of March (maximum 10 hours per day). There are no time limits imposed by the Italian law for the cooling system. For these reasons, the following schedules have been chosen for the heating and cooling systems:

- Heating system: 10 hours per day, from 15th of November to 31st of March [53], from 6:00 to 10:00 and from 16:00 to 22:00.

- Cooling system: 7 hours per day, from 1st of June to 30th of September, from 9:00 to 11:00 and from 15:00 to 20:00.

The electrical equipment is as follows:

- for bathrooms, the hair dryer with an electrical power of 600 W;
- for the kitchen, an electric stove (for the preparation of the food) with an electrical power of 3000 W and the refrigerator with an electrical power of 100 W;
- for the living-dining room, a computer with an electrical power of 250 W and a TV with an electrical power of 50 W.

For the lighting of the existing building, a led lighting with a normalized power density value equal to 5 W/m^2 * 100 lux is assumed.

4.1.2 Retrofit scenarios

To obtain an NZEB, the energy retrofit consists in the improvement of the building envelope, the insertion of a mechanical ventilation plant and the insertion of a more efficient heating and cooling systems.

Considering that the intervention area has a garden, this area can be suitable for the installation of geothermal probes of the GSHP or the pipes of the EAHX.

Four scenarios have been proposed in order to individuate the best retrofit strategy using the low enthalpy geothermal energy to obtain an NZEB:

- Scenario 0: Existing building and related systems.
- Scenario 1: The building envelope has been improved and a new heating and cooling system is considered, based on reversible (invertible) air-to-water heat pump and radiant floor as terminals. Moreover, a mechanical ventilation system and a dedicated heat pump for DHW production are foreseen.
- Scenario 2: equal to scenario 1, but a earth-to-air heat exchanger (EAHX) is added to the mechanical ventilation system.
- Scenario 3: The building envelope has been improved and a new heating and cooling system is considered, based on a ground source heat pump with radiant floor as terminals. Even

in this case there is a mechanical ventilation system and a dedicated heat pump for DHW production.

- Scenario 4: equal to scenario 3, but an earth-to-air heat exchanger (EAHX) is added to the mechanical ventilation system.

In the Table 23 different energy retrofit scenarios are summarized.

Table 23. Different energy retrofit scenarios.

Systems	Scenario 0	Scenario 1	Scenario 2	Scenario 3	Scenario 4
Heating	traditional gas boiler + radiators	invertible air-to-water heat pump	invertible air-to-water heat pump	ground source heat pump	ground source heat pump
Cooling	split systems				
Ventilation	natural	mechanical ventilation	mechanical ventilation + EAHX	mechanical ventilation	mechanical ventilation + EAHX
DHW	the same boiler of the heating system	dedicated heat pump	dedicated heat pump	dedicated heat pump	dedicated heat pump
Building envelope	poor	improved	improved	improved	improved

In the Table 24 the nominal capacity, the coefficient of performance (COP) and the energy efficiency ratio (EER) of the proposed heat pumps are reported.

Table 24. Thermal and energy parameters of the proposed heat pumps.

Air-to-Water heat pump	Nominal capacity [kW]	COP/EER [-]
Heating	7.0	4.6
Cooling	12.2	4.7
Geothermal heat pump		
Heating	7.5	4.7
Cooling	12.5	8.2
DHW Dedicated heat pump		
	1.9	3.7

The main characteristics of the designed geothermal energy systems are reported in Table 25.

Table 25. Characteristics of EAHX and GSHP systems [99] .

Ground-to-air Heat Exchanger		**Ground source heat pump**	
Soil			
Unitary thermal capacity		2 MJ/m^{3}K	
Thermal conductivity		1.5 W/mK	
Undisturbed ground T		17 °C	
Characteristics of EAHX system		**Characteristics of probes for GHSP system**	
Type	horizontal	Type	vertical
Material	PP	Material	PE-Xa
Thermal conductivity	0.28 W/mK	Thermal conductivity	0.40 W/mK
Depth of installation	3 m	Start depth of installation	1.5 m
Length	80 m	Length	60 m
Diameter	0.2 m	Shape	single U
Tube slope	2.50%	Number of probes	2

The indoor air set point temperature is 20°C and 26°C for heating and cooling, respectively. The total airflow of the EAHX is 460.8 m^3/h, calculated using the technical standard UNI 10339:2005 [100].

Moreover, as previously mentioned, each retrofit scenario contemplates the improvement of the building envelope. Indeed, a 4 cm and 10 cm thick layer of tuff insulation are added to the vertical walls of the building envelope, and a 10 cm hemp fibre panel is foreseen for the roof slab. Finally, a 5 cm cork panel is added to the first-floor slab. The replacement of the current windows with others in thermal break aluminium with double low-emission glass is also foreseen.

In Table 26 the unitary thermal transmittance U and the periodic (or dynamic) thermal transmittance Yie of the improved building opaque envelope components are shown. All the values respect the rule in force [38] in Italy about energy saving and environmental sustainability.

Even lighting and indoor mechanical ventilation are improved. The ventilation outdoor air is guaranteed for each zone: for the bedrooms and the living-dining room a minimum fresh air value of 10 l/s per person is considered, for the bathrooms and the kitchen a value of 12 l/s per person.

For lighting, the different illuminance values required for the various rooms are: 150 lux for the bathrooms and bedrooms, and 250 lux for the kitchen and living-dining room. LED lighting with a normalized power density value equal to 2 W/m² * 100 lux is considered even to reduce the related energy demand.

Table 26. Unitary thermal transmittances of the improved building opaque envelope components.

ELEMENT	**Thickness**	**Stationary Thermal Transmittance**		**Limit values of stationary Thermal Transmittance**	**Dynamic Thermal Transmittance**		**Limit values of Dynamic Thermal Transmittance**	**Mass per unit area**		**Limit value of M-ass per unit area**
	s [m]	**U [W/m²K]**		**U [W/m²K]**	**Yie [W/m²K]**		**Yie [W/m²K]**	**M [kg/m²]**		**M [kg/m²]**
Floow	0.635	0.21	<	0.38	0.004	<	0.18	546.50		-
Roof	0.367	0.27	<	0.33	0.098	<	0.18	370.84		-
Wall 35 cm (S, E, O)	0.51	0.22	<	0.34	0.003	<	0.1	520.78	>	230
Wall 60 cm (N)	0.7	0.27	<	0.34	0.000	<	0.1	836.18	>	230

4.2 RESULTS AND DISCUSSION

The first results concern the comparison of primary energy consumption between the real building, characterized by a high thermal transmittance of the building envelope components and an obsolete heating and cooling systems, and the different proposed energy retrofit scenarios.

As can be seen in Figure 47, the total yearly primary energy consumption of the existing building is quite high (203.5 kWh/m^2), mainly that of the heating system (118.8 kWh/m^2).

By intervening on the building envelope and proposing an air-to-water heat pump as a heat generator (scenario 1), the yearly consumption of primary energy is considerably reduced, reaching the global value of 92.1 kWh/m^2 and only 23.7 kWh/m^2 for the heating system (Figure 48).

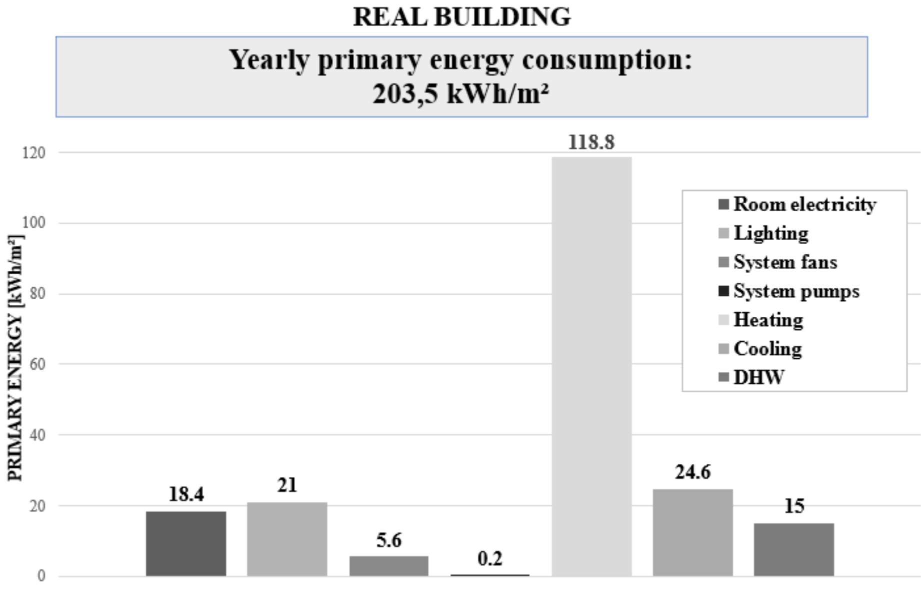

Figure 47. Primary energy consumption of the existing building.

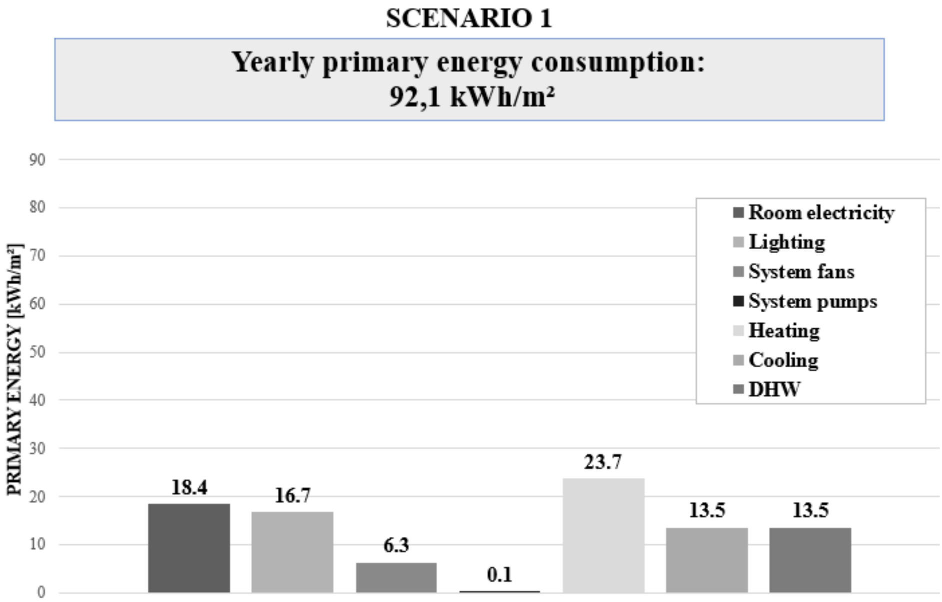

Figure 48. Yearly primary energy consumption for scenario 1.

Figure 49 shows a total reduction of 55% by comparing the existing building and scenario 1; the highest primary energy reduction concerns both heating (80%) and cooling (45%). This is due to the improvement of the thermal characteristics of the building envelope but also to the use of a type of heat generator more efficient than a traditional boiler.

Once the effectiveness of traditional energy improvement interventions has been assessed, it was examined which improvement could be obtained when considering systems that use low enthalpy geothermal energy.

In scenario 2 the effectiveness of EAHX in the HVAC system is noticeable. In fact, the total primary energy consumption is lower than scenario 1 and equal to 80.1 kWh/m^2. As Figure 50 shows, this technology has a positive effect on the primary energy saving referred to heating and cooling. Particularly, the energy saving for the cooling system is 85 % (compared to existing building), as the outdoor air is pre-cooled in the EAHX in summer.

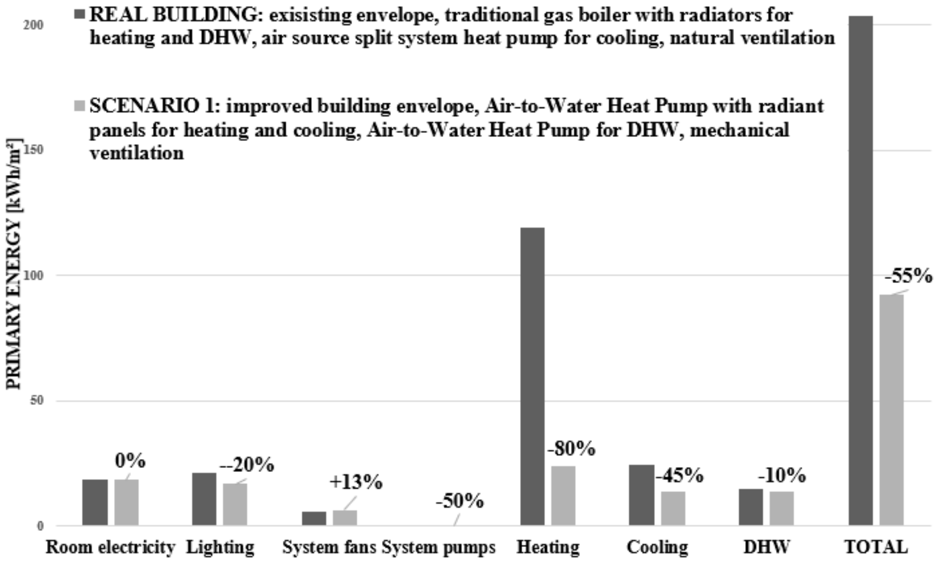

Figure 49. Comparison in terms of primary energy consumptions between existing building and scenario 1.

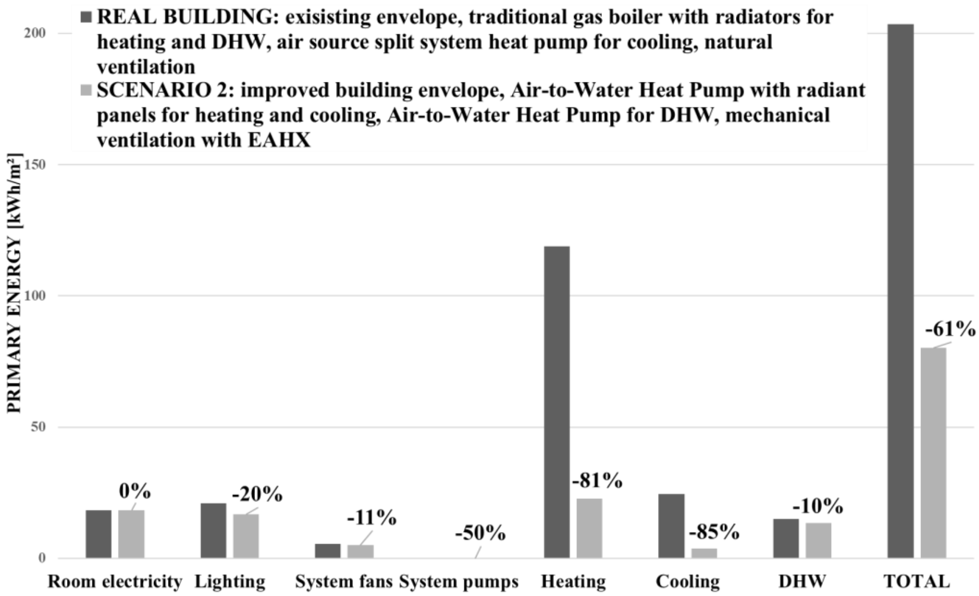

Figure 50.Comparison in terms of primary energy consumptions between existing building and scenario 2.

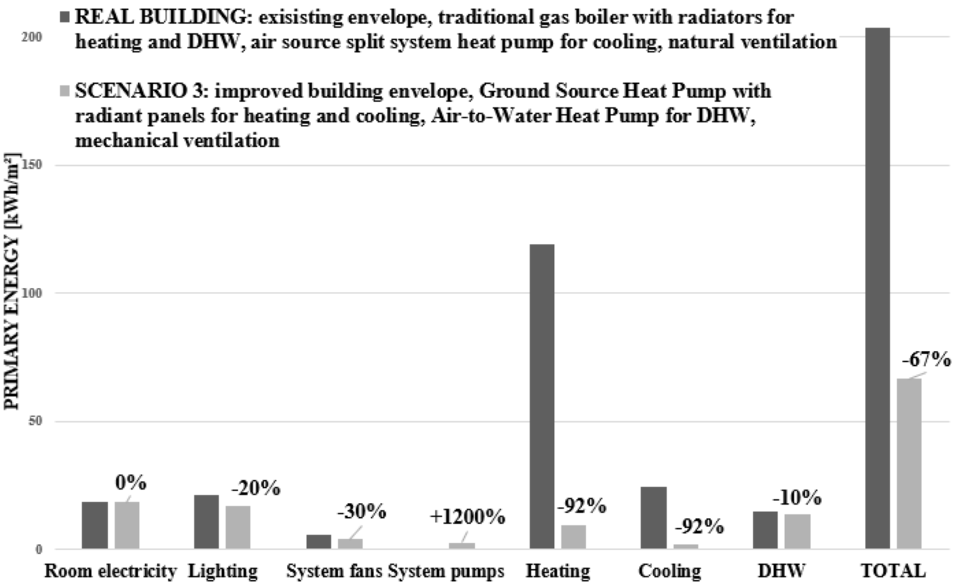

Figure 51. Comparison in terms of primary energy consumptions between existing building and scenario 3.

When considering scenario 3 (Figure 51), the yearly primary energy consumption is equal to 66.6 kWh/m^2: by using a GSHP as the generator for the heating and cooling system and by improving the building envelope, the energy consumption for heating and cooling decreased by 92% and there is a reduction of total primary energy consumption of 67% compared to the existing building.

These remarkable results led to the proposal of scenario 4, i.e., the coupling of both the analysed low enthalpy geothermal technologies (the GSHP and the EAHX) in the HVAC system.

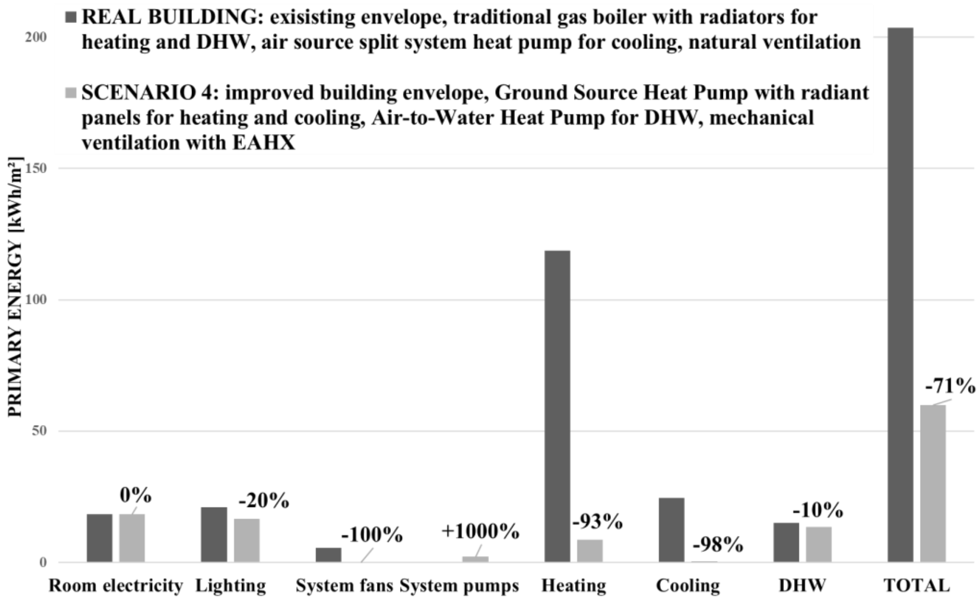

Figure 52.Comparison in terms of primary energy consumptions between existing building and scenario 4.

With this solution, the building with the related systems presents the highest yearly primary energy saving compared to the existing building, i.e., 71% (Figure 52). The savings for heating and cooling are remarkable, i.e., 93% and 98%, respectively. The total primary energy requirement is equal to 59.9 kWh/m^2 and this value is very close to the consumption values of a Net Zero Energy Building found in literature; for example, the definition reported by the New Building Institute of the U.S. [54] indicates a maximum primary energy consumption of 57 kWh/m^2 for an NZEB; a very similar value is reported in [20].

Also, in Blàzquez et al. [55], the value of the total yearly primary energy when using the geothermal heat pump is compared with the results herein obtained for one of the analysed different case studies. In particular, in [55], the yearly primary energy values have been obtained for three cities with different climates conditions: 65, 57, and 97 kWh/m^2 for Ancona, Edinburgh, and Karlstad, respectively. It can be noted that the value in the case of Ancona (Italian climate) is very similar to that obtained for the case study in this research, which is 66.6 kWh/m^2 for scenario 3.

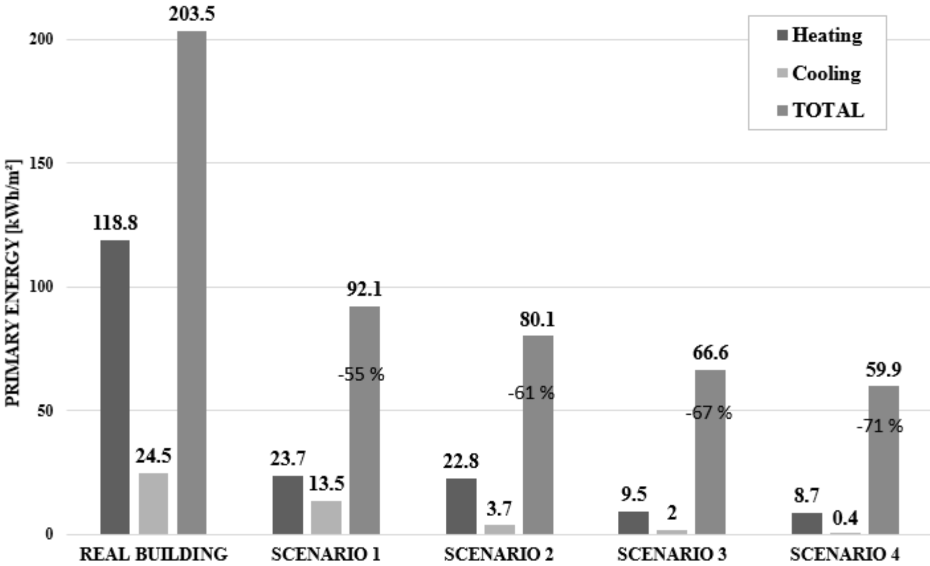

Figure 53. Comparison between the different scenarios in terms of primary energy.

Figure 53 shows that scenario 4 is the best solution from the primary energy point of view. However, even scenario 3 (i.e., GSHP as a generator for heating and cooling) represents an excellent compromise, allowing significant savings of primary energy.

These trends also regard the reduction of CO_2 emissions (Figure 54). When the building improvements and an air source heat pump (scenario 1) instead of a gas boiler are considered, there is a reduction of 42% compared to the real building, while this percentage increases up to 58% when the building envelope is more thermal efficient and a ground source heat pump in the HVAC system is proposed (scenario 3).

It is important to notice that although scenario 4 is the best proposal from an energy and environmental point of view, a technical-economic analysis would be useful to compare scenarios 3 and 4.

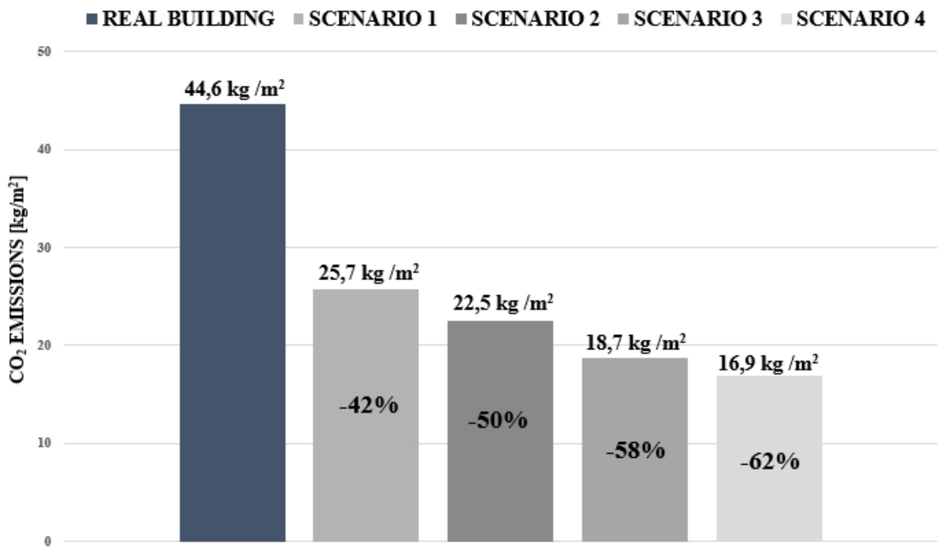

Figure 54. Comparison between the different scenarios in terms of CO_2 emissions.

Once obtained the yearly energy consumption for the different scenarios, an energy balance is made between energy needs and energy production from renewable energy sources in order to achieve the NZEB target. Due to the high solar radiation, the renewable energy system chosen is a monocrystalline silicon photovoltaic system (300 Wp for each panel). The solar radiation is calculated based on the data measured by Joint Research Centre (JRC) of European Commission [56].

By using the calculation software PVGIS [57], the yearly electric energy production of 1361 kWh is evaluated for a 1 kWp of PV system with a tilt angle of 8° and oriented to the southwest (like the pitch of the building roof). Based on this value, the global electric power of the PV system necessary to obtain an NZEB is calculated.

In

Table 27 different pick power values and number of panels for the PV system are reported for the different scenarios.

It can be noted that in all these cases the number of PV panels to entirely balance the energy need is quite low (5-7). But particularly in the case of ground source heat pump, the number of PV panels is 5 with 1.5 or 1.3 peak power of the system. This last value is very low considering that the building is a residential one (while 3 kWp per apartment are usually considered).

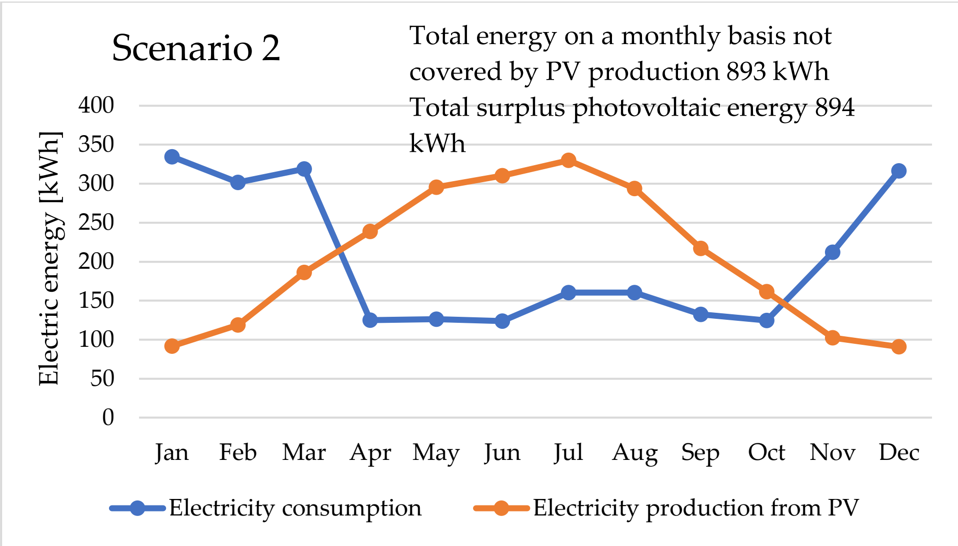

(a)

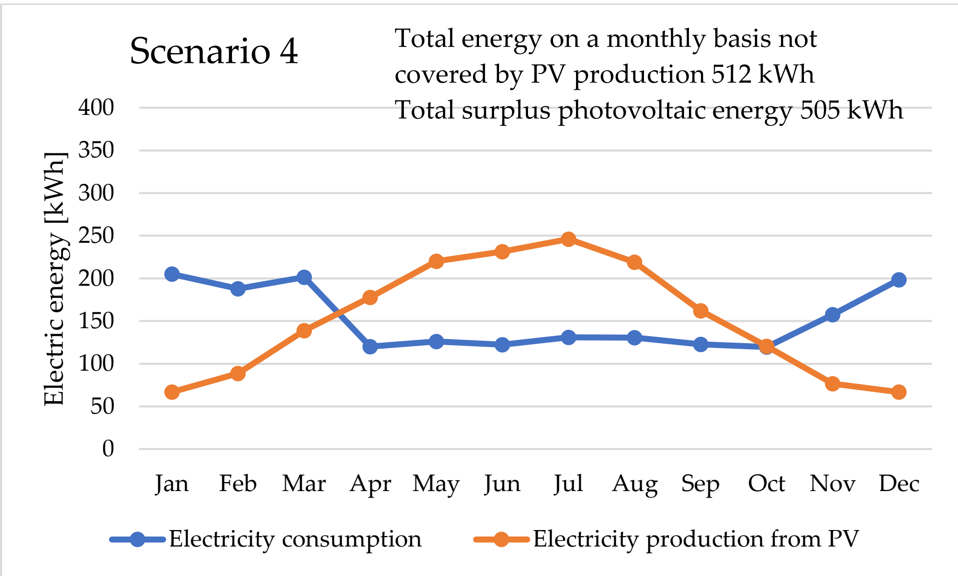

(b)

Figure 55. Electric energy needs and electric energy production from PV system on monthly basis: a) scenario 2; b) scenario 4.

Table 27. Power and number of panels of the PV system necessary to obtain an NZEB for the different scenarios.

	SCENARIO 1 Improved building envelope Air-to-Water Heat Pump Mechanical ventilation Radiant panels	**SCENARIO 2** Improved building envelope Air-to-Water Heat Pump EAHX + mechanical ventilation Radiant panels	**SCENARIO 3** Improved building envelope Ground Source Heat Pump Mechanical Ventilation Radiant panels	**SCENARIO 4** Improved building envelope Ground Source Heat Pump EAHX + mechanical ventilation Radiant panels
Yearly electricity consumption [kWh]	2801.2	2436.3	2025.7	1821.9
Yearly production [kWh/kWp]	1361.0	1361.0	1361.0	1361.0
Necessary power of PV system to obtain a NZEB [kW]	2.1	1.8	1.5	1.3
Number of necessary PV panels	7	6	5	5

Another important result comes from the comparison between the building electricity needs and the production of electricity from PV systems on a monthly basis. By way of example, Figure 55 (a) shows the trend in the case of scenario 2 and Figure 55(b) shows the trend for scenario 4.

Table 27 highlights the convenience of GSHP in reducing the photovoltaic surface for the NZEB. Furthermore, Figure 55 shows that when the NZEB target is reached with an air-to-water heat pump, there is a need to withdraw from the national electricity grid a greater amount of energy than in the case in which the NZEB target is reached with a GSHP (893 kWh vs 512 kWh). Furthermore, in the scenario 2 (Air-to-Water Heat Pump + EAHX) the PV system has a surplus of untapped energy in the summer months equal to 43% more than in the scenario 4 (GSHP+EAHX). Finally, Figure 55 shows that monthly energy self-sufficiency of the building is greater when the NZEB target is reached with low enthalpy geothermal systems.

Table 28. Energy costs and savings for different scenarios compared to the existing building.

	Electricity	**Gas**	**Primary energy**	**Energy costs**	**Saving compared to the real building**
	[kWh/m²]	[kWh/m²]	[kWh/m²]	[€]	[%]
REAL BUILDING	32.3	133.8	203.5	1172	-
SCENARIO 1	42.5	-	92.1	646	-45%
SCENARIO 2	36.9	-	80.1	562	-52%
SCENARIO 3	30.7	-	66.6	467	-60%
SCENARIO 4	27.6	-	59.9	420	-64%

Considering the prices of both electricity and natural gas, an economic evaluation on savings is made. The prices are referred to Eurostat data [58] referred to 2019: 0.230 EUR/kWh for electricity and 0.0769 EUR/kWh for natural gas. The economic analysis highlighted in Table 28 has shown that the scenario 1 allows a saving of 45% on yearly energy bills compared with the existing building. This percentage increases up to 64% when using both the analysed low enthalpy geothermal plants (i.e., scenario 4). This means a saving of 725.00 EUR/year when comparing scenario 4 and the existing building and a saving of 220.00 EUR/year when comparing scenarios 4 and 1.

4.3 CONCLUSIONS

In this chapter an analysis of different energy retrofit scenarios exploiting the low geothermal energy is proposed. The retrofit strategies (all including a suitable improvment of the building envelope) aim to transform an existing building into an NZEB. Four scenarios have been hypothesized:

- Scenario 1. The building envelope has been improved and a new heating and cooling system is considered, based on reversible (invertible) air-to-water heat pump and radiant floor as terminal. Moreover, a mechanical ventilation system and a dedicated heat pump for DHW production are foreseen.
- Scenario 2. Equal to scenario 1, but a ground-to-air heat exchanger (EAHX) is added to the mechanical ventilation system.
- Scenario 3. The building envelope has been improved and a new heating and cooling system is considered, based on a ground source heat pump (GSHP) with radiant floor as terminals. Even in this case there is a mechanical ventilation system and a dedicated heat pump for DHW production.
- Scenario 4. Equal to scenario 3, but an earth-to-air heat exchanger (EAHX) is added to the mechanical ventilation system.

In particular, the difference between the use of two different systems that exploit low enthalpy geothermal energy (i.e., ground source heat pump, ground-to-air heat exchanger) and more common plants such as an air-source heat pump is evaluated from an energy and economic point of view.

After validating the model, the dynamic simulations highlight how all scenarios that contemplate the use of low enthalpy geothermal energy are better than those with an air-to-water heat pump. Compared to the existing building, scenario 1 allows a total primary energy saving of 55%. This saving increases for scenarios 2 (61% - EAHX), 3 (67% - GSHP) and 4 (71% - EAHX plus GSHP).

Similar values have been obtained also for the reduction of CO_2 emissions.

The number of PV panels necessary to entirely balance the building energy need, so obtaining an NZEB, is quite low (5-7) for all the scenarios, but in the case of the NZEB with HVAC based on low enthalpy geothermal systems, the monthly energy needs of the building and the surplus of energy from PV system take on the lowest values (about 40% less than NZEB with air-to-water heat pump).

Also, substantial annual savings on the energy bill are obtained in all the scenarios proposed. Starting from the existing building where the user spends around 1172 € in one year, this value becomes 646 € in the case of scenario 1, 562 € in the case of scenario 2, and 467 € for scenario 3. The best result corresponds to the coupling of the GSHP and the EAHX, reaching an annual energy cost of only 420 €.

Therefore, the results confirm that NZEBs represent the means for a considerable energy and economic saving in the construction sector. This saving can be significantly increased when the exploitation of the geothermal energy (free and almost constant throughout the year) is performed, mainly by using a GSHP. On the other hand, air source heat pumps can be subject to malfunctions in winter for particularly cold climates.

Possible further analyses on the topic could concern an in-depth energy-economic evaluation which also considers the component costs and different photovoltaic technologies.

The contents of this chapter are an extension of the following publications in which I am the corresponding author:

- D'Agostino, D., Minichiello, F. and A. Valentino. "Contribution of Low Enthalpy Geothermal Energy in the Retrofit of a Single-Family House: A Comparison between Two Technologies". *Journal of Advanced Thermal Science Research,* 2020, 7, 30-39.
- D'Agostino, D., Minichiello, F., Renno, C. and A. Valentino. "Retrofit strategies to obtain a NZEB using low enthalpy geothermal energy plants" submitted and under review on *Energy,2021*.

5 CONCLUSIONS AND FUTURE DEVELOPMENTS

This thesis work investigated low enthalpy geothermal systems such as the Ground Source Heat Pump (GSHP) and the Earth-to-Air Heat eXchanger (EAHX). The work was carried out using the dynamic simulation tool and the results were validated through comparisons with international scientific literature and, when the data were available, the model was calibrated with energy bills. Furthermore, an in-depth study was carried out on the EAHX technology with a parametric analysis, evaluating the efficiency of this system and the energy savings achievable for different climatic zones in the World for different lengths and diameters of the pipes.

The final aim of the thesis was to demonstrate how the use of technologies that exploit low enthalpy geothermal energy implemented in a Net Zero Energy Building contributes to substantial energy savings and reduction in the required photovoltaic surface. This, especially in highly urbanized contexts, would facilitate the desired widespread of the NZEBs, contributing to the objectives of energy saving and GHGs reduction of the European Community in the near future. It has been demonstrated that the geothermal heat pump is a system suitable for different climates unlike the air source heat pump which often in very cold climates can be affected not only by malfunctions but by a significant reduction in COP.

Another important advantage is that these systems in the NZEB can reduce the overload for the electricity grid that an excessive surplus of electricity from photovoltaics can entail. Moreover, it has been shown that an NZEB that uses low enthalpy geothermal energy has a lower amount of energy on a monthly basis not covered by photovoltaics.

It is from this last consideration that future research developments will come to life which will analyse the behaviour of NZEB not only on the basis of an yearly balance, as indicated today by the directives, but by reducing the timestep and evaluating the performance of the NZEBs on monthly or weekly balance between energy consumption and energy production from renewable energy sources.

In literature different balancing methods for ZEBs can be impacted by the variation in time step in the evaluation of grid interaction [101] and several approaches exist on the optimization of the energy balance of buildings. To optimise the energy exchanged with the national electric grid, it is important to define the type of energy balance by varying the time step resolution to be considered when dealing with the energy balance of an NZEB integrated with a solar PV system. By setting the energy balance on yearly basis often is not adequate for covering all operational circumstances, considering the seasonal variability of the weather conditions and consequently of production of PV systems. However, when considering a lower time step, i.e., monthly or weekly, would involve a much more demanding and expensive initial investment.

A careless design may induce not only the failure to really achieve the NZEB target, but also an overload for the electricity grid, considering that in the next years the use of energy from renewable sources will increase significantly.

6 APPENDIX: EXPERIMENTAL CPV/T SYSTEM

During my PhD course I collaborated with Prof. Carlo Renno, head of the Laboratory of Applied Thermodynamics at University of Salerno (Italy). The collaboration involved the experimental study of a concentrating photovoltaic and thermal (CPV/T) system with a linear focus optics.
This system was analysed in order to determine its electrical and thermal performance under different working conditions by changing the outdoor temperature, the weather conditions, i.e., sunny or cloudy and, the focal length of the optics. The results were applied to a case studies. Unfortunately, the pandemic situation has stopped activity for a while, which is currently still ongoing. In the following paragraph the experimental plant is described in detail and some results on the application on a case study are shown.

6.1 CPV/T DESCRIPTION

The experimental Concentrating Photovoltaic and Thermal (CPV/T) system, shown in Figure 56 and realized at Laboratory of Applied Thermodynamics coordinated by Prof. Carlo Renno (University of Salerno, Southern Italy), presents a line-focus configuration with reflective optics consisting of a parabolic trough concentrator [102].

a) b) c)

Figure 56. Linear focus experimental plant: a) Triple-Junction solar cell; b) cooling fluid circuit; c) global CPV/T system.

In particular, a parabolic optics and Triple-Junction (TJ) solar cells (InGaP/GaAs/Ge) have been used in the experimental plant. The TJ cell characteristics are reported in Table 29.

Table 29. TJ cell characteristics.

Triple-Junction cell	
parameter	*value*
material	InGaP/InGaAs/Ge
dimensions	1.0 cm x 1.0 cm
reference efficiency η_r (at 298 K, 50 W/cm^2)	38.7%
temperature coefficient (σ_t)	-0.04%/K

The concentration of the line-focus system takes place along a tube where the TJ cells are located on its surface and where the refrigerant fluid flows. Thirty cells are present along a line of 1.2 m. The experimental system presents also a tracking system able to converge the maximum direct solar radiation on the TJ cells. The TJ cells are placed at a variable distance from the optics and the focal length is a variable in the experimental analysis. The experimental system allows to move the parabolic optics on a vertical axis in order to modify its height respect to the cells, and then the incident radiation on the solar cells can be modified varying the concentration factor value. The main parameters that characterize a parabolic optic are its focal length (f) on which the size of the focused image depends, and the truncation value (a) on which the amount of energy that reaches the tube depends. Hence, the concentration factor C will be proportional to the ratio of the two parameters (f/a). The input data considered in the sizing of the CPV/T system are: C equal to 107, tube length and diameter respectively equal to 1.2 m and 2.8 cm. Referring to these data, it has been possible to determine the parameters and the characteristic dimensions of the parabola necessary to achieve the optimal concentration factor. Corresponding to a proper focal length, the maximum value of C, obtained during the operation hours of the CPV/T system, has been about 90.

A mobile structure is necessary in order to support the optics and to move the CPV/T system either by rotating with its base on a plane, or by rotating around the axis of the tree on a plane orthogonal to the first, to allow the tracking system and to obtain always the maximum concentration factor during the day. The degrees of freedom of the system allow its movement in the north-south and east-west directions, and the change of the focal length (Figure 57). In particular, if a plane parallel to the cell area and another tangent to the vertex of the parabola constituting the concentrator are considered, it is necessary that such planes remain parallel during the movement of the system. What happens is that the rotation of the shaft, which allows the concentrator to chase the sun, does not coincide with the rotation of the tube where the fluid flows, but the rotations tend to be opposite (Figure 57). Finally, the system thus designed will allow to modify parameters such as the focal distance and the positioning of the CPV/T system.

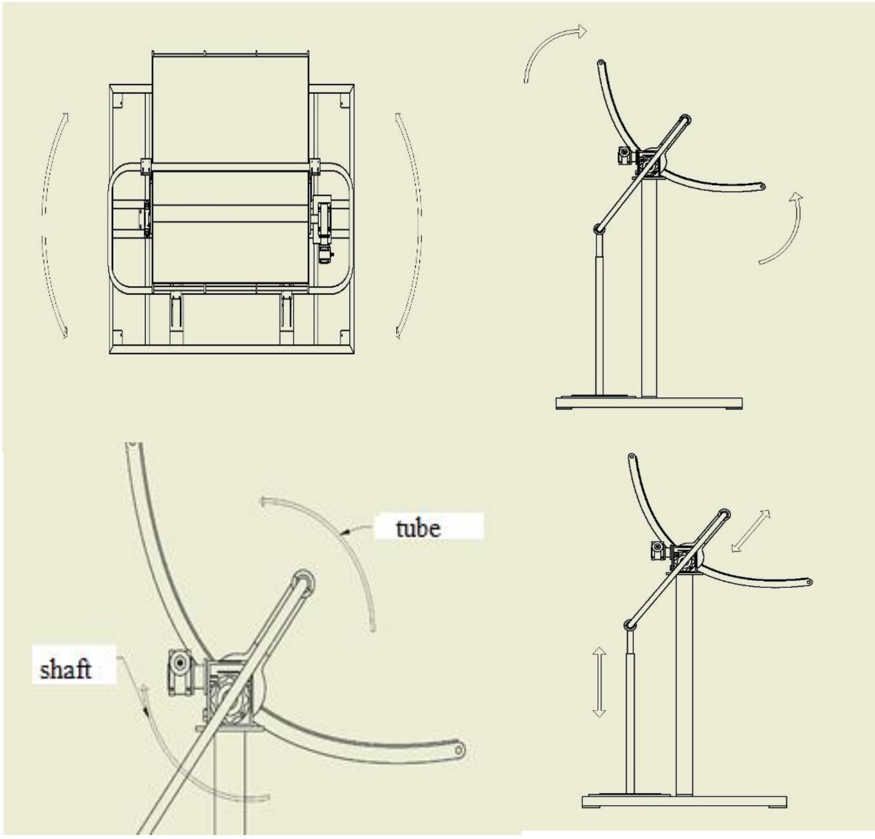

Figure 57. Degrees of freedom of the experimental plant.

Some PT100 thermo-resistances, with an accuracy of ±0.2 K, are adopted to measure the fluid, TJ cell and environmental temperatures. The electrical energy production of the CPV/T system is also evaluated by the voltage and current measurements. A pyrheliometer with an accuracy of 2% is adopted to measure the direct solar radiation. Generally, all the measurements of current and voltage have been monitored during the CPV/T system working by means of a data logger (data tracker series DT80, accuracy 2%). The sampling rate for the energy analysis has been of 15 s.

6.2 APPLICATIONS ON CASE STUDIES

Based on the realization, setting and modelling of a linear focus CPV/T system in the high concentration field, in [103] an experimental linear focus CPV/T plant was set up and analysed in order to determine its electrical and thermal performance by varying the outdoor temperature, the weather conditions, focal length, etc.
The electrical production of the CPV/T system depends generally on the TJ cell characteristics and the concentration factor, while the thermal production is above all linked to the system configuration and the direct normal irradiance (DNI) values. From the results found in [103] two applications on a case study were made and the papers [104] [105]resulted from the above mentioned collaboration.

6.2.1 Performance analysis on CPV/T coupled to a Desiccant Cooling (DC) system

In [104] the performance of a CPV/T coupled to a Desiccant Cooling system in order to satisfy the energy need of a supermarket has been evaluated. The coupling between the CPV/T and DC systems allows to obtain energy and economic savings during the year compared with a conventional solution (without CPV/T and DC systems), considering accurately in the modelling: supermarket energy loads, solar radiation, environmental conditions, etc. In particular, the analysis of three case studies was performed, where the main aim has been to size the CPV/T-DC integrated system and to study how it can match the different supermarket energy needs.

Evaluation of alternative energy solutions has high importance for large users such as a supermarket. A theoretical model of the coupling of a CPV/T system and a DC system have been developed (Figure 58) to satisfy the energy loads The proposed air-conditioning system is an all-air system (with partial recirculation of the air) equipped with a desiccant wheel to balance the latent thermal loads (both internal latent load and that related to the ventilation outdoor air). The DC requires to be regenerated by means of thermal energy derived from the CPV/T system and, only if necessary, from the condensing boiler. The thermal energy derived from the the CPV/T system and, only if necessary, from the condensing boiler is used also for the domestic or sanitary hot water. The sensible thermal load of the supermarket is handled by means

of the cooling/heating direct expansion coil (in summer, part of the sensible load is balanced by the open case refrigerators for food).
In Figure 59, the flow-chart of the model has been reported.
A detailed analysis of the supermarket electrical and thermal needs has been conducted with reference to three different periods: summer, winter and half season; moreover, the DNI model allows a more accurate analysis of the available solar radiation.

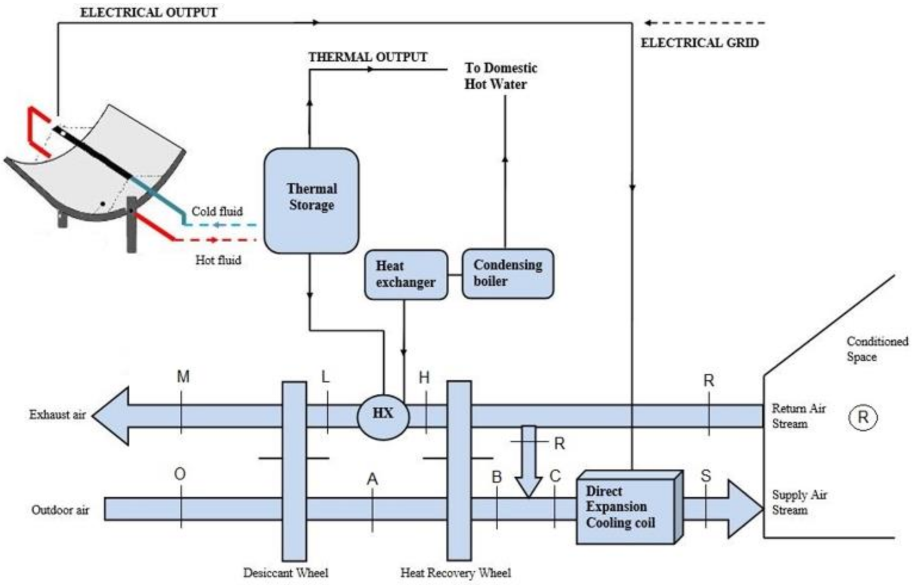

Figure 58. Scheme of the CPV/T coupled to the desiccant cooling system in summer conditions.

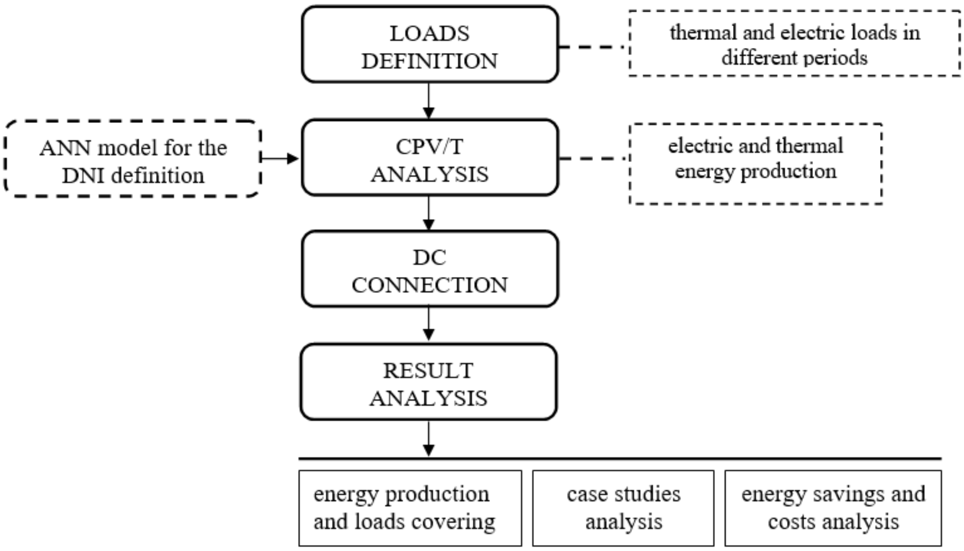

Figure 59. Flow-chart of the model.

The CPV/T system presents a linear focus configuration that allows a modular sizing in order to meet the energy needs of the supermarket. The CPV/T system can satisfy the electrical load as well as the thermal and cooling loads, totally or partially according to the choice, by using the system based on DC, thermal storage, electric heat pump (EHP) and absorption heat pump (AHP). The electrical and thermal energy modelling of the CPV/T system allows to evaluate the system production for each period. The DNI has been modelled to obtain its hourly, daily and monthly distribution for the target location of Naples. The ANN (Artificial Neural Network) model has been validated with experimental data of about two months and the good correspondence between the measured and predicted data can be observed in Figure 60, where the scatterplot of the validation phase is shown.

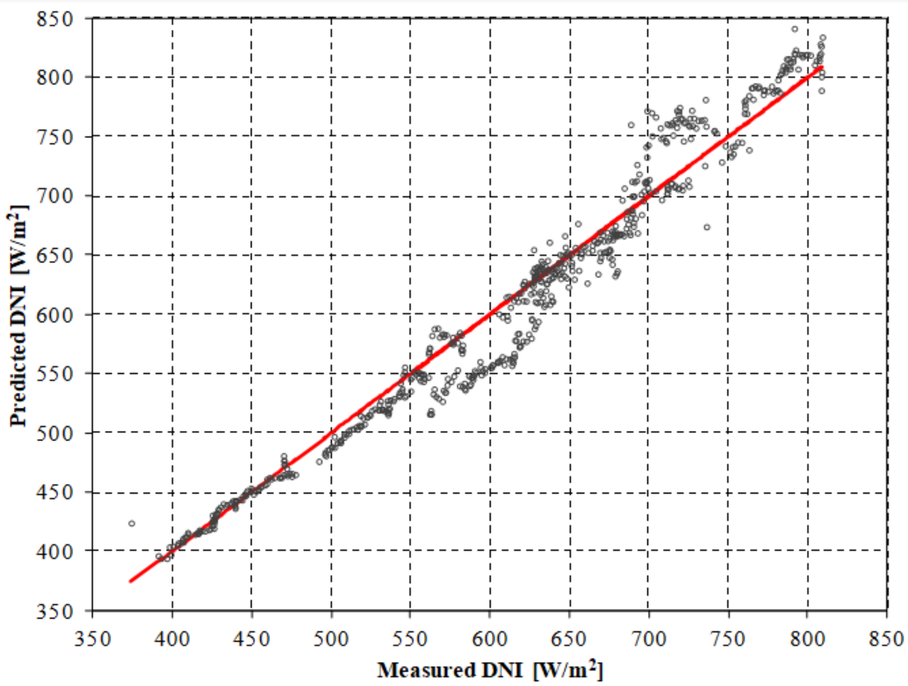

Figure 60. Scatterplot of the ANN configuration for predicting the DNI.

In addition, the mean absolute percentage error (MAPE) of about 2.6% and the root mean squared error (RMSE) of about 22 W/m^2 have been calculated allowing to verify the goodness of the designed network. So, starting from the CPV/T-DC system modelling, which considers the electrical and thermal energy and takes into account the DNI distribution as input, different load solutions have been analysed. In particular, with reference to the energy needs of the supermarket, three case studies have been considered.

The first considers as thermal needs the sanitary hot water (SHW, also called domestic hot water) and latent loads (thermal energy for the regeneration of the DC); so, in this case a great part of the energy needs is represented by the electrical load. In fact, both the winter heating and the summer cooling are obtained by means of an EHP. The electrical loads are also due to illumination, refrigerators for food and different electrical devices. In the Figure 61(a) and Figure 61(b) , the thermal and electrical load annual trends are presented.

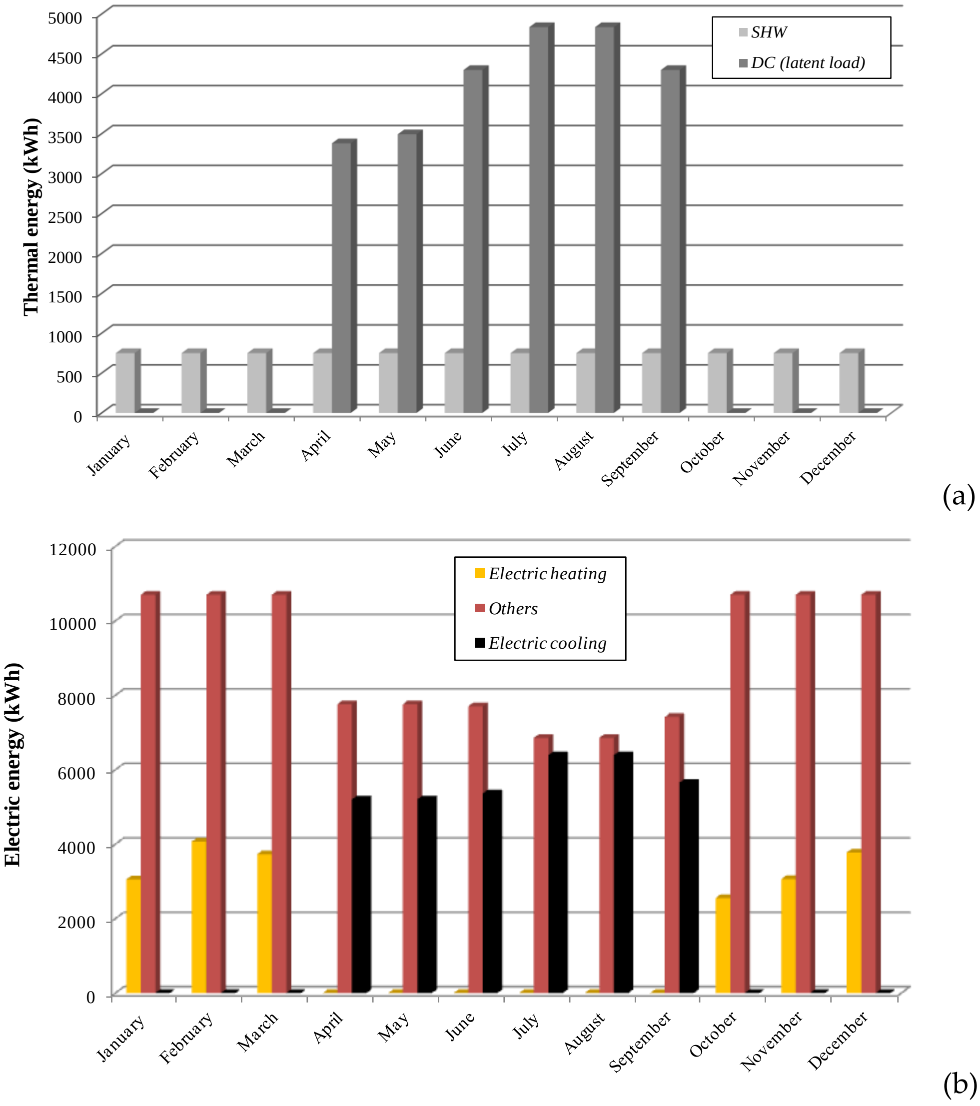

Figure 61. Thermal (a) and electrical (b) loads annual trend for the case 1.

The second case study considers an intermediate solution where the CPV/T-DC system is partially adopted also for heating in winter. In the Figure 62(a) and Figure 62 (b), the thermal and electrical loads are reported. In particular, it can be observed that an increase of the thermal needs, due to the building heating mainly by means of the thermal energy from the CPV/T system, leads to a decrease of the electrical requirements for heating; the summer cooling is still realized with an EHP.

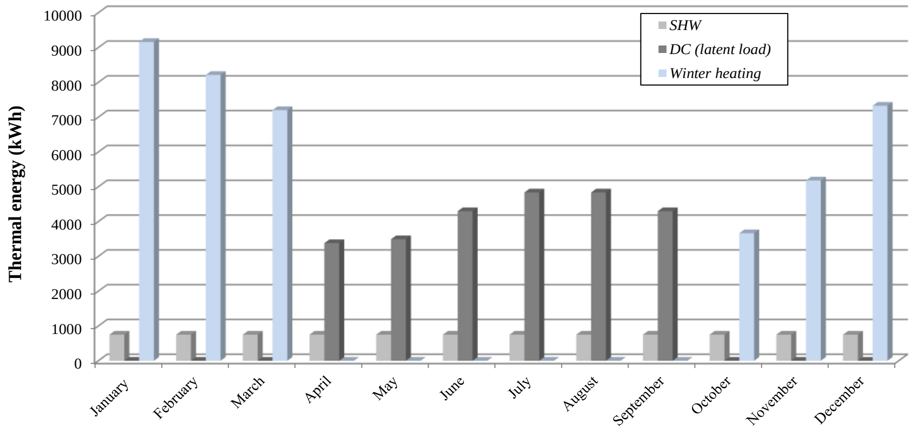

(a)

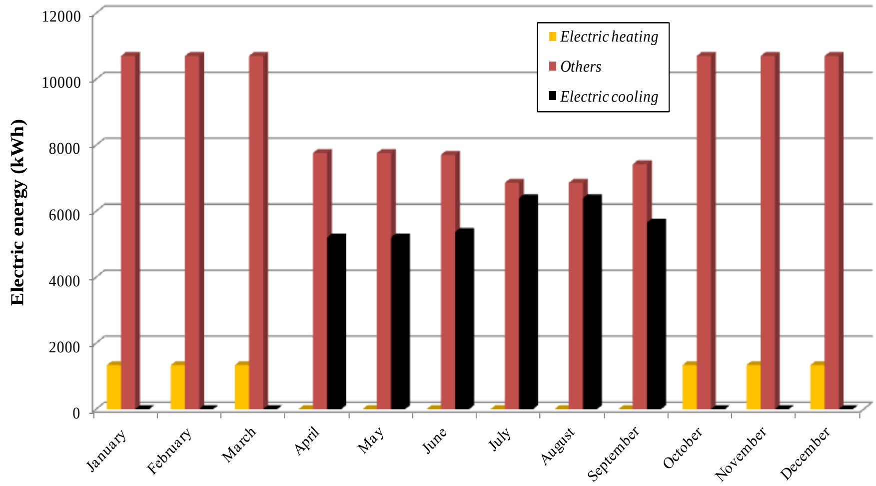

(b)

Figure 62. Thermal (a) and electrical (b) loads annual trend for the case 2.

In the last case study, a high thermal energy recovery from the CPV/T system is considered in winter and summer seasons, in order to satisfy the following thermal loads: SHW, latent load (DC), winter heating and summer cooling. In particular, the heat recovered by the CPV/T system is used to supply both the DC system and the AHP for the summer cooling. Hence, the Figure 63(a) Figure 63(b), where the thermal and electrical loads are reported respectively, show that the thermal needs increase while the electrical needs decrease compared to the first two cases. In particular, electrical loads are due only to electrical devices ("others") and partially due to the winter heating ("electrical heating").

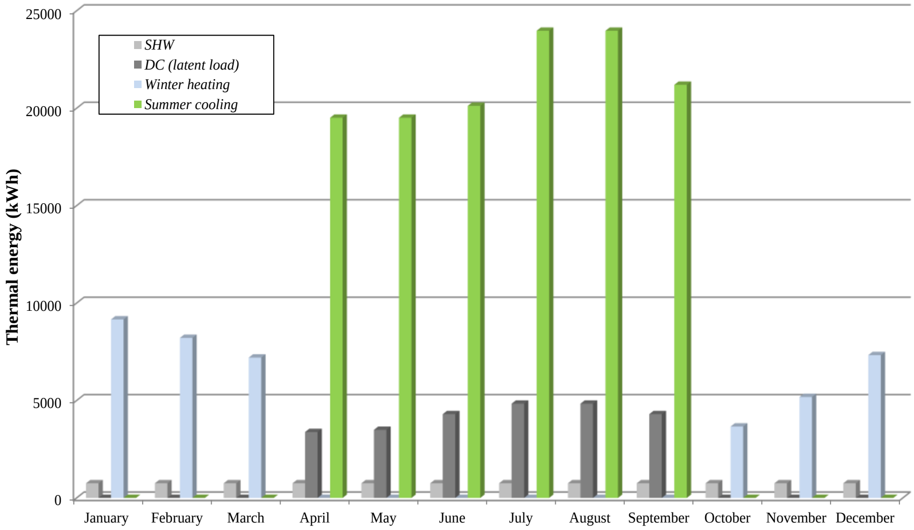

(a)

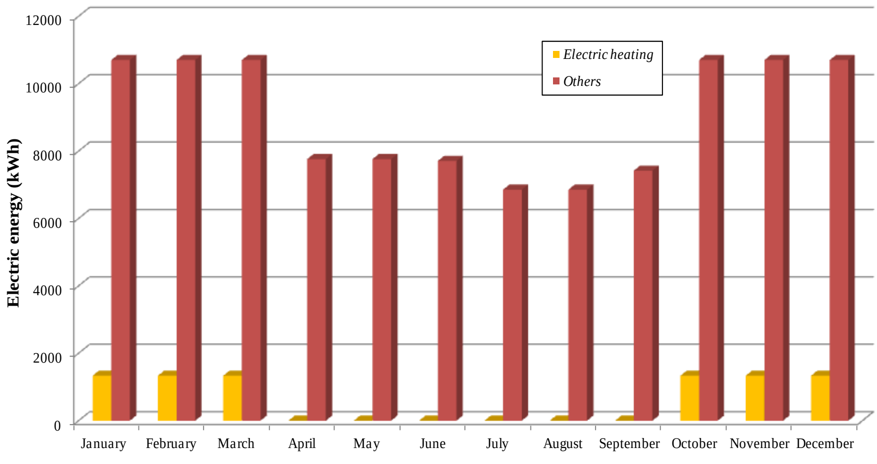

(b)

Figure 63.Thermal (a) and electrical (b) loads annual trend for the case 3.

The analysis of these three case studies allows dimensioning of the CPV/T-DC integrated system and studying how it matches the different energy needs of the supermarket. The three solutions have been analysed from an energy and

economic point of view, as shown in the next section, in order to evaluate the effectiveness of the proposed solution.
In the first case, the CPV/T system matches the thermal energy for SHW and for the latent load and part of the electrical energy needs. In this case, starting from the values of the DNI, and sizing the CPV/T system according to the thermal needs, 3.500 TJ cells, subdivided into 7 modules of 500 cells, are needed. In Table 30, the energy needs and the energy production together with the electrical and thermal loads cover rate, have been reported with reference to the first case.

Table 30. Energy loads and energy production together with the electrical and thermal loads cover rate in the case 1.

Months	*Thermal Loads (SHW+DC) (kWh)*	*Electric Loads (kWh)*	*Thermal Production (kWh)*	*Electric Production (kWh)*	*Thermal Coverage*	*Electric Coverage*
Jan	750	13755	1890	1217	252,0%	8,9%
Feb	750	14772	2272	1464	302,9%	9,9%
Mar	750	14435	4378	2821	583,7%	19,5%
Apr	4130	12963	5428	3497	131,4%	27,0%
May	4242	12963	6453	4157	152,1%	32,1%
Jun	5048	13071	7467	4811	147,9%	36,8%
Jul	5586	13249	7867	5068	140,8%	38,3%
Aug	5586	13249	7417	4779	132,8%	36,1%
Sep	5048	13071	5056	3258	100,2%	24,9%
Oct	750	13256	3713	2392	495,1%	18,0%
Nov	750	13762	1863	1200	248,4%	8,7%
Dec	750	14477	1799	1159	239,9%	8,0%

It is possible to observe that the thermal loads have been always satisfied; on the contrary, the maximum values of covering of the electrical needs are obtained in July with a rate of about 38%, while the annual mean value of covering is of about 22%. Hence, the thermal loads (SHW and latent load) are totally matched by the innovative system compared to the conventional solution, while the electrical loads are partially covered and thus an integration by the electrical national grid is necessary.
The data related to the second case have been reported in Table 31. In this case the CPV/T-DC system is also partially adopted for the winter heating.

Table 31. Energy loads and energy production together with the electrical and thermal loads cover rate in the case 2.

Mon ths	Thermal Loads (SHW+DC) (kWh)	Electric Loads (kWh)	Thermal Production (kWh)	Electric Production (kWh)	Thermal Coverage	Electric Coverage
Jan	9909	12035	3779	2435	38,1%	20,2%
Feb	8962	12035	4543	2927	50,7%	24,3%
Mar	7951	12035	8756	5641	110,1%	46,9%
Apr	4130	12963	10856	6995	262,9%	54,0%
May	4242	12963	12905	8315	304,2%	64,1%
Jun	5048	13071	14933	9621	295,8%	73,6%
Jul	5586	13249	15733	10137	281,7%	76,5%
Aug ust	5586	13249	14835	9558	265,6%	72,1%
Sep	5048	13071	10113	6516	200,3%	49,8%
Oct	4414	12035	7426	4785	168,3%	39,8%
Nov	5930	12035	3726	2400	62,8%	19,9%
Dec	8077	12035	3599	2319	44,6%	19,3%

Again, the system has been sized to match the thermal load; 7.000 TJ cells in 14 modules of 500 cells have been selected. As observed in Table 31, the thermal load cover rate is equal to 100% except in the winter months where the integration with the boiler is required. However, the annual mean rate of thermal energy covering is about 84%. Moreover, as previously observed, a decrease of the electrical energy needs is expected; this aspect, together with the increase of the plant size, allows to strongly reduce the electrical energy required to the national grid. In fact, the electrical energy cover rate reaches the highest value of 76.5% in July, with an annual average covering of about 48%.

In Table 32 the energy results of the last case study have been reported. In this case, the innovative CPV/T-DC system is equipped with an AHP in order to match the summer cooling needs. As observed in Table 32, the thermal loads have been strongly increased compared to the previous two cases. In fact, the thermal energy has been used for SHW, the latent load, winter heating and summer cooling. Hence, the electrical energy needs to cover only part of winter heating and other electrical equipments. The CPV/T system has been sized to about 10.000 TJ solar cells divided into 20 modules. The thermal energy cover rate is reduced to an annual mean value of 76%; the thermal needs that include the cooling loads are covered for about 80% in the summer period. On the other hand, the electrical energy cover rate increases to a mean annual value of 70%, making the user completely independent from the national grid in the period between April and September. Moreover, in the same period the electrical energy production is greater than the requirements and then the surplus can be sold. So, the third case has a more expensive initial solution but allows greater energy savings and economic revenues.

Table 32. Energy loads and energy production together with the electrical and thermal loads cover rate in the case 3.

Months	*Thermal Loads (SHW+DC) (kWh)*	*Electric Loads (kWh)*	*Thermal Production (kWh)*	*Electric Production (kWh)*	*Thermal Coverage*	*Electric Coverage*
Jan	9909	12035	5399	3479	54,5%	28,9%
Feb	8962	12035	6490	4182	72,4%	34,7%
Mar	7951	12035	12508	8059	157,3%	67,0%
Apr	23638	7761	15509	9992	65,6%	128,8%
May	23750	7761	18436	11878	77,6%	153,1%
Jun	25168	7706	21333	13745	84,8%	178,4%
Jul	29558	6856	22476	14481	76,0%	211,2%
Aug	29558	6856	21192	13654	71,7%	199,2%
Sep	26248	7418	14447	9308	55,0%	125,5%
Oct	4414	12035	10609	6835	240,4%	56,8%
Nov	5930	12035	5322	3429	89,8%	28,5%
Dec	8077	12035	5141	3313	63,7%	27,5%

Once evaluated the three case studies from the energy production and loads covering point of view, the second case has been selected for a further analysis. In particular, starting from the monthly loads, a daily analysis for three different periods of the year has been conducted. Adopting the ANN results for the hourly DNI and the CPV/T-DC system model, the daily electrical and thermal energy production of the plant proposed has been evaluated in the second case. Considering a summer day, in Figure 64 (a) it can be noted that the thermal energy production is always greater than the needs, while in Figure 64 (b) the electrical loads are greater than the electrical production only in few hours, but this difference can be covered by the surplus in the central hours of the day.

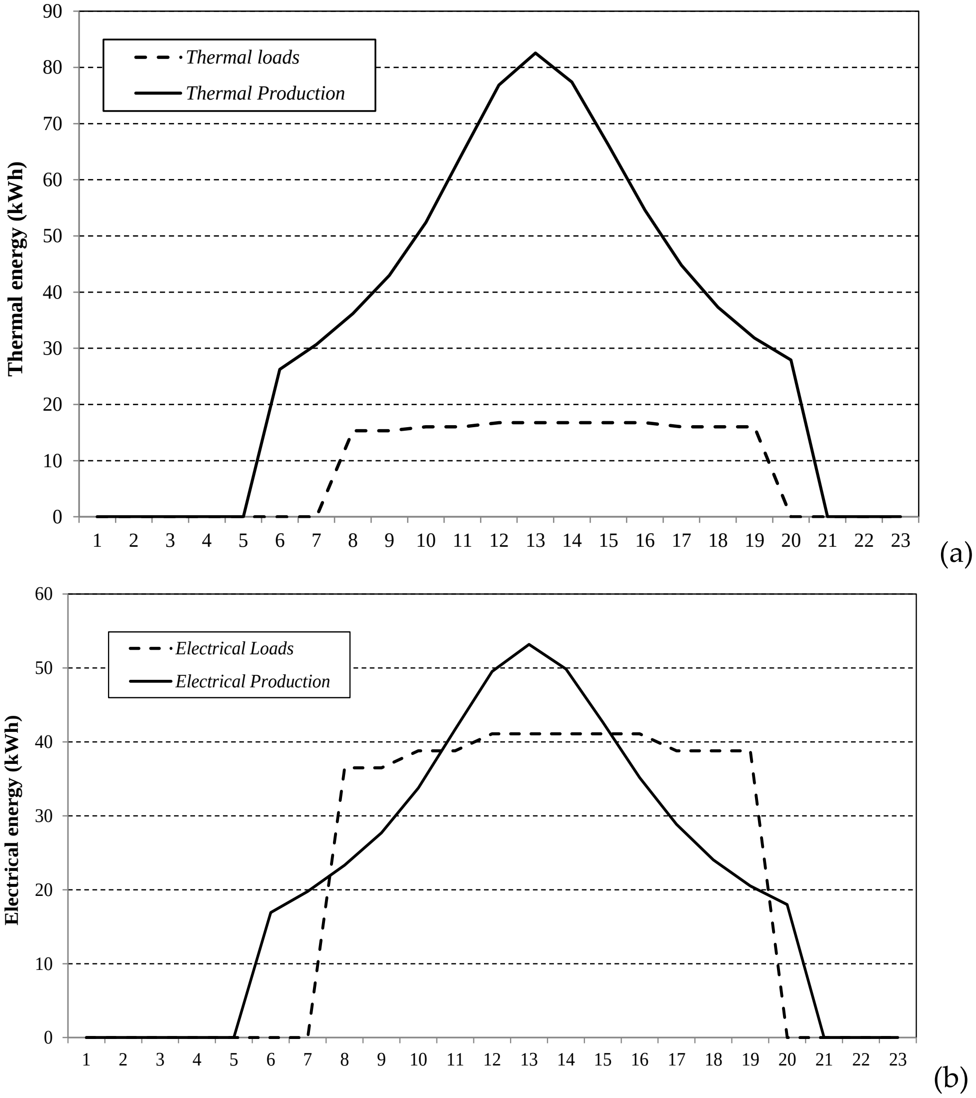

Figure 64.Thermal (a) and electrical (b) energy production and loads for a summer day.

In Figure 65(a) and Figure 65 (b), the thermal and electrical energy production and the loads have been respectively shown considering a winter day. The low incident DNI of this period, as previously shown in Table 31 , leads to an integration requirement for the thermal and electrical needs.

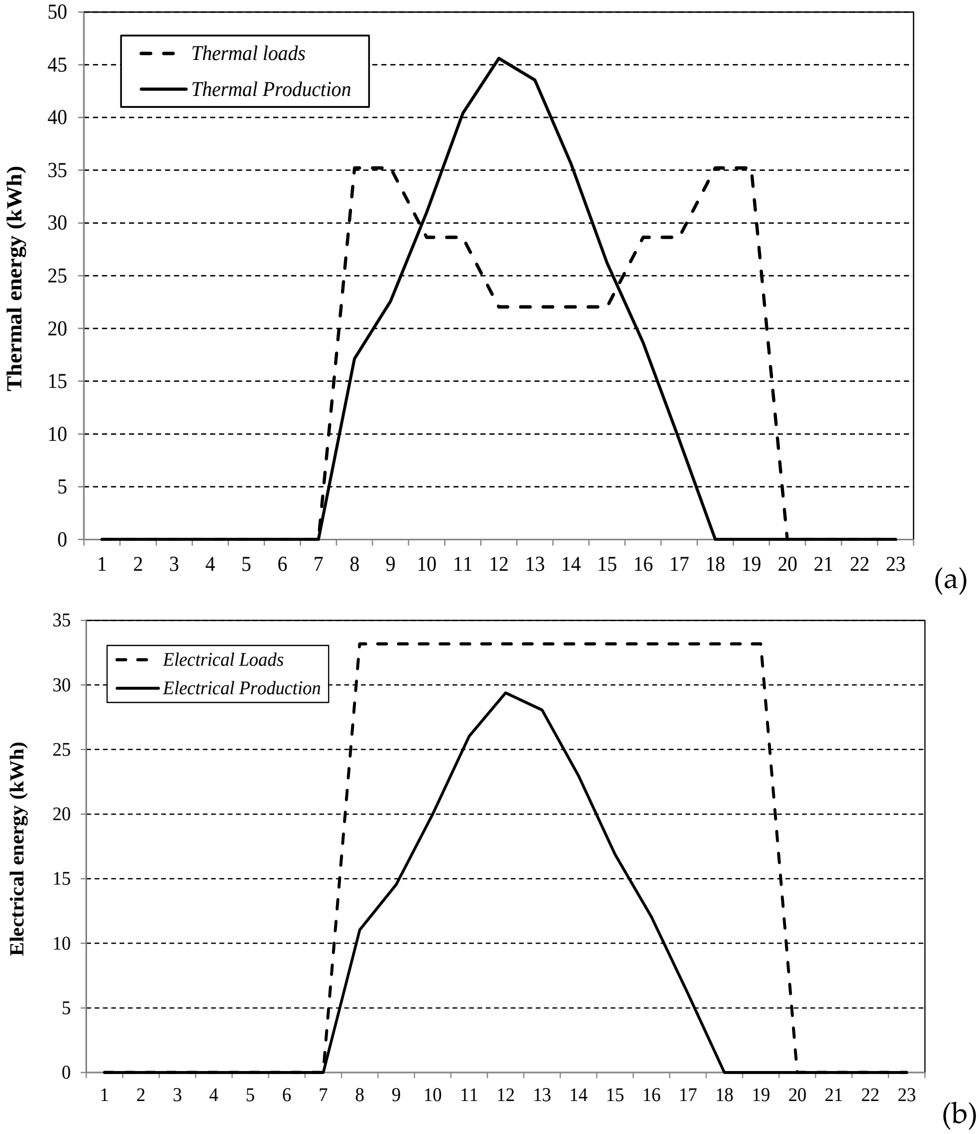

Figure 65.Thermal (a) and electrical (b) energy production and loads for a winter day.

Finally, in the Figure 66 the situation for a half season day has been indicated. In this case, the thermal loads are always covered by the plant thermal energy production (Figure 66 (a)), while the electricity from the grid is required (with a daily percentage less than 15% - Figure 66 (b)).

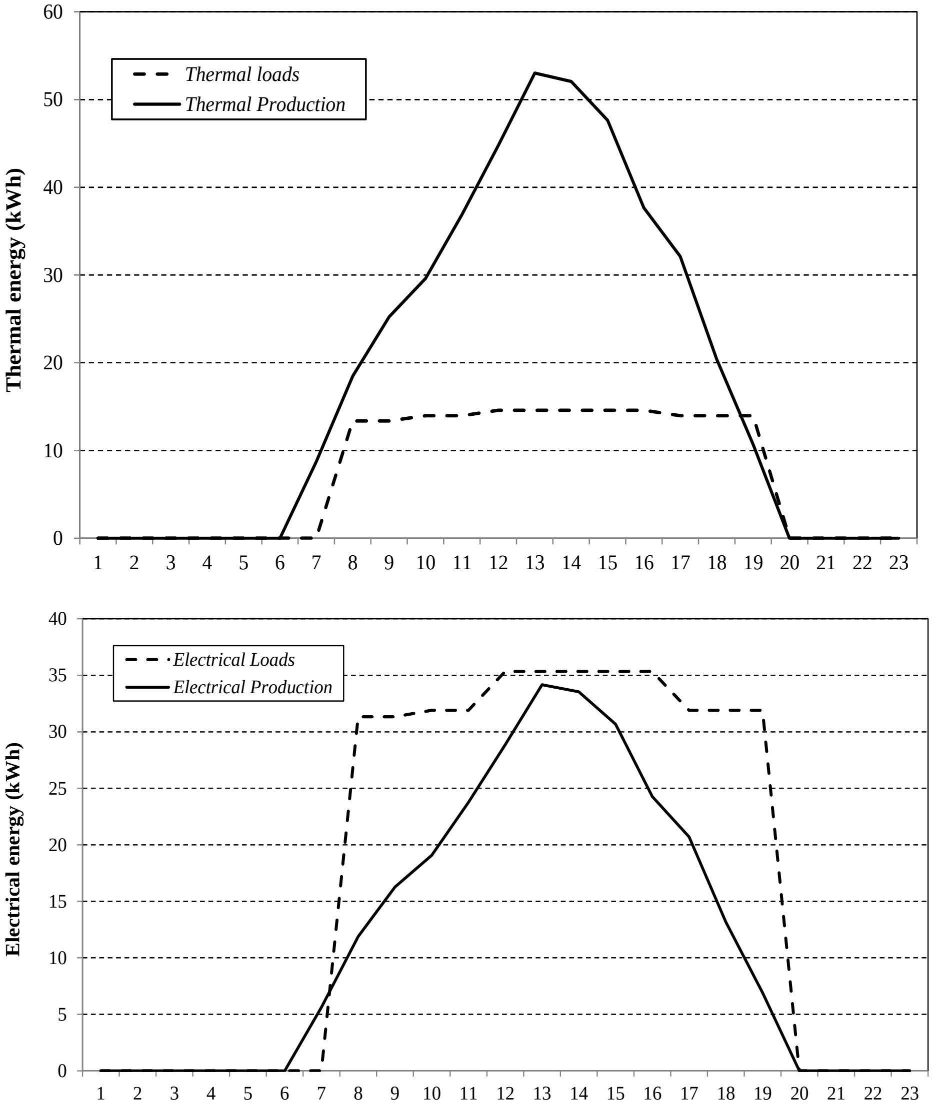

(a)

(b)

Figure 66. Thermal (a) and electrical (b) energy production and loads for a half season day.

The analysis conducted during the different periods of the year, together with the previous global evaluation, shows that the plant proposed can almost match the user all year energy demands, thus it could represent a good alternative to the conventional system, especially for the second case. In fact,

this solution represents a good compromise between costs and loads covering rate.
Moreover, the values of the primary energy saving (PES) are evaluated, by comparing the primary energy required by the conventional system ($E_{prim\text{-}CS}$) with those of the proposed innovative CPV/T-DC system ($E_{prim\text{-}prop\ sys}$):

$$PES = \frac{E_{prim-CS} - E_{prim-prop\ syst}}{E_{prim-CS}} \cdot 100 \qquad (30)$$

Based on the values reported in the Table 30, Table 31 and Table 32, the following relevant PES values have been obtained: 41%, 61% and 74%, respectively for the cases 1, 2 and 3.
Finally, a costs analysis has been also conducted for the three case studies in order to definitively demonstrate the goodness of the solutions proposed. In Table 33, the costs of the plant have been separately reported referring to CPV/T system, DC system and AHP.

Table 33. CPV/T-DC system costs.

	CPV/T-DC system costs		
	Unitary cost		*Total cost*
DC	1800	€/kW	€ 90.000
CPV/T	16	€/cell	€ 112.000
AHP	450	€/kW$_f$	€ 22.500
		Total	€ 224.500

In Figure 67, the Net Present Value (NPV) trend for the three solutions has been reported, with respect to the conventional system. The first case presents an initial additional cost of about 150 k€ with a SPB of 9 years and the second case shows an initial extra-cost of 200 k€ with a SPB of 8 years. Finally, the third case, which corresponds to the tri-generation solution, represents the most advantageous case with a SPB of about 5-6 years and a higher NPV (more than 550 k€ after 20 years), even if this solution presents higher initial costs, larger overall dimensions and the required temperatures of the working fluid cannot always be reached during the year.

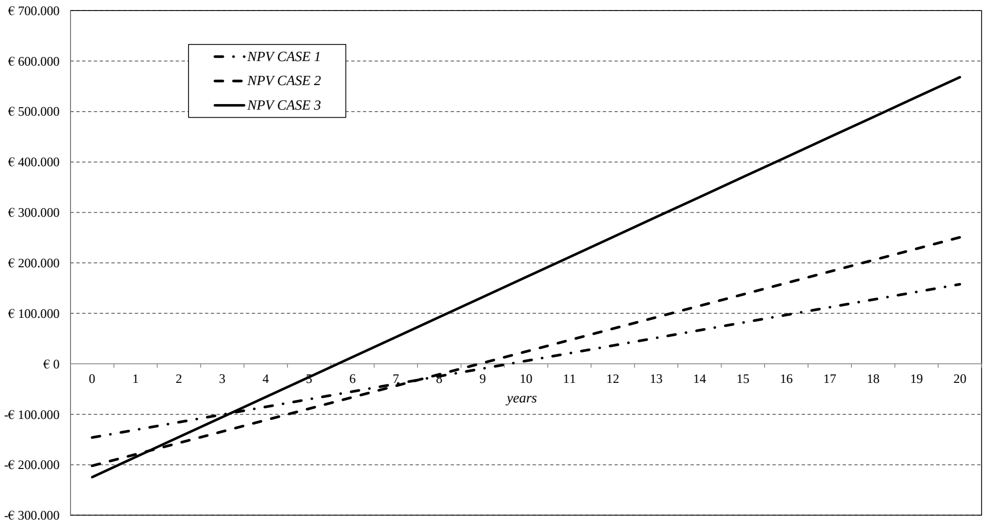

Figure 67. NPV (Net Present Value) for the proposed CPV/T-DC system in the cases 1, 2, 3.

6.2.2 Conclusions

The coupling of a concentrating photovoltaic thermal system (CPV/T) with a desiccant cooling (DC) system has enabled to obtain energy and economic savings during the year, compared with a conventional solution (without CPV/T and DC). In particular, three case studies have been conducted and in each of them the CPV/T-DC integrated system has been sized to satisfy, totally or partially, the different energy needs of the supermarket. The three case studies have been analyzed from an energy and economic point of view, evaluating the thermal and electrical energy production and the Net Present Value (NPV).

The coupling between the CPV/T and DC system has been modelled in order to satisfy the energy loads required by a supermarket. An accurate analysis of the electrical and thermal loads of the supermarket has been realized considering three different periods of the year: summer, winter and half season. The size of the CPV/T system as a function of the Direct Normal Irradiance (DNI) for each period of the year, has been obtained. For this purpose, an accurate DNI modelling by means of the Artificial Neural Network (ANN) has been also considered. The coupling between the CPV/T and DC systems has allowed to obtain energy and economic savings during the year, compared with the conventional solution. In particular, three case

studies have been analysed and in each of them the CPV/T-DC integrated system has been sized to satisfy, totally or partially, the different energy needs of the supermarket. The three solutions have been analysed from an energy and economic point of view, evaluating the thermal and electrical energy production, the Primary Energy Savings (PES) and the economical parameters Simple PayBack (SPB) and the Net Present Value (NPV).
In the first case the thermal loads have been always satisfied while the annual mean value of electrical energy covering is about 22%. In the second case the annual mean rate of thermal energy covering is about 84%, while the electrical annual average covering is about 48%. In the last case the thermal energy cover rate is reduced to an annual mean value of 76%, but the electrical energy cover rate increases to a mean annual value of 70%. By comparing the primary energy required by both the conventional system and the proposed innovative CPV/T-DC system, the following relevant PES values have been obtained: 41%, 61% and 74%, respectively for the cases 1, 2 and 3.
The third case represents a more expensive initial solution, but it allows greater energy savings and economic revenues, presenting a SPB of about 6 years and the highest NPV (more than 550 k€ after 20 years) and PES (74%), even if the second case represents a good compromise between costs and loads covering rate with a SPB of 8 years, a NPV more than 250 k€ and a PES of 61%. Finally, the obtained energy and economic results are consistent with other literature values.

The contents of this chapter are a summary of the following publication:

- Renno, C., D'Agostino, D., Minichiello, F., Petito, F., Balen, I. "Performance analysis of a CPV/T-DC integrated system adopted for the energy requirements of a supermarket". *Applied Thermal Engineering*, 2019, 149, 231-2

BIBLIOGRAPHY

1. Euopean Parliament, *Directive 2002/91/EC on Energy performance of buildings. OJ L 1, 4.1.2003*. 2002: European Union.
2. European Parliament, *Directive 2010/31/EU on energy performance of buildings.* 2010: European Union.
3. Gilijamse, W., *Zero-energy houses in the Netherlands.* Proceedings of Building Simulation '95. Madison, Wisconsin, USA, August 14–16 1995, 1995.
4. Torcellini, P.P., S; Deru, M; Crawley, D, *Zero Energy Buildings: A Critical Look at the Definition.* Conference: Presented at ACEEE Summer Study, 14-18 August 2006, Long Beach, California, 2006.
5. Evola, G., Marganu, G., and Marletta, L., *Cost - effective design solutions for low rise residential Net ZEBs in Mediterranean climate.* Energy and Buildings, 2014. 68(7-18).
6. Magrini, A., et al., *From nearly zero energy buildings (NZEB) to positive energy buildings (PEB): The next challenge - The most recent European trends with some notes on the energy analysis of a forerunner PEB example.* Developments in the Built Environment, 2020. 3: p. 100019.
7. Belussi, L., et al., *A review of performance of zero energy buildings and energy efficiency solutions.* Journal of Building Engineering, 2019. 25: p. 100772.
8. Li, X., et al., *Energetic and economic evaluation of hybrid solar energy systems in a residential net-zero energy building.* Applied Energy, 2019. 254: p. 113709.
9. Hermelink, A.S.S.; Boermans, T.; Pagliano, L.; Zangheri, P.; Armani, R.; Voss, K.; Musall, E, *Towards Nearly Zero-Energy Buildings. Definition of Common Principles under the EPBD; Final Report. Project Number: BESDE10788*. 2013.
10. Harkouss, F., Fardoun, F., Biwole, P.H. , *Optimal design of renewable energy solution sets for net zero energy buildings. .* Energy, 2019. 179: p. 1155–1175.

11. Sartori, I., Napolitano, A., Voss, K., *Net zero energy buildings: A consistent definition framework.* . Energy and Buildings, 2012. 48: p. 220–232.
12. Bandeiras, F., et al., *Towards net zero energy in industrial and commercial buildings in Portugal.* Renewable and Sustainable Energy Reviews, 2020. 119: p. 109580.
13. Tumminia, G., et al., *Grid interaction and environmental impact of a net zero energy building.* Energy Conversion and Management, 2020. 203: p. 112228.
14. Basta, S. and Minchio, F., *Geotermia e pompe di calore. Guida pratica agli impianti geotermici di climatizzazione.* 2007, Verona: Savino Basta (in Italian)
15. Sommaruga, C., and Verdiani, G., *Geotermia: Principi, Ricerca, Produzione.*, ed. L.N.I. Scientifica. 1995, Roma. (in Italian)
16. Lund, J.W., Freestone., D. H. and Boyd, T. L. , *Direct Utilization of Geothermal Energy 2010 Worldwide Review.* Proceedings World Geothermal Congress 2010 Bali, Indonesia, 25-29 April 2010, 2010.
17. European Geothermal Market Report, *European Geothermal Energy Council*. 2020.
18. ASHRAE, *ASHRAEhandbook: Heating, ventilating, and air-conditioning applications*, in *Geothermal Energy*, R.A.-C.E. American Society of Heating, Editor. 2007: Atlanta. p. 32.31-32.30.
19. Raymond, J. Therrien, R. and Gosselin, L., Université Laval, Québec, Québec, *Low-temperature geothermal energy in mining environments.* CIM journal, 2010. 1 (2).
20. Budinski, K.G. and Budinski, M. K., *Engineering Materials: Properties and Selection*, ed. N. Edition. 2009.
21. Lund, J.W., Freeston, D. H. and Boyd, T.L., *Direct utilization of geothermal energy 2010 worldwide review.* Geothermics, 2011. 40(3): p. 159-180.
22. Noorollahi, Y., et al., *The effects of ground heat exchanger parameters changes on geothermal heat pump performance – A review.* Applied Thermal Engineering, 2018. 129: p. 1645-1658.
23. Baietto, A., Pochettino, M. and Salvatici, E. , *Progettazione di Impianti Geotermici – Sonde verticali e pozzi d'acqua.*, ed. D. Flaccovio. 2020. (in Italian)

24. Marrasso, E., et al., *Global and local environmental and energy advantages of a geothermal heat pump interacting with a low temperature thermal micro grid.* Energy Conversion and Management, 2018. 172: p. 540-553.
25. Massarotti, N., et al., *Innovative Solutions to Use Ground-Coupled Heat Pumps in Historical Buildings: A Test Case in the City of Napoli, Southern Italy.* Energies, 2021. 14(2).
26. Kotarela, F., A. Kyritsis, and N. Papanikolaou, *On the Implementation of the Nearly Zero Energy Building Concept for Jointly Acting Renewables Self-Consumers in Mediterranean Climate Conditions.* Energies, 2020. 13(5).
27. Carotenuto, A., et al., *Energy piles for ground source heat pump applications: Comparison of heat transfer performance for different design and operating parameters.* Applied Thermal Engineering, 2017. 124: p. 1492-1504.
28. Revesz, A., et al., *Ground source heat pumps and their interactions with underground railway tunnels in an urban environment: A review.* Applied Thermal Engineering, 2016. 93: p. 147-154.
29. Sáez Blázquez, C., et al., *Technical optimization of the energy supply in geothermal heat pumps.* Geothermics, 2019. 81: p. 133-142.
30. Buonomano, A., et al., *Energy and economic analysis of geothermal–solar trigeneration systems: A case study for a hotel building in Ischia.* Applied Energy, 2015. 138: p. 224-241.
31. Huang, J., Fan, J. and Furbo, S., *Demonstration and optimization of a solar district heating system with ground source heat pumps.* Solar Energy, 2020. 202: p. 171-189.
32. Lazzarin, R. and Noro, N., *Photovoltaic/Thermal (PV/T)/ground dual source heat pump: Optimum energy and economic sizing based on performance analysis.* Energy and Buildings, 2020. 211: p. 109800.
33. Abu-Rumman, M., M. Hamdan, and O. Ayadi, *Performance enhancement of a photovoltaic thermal (PVT) and ground-source heat pump system.* Geothermics, 2020. 85: p. 101809.
34. Litjens, G.B.M.A., Worrell, E., and van Sark, W.G.J.H.M. *Lowering greenhouse gas emissions in the built environment by combining ground source heat pumps, photovoltaics and battery storage.* Energy and Buildings, 2018. 180: p. 51-71.

35. De Carli, M., et al., *Energetic and economic aspects of a heating and cooling district in a mild climate based on closed loop ground source heat pump.* Applied Thermal Engineering, 2014. 71(2): p. 895-904.
36. Fadejev, J., et al., *Geothermal Heat Pump Plant Performance in a Nearly Zero-energy Building.* Energy Procedia, 2016. 96: p. 489-502.
37. Gao, J., et al., *Ground heat exchangers: Applications, technology integration and potentials for zero energy buildings.* Renewable Energy, 2018. 128: p. 337-349.
38. Ministry of Economic Development, *Decreto interministeriale 26 giugno 2015 - Applicazione delle metodologie di calcolo delle prestazioni energetiche e definizione delle prescrizioni e dei requisiti minimi degli edifici (in Italian)*. 2015.
39. Feng, W.Z., Q.; Ji, H.; Wang, R.; Zhou, N.; Ye, Q.; Hao, B.; Li, Y.; Luo, D.; Lau, S.S.Y. , *A review of net zero energy buildings in hot and humid climates: Experience learned from 34 case study buildings.* Renewable and Sustainable Energy Reviews, 2019. 114: p. 109303.
40. DesignBuilder, *DesignBuilder Software V.6.1.0.006*. 2019: Designbuilder Software Limited Clarendon Court 1st Floor 54/56 London Rd Stroud,Gloucestershire GL5 2AD(UK).
41. ANSI/ASHRAE, *ANSI/ASHRAE Standard 140-2017 (aka BESTEST) validation test results for DesignBuilder v6.1 with EnergyPlus v8.9*. 2017.
42. ASHRAE, *International Weather Files for Energy Calculations (IWEC Weather Files)*, R.a.A.-C.E.A. American Society of Heating, GA, USA, 2017, Editor. 2017.
43. Tool, B.E.U.a.C.A., *38.DOE-2* 2016.
44. Program, T.A.R., *TARP*. 2018.
45. DesignBuilder. *HVAC component hierarchy and navigation*. Available from: https://designbuilder.co.uk/helpv4.2/Content/Detailed_HVAC/HVAC_Component_Hierarchy_and.htm.
46. DesignBuilder. *Cooling capacity function of temperature curve (CAPFT)*. Available from: https://designbuilder.co.uk/helpv4.2/Content/Performance_Curves.htm#Curve:Bi.
47. DesignBuilder, *Quadratic curve EIRPLR.*
48. Tang, C.C., *Modelling Packaged Heat Pumps in a Quasi-Steady State Energy Simulation Program.* , in *Department of Mechanical and Aerospace*

Engineering, Oklahoma State University, Stillwater, OK, USA. 2005, Oklahoma State University.
49. Jones, A.T.F., D. , *Ground source heat pump modelling with thermal storage-simulation and integration issues in EnergyPlus.* Proceedings of the BS2013 13th Conference of International Building Performance Simulation Association; Chambéry, France, 26–28 August 2013, 2013.
50. Kusuda, T.A., P.R. , *Earth Temperature and Thermal Diffusivity at Selected Stations in the United States.* ASHRAE Transactions., 1965. Department of Commerce – National Bureau of Standards, Volume 71.
51. Mayors, E., *Greenhouse Gas Emission Coefficients: Fuels.* . 2020.
52. *ASHRAE Handbook Fundamentals, SI.* ASHRAE: Atlanta, GA, USA, 2017.
53. President of Italian Republic, *D.P.R. 26 agosto 1993, n. 412, Regolamento recante norme per la progettazione, l'installazione, l'esercizio e la manutenzione degli impianti termici degli edifici, in attuazione dell'art. 4, comma 4, della L. 9 gennaio 1991, n. 10 (in Italian).* 1993.
54. President of Italian Republic, *D.P.R. 74/2013 Regolamento recante definizione dei criteri generali in materia di esercizio, conduzione, controllo, manutenzione e ispezione degli impianti termici per la climatizzazione invernale ed estiva degli edifici e per la preparazione dell'acqua calda per usi igienici sanitari*. (in Italian) 2013.
55. García-Céspedes, J.A., G.; Herms, I.; de Felipe, J.J. , *Characterisation of efficiency losses in ground source heat pump systems equipped with a double parallel stage: A case study.* Renewable Energy, 2020. 147: p. 2761–2773.
56. Ministry Of Economic Development and ENEA, *REPORT RSE/2009/162. Ricerca Sistema Elettrico—Caratterizzazione energetica del settore alberghiero in Italia*. 2009, Milan. (In Italian).
57. *Joint Research Centre of the European Commision, PVGIS performance tool*. 2020.
58. D'Agostino, D., et al., *The use of ground source heat pump to achieve a net zero energy building*. Energies, 2020. 13(13).
59. European Union, *Eurostat Statistic Explained - Energy costs referred to 2019*. 2019.
60. Peretti, C., et al., *The design and environmental evaluation of earth-to-air heat exchangers (EAHE). A literature review.* Renewable and Sustainable Energy Reviews, 2013. 28: p. 107-116.

61. De Carli, M. and Zarrella, A., *Nuova frontiere in tema di trasmissione del calore: Scambiatori aria-terreno (Earth to Air Heat Exchanger) (in Italian)*, in *XI Scuola Estiva di Fisica Tecnica*, U.d.S.d.P.-. DII, Editor. 2019.
62. Agrawal, K.K., et al., *A review on effect of geometrical, flow and soil properties on the performance of Earth air tunnel heat exchanger.* Energy and Buildings, 2018. 176: p. 120-138.
63. Singh, R., et al., *Recent advancements in earth air tunnel heat exchanger (EATHE) system for indoor thermal comfort application: A review.* Renewable and Sustainable Energy Reviews, 2018. 82: p. 2162-2185.
64. de Jesus Freire, A., et al., *Compact buried pipes system analysis for indoor air conditioning.* Applied Thermal Engineering, 2013. 51(1): p. 1124-1134.
65. D'Agostino, D., et al., *The Energy Performances of a Ground-to-Air Heat Exchanger: A Comparison Among Köppen Climatic Areas.* Energies, 2020. 13(11).
66. Bordoloi, N., et al., *An intense review on the latest advancements of Earth Air Heat Exchangers.* Renewable and Sustainable Energy Reviews, 2018. 89: p. 261-280.
67. Bisoniya, T.S., A. Kumar, and P. Baredar, *Study on Calculation Models of Earth-Air Heat Exchanger Systems.* Journal of Energy, 2014. 2014: p. 859286.
68. Kabashnikov, V.P., et al., *Analytical and numerical investigation of the characteristics of a soil heat exchanger for ventilation systems.* International Journal of Heat and Mass Transfer, 2002. 45(11): p. 2407-2418.
69. De Paepe, M. and A. Janssens, *Thermo-hydraulic design of earth-air heat exchangers.* Energy and Buildings, 2003. 35(4): p. 389-397.
70. Cucumo, M., et al., *A one-dimensional transient analytical model for earth-to-air heat exchangers, taking into account condensation phenomena and thermal perturbation from the upper free surface as well as around the buried pipes.* International Journal of Heat and Mass Transfer, 2008. 51(3): p. 506-516.
71. Sehli, A., A. Hasni, and M. Tamali, *The Potential of Earth-air Heat Exchangers for Low Energy Cooling of Buildings in South Algeria.* Energy Procedia, 2012. 18: p. 496-506.
72. Serageldin, A.A., Abdelrahman, A.K., and Ookawara, S., *Earth-Air Heat Exchanger thermal performance in Egyptian conditions: Experimental*

results, mathematical model, and Computational Fluid Dynamics simulation. Energy Conversion and Management, 2016. 122: p. 25-38.
73. Cuny, M., et al., *Multi-criteria optimization of an earth-air heat exchanger for different French climates.* Renewable Energy, 2020. 157: p. 342-352.
74. Lin, J., et al., *Impact of soil moisture on the long-term energy performance of an earth-air heat exchanger system.* Renewable Energy, 2020. 147: p. 2676-2687.
75. Ahmed, S.F., et al., *Parametric study on thermal performance of horizontal earth pipe cooling system in summer.* Energy Conversion and Management, 2016. 114: p. 324-337.
76. Niu, F., et al., *Investigation on soil thermal saturation and recovery of an earth to air heat exchanger under different operation strategies.* Applied Thermal Engineering, 2015. 77: p. 90-100.
77. Zhao, Y., et al., *Parametric study and design of an earth-air heat exchanger using model experiment for memorial heating and cooling.* Applied Thermal Engineering, 2019. 148: p. 838-845.
78. Bisoniya, T.S., A. Kumar, and P. Baredar, *Energy metrics of earth–air heat exchanger system for hot and dry climatic conditions of India.* Energy and Buildings, 2015. 86: p. 214-221.
79. Bansal, V., et al., *'Derating Factor' new concept for evaluating thermal performance of earth air tunnel heat exchanger: A transient CFD analysis.* Applied Energy, 2013. 102: p. 418-426.
80. Bansal, V., et al., *Performance evaluation and economic analysis of integrated earth–air–tunnel heat exchanger–evaporative cooling system.* Energy and Buildings, 2012. 55: p. 102-108.
81. Ascione, F., et al., *Earth-to-air heat exchanger for NZEB in Mediterranean climate.* Renewable Energy, 2016. 99: p. 553-563.
82. Li, H., et al., *Annual performance experiments of an earth-air heat exchanger fresh air-handling unit in severe cold regions: Operation, economic and greenhouse gas emission analyses.* Renewable Energy, 2020. 146: p. 25-37.
83. D'Agostino D., M.C., Minichiello F., *The Use of Earth-to-Air and Air-to-Air Heat Exchangers for Different Italian Climates.* International Journal of Heat and Technology, 2016. 34.
84. UNI 10339: Impianti aeraulici a fini di benessere. Generalità, c., requisiti. Regole per la richiesta d'offerta, l'offerta, l'ordine e la fornitura. . 1995.

85. Chiesa, G., *EAHX – Earth-to-air heat exchanger: Simplified method and KPI for early building design phases.* Building and Environment, 2018. 144: p. 142-158.
86. Ascione, F., L. Bellia, and F. Minichiello, *Earth-to-air heat exchangers for Italian climates.* Renewable Energy, 2011. 36(8): p. 2177-2188.
87. Chen, D. and H.W. Chen, *Using the Köppen classification to quantify climate variation and change: An example for 1901–2010.* Environmental Development, 2013. 6: p. 69-79.
88. Spitler, J.D. and S.E.A. Gehlin, *Thermal response testing for ground source heat pump systems—An historical review.* Renewable and Sustainable Energy Reviews, 2015. 50: p. 1125-1137.
89. Badescu, V., *Simple and accurate model for the ground heat exchanger of a passive house.* Renewable Energy, 2007. 32(5): p. 845-855.
90. N. Hatraf, F.C., A. Brima, N. Moummi, and A. Moummi, *Parametric Study of to Design an Earth to Air Heat Exchanger with Experimental Validation.* Eng. J., 2014. 18(2): p. 41-54.
91. Khabbaz, M., et al., *Experimental and numerical study of an earth-to-air heat exchanger for air cooling in a residential building in hot semi-arid climate.* Energy and Buildings, 2016. 125: p. 109-121.
92. Qiu, S., et al., *An energy exchange efficiency prediction approach based on multivariate polynomial regression for membrane-based air-to-air energy recovery ventilator core.* Building and Environment, 2019. 149: p. 490-500.
93. Rojas, G., R. Pfluger, and W. Feist, *Cascade ventilation—Air exchange efficiency in living rooms without separate supply air.* Energy and Buildings, 2015. 100: p. 27-33.
94. U.S. Department of Energy, F.E.M.P.F., *M&V Guidelines: Measurement and Verification for Performance-Based Contracts*. 2015: FEMP: Washington, DC, USA.
95. Engineers, A.A.S.o.H.R.a.A.-C., *Guideline 14 2002, Measurement of Energy and Demand and Savings*. 2002: ASHARE: Atlanta, GA, USA.
96. 2:2019-06, V.B., *Thermal use of the underground - Ground source heat pump systems. Technical rule (in German and English)*. 2019.
97. Urraca, R., et al., *Sources of uncertainty in annual global horizontal irradiance data.* Solar Energy, 2018. 170: p. 873-884.

98. Gracia-Amillo, A.M., et al., *Energy-based metric for analysis of organic PV devices in comparison with conventional industrial technologies.* Renewable and Sustainable Energy Reviews, 2018. 93: p. 76-89.
99. D'Agostino, D., Minichiello, F. and Valentino, A., *Contribution of low enthalpy geothermal energy in the retrofit of a single-family house: a comparison between two technologies.* Journal of Advanced Thermal Science Research, 2020. 7 (1).
100. UNI EN 10339:2005,., *Impianti aeraulici a fini di benessere. Generalità, classificazione, requisiti. Regole per la richiesta d'offerta, l'offerta, l'ordine e la fornitura.* 2005.
101. Hall, M., and Geissler, A., *Different balancing methods for Net Zero Energy Buildings - Impact of time steps, grid interaction and weighting factors.* Energy procedia, 2017. 122: p. 379–384.
102. Renno, C., *Experimental and Theoretical Analysis of a Linear Focus CPV/T System for Cogeneration Purposes.* Energies, 2018. 11(11).
103. Renno, C., *Experimental and Theoretical Analysis of a Linear Focus CPV/T System for Cogeneration Purposes.* Energies, 2018. 11: p. 2960.
104. Renno, C., et al., *Performance analysis of a CPV/T-DC integrated system adopted for the energy requirements of a supermarket.* Applied Thermal Engineering, 2019. 149: p. 231-248.
105. Renno, C., et al., *Modeling of a CPV/T-ORC Combined System Adopted for an Industrial User.* Energies, 2020. 13(13)

PUBLICATIONS

The publications published during the PhD program are indicated in bold type.

1. Calise F., Cappiello F., D'Agostino D., Vicidomini M., “**A novel approach for the calculation of the energy savings of heat metering for different kinds of buildings**”, 2021, *Energy and Buildings*, 252, 111408.
2. Calise F., Cappiello F., D'Agostino D., Vicidomini M., "**Heat metering for residential buildings: A novel approach through dynamic simulations for the calculation of energy and economic savings**",2021,*Energy*,234,121204.
3. D'Agostino D., D'Agostino P., Minelli F., Minichiello F., "**Proposal of a new automated workflow for the computational performance-driven design optimization of building energy need and construction cost**",2021,*Energy and Buildings*,239,110857.
4. Renno C., Perone A., D’Agostino D., Minichiello F. “**Experimental and economic analysis of a concentrating photovoltaic system applied to users of increasing size**”, 2021, *Energies*, 14(16), 4968.
5. D'Agostino, D., Minichiello, F. and A. Valentino. “**Contribution of Low Enthalpy Geothermal Energy in the Retrofit of a Single-Family House: A Comparison between Two Technologies**”. *Journal of Advanced Thermal Science Research,* 2020, 7, 30-39.
6. D'Agostino D., Greco A., Masselli C., Minichiello F., "**The employment of an earth-to-air heat exchanger as pre-treating unit of an air conditioning system for energy saving: A comparison among different worldwide climatic zones**", 2020, *Energy and Buildings*, 229, 110517.
7. D'Agostino D., Marino C., Minichiello F., "**Earth-to-Air Versus Air-to-Air Heat Exchangers: A Numerical Study on the Energetic, Economic, and Environmental Performances for Italian Office Buildings**", 2020, *Heat Transfer Engineering*, 41,12,1040,1051.

8. D'Agostino D., Mele L., Minichiello F., Renno C., "**The use of ground source heat pump to achieve a net zero energy building**", 2020, *Energies*, 13,13,3450.
9. Renno C., Petito F., D'Agostino D., Minichiello F., "**Modeling of a CPV/T-ORC combined system adopted for an industrial user**", 2020, *Energies*, 13, 13, 33476.
10. D'Agostino D., Esposito F., Greco A., Masselli C., Minichiello F., "**Parametric analysis on an earth-to-air heat exchanger employed in an air conditioning system**", 2020, *Energies*, 13,11, 2925.
11. D'Agostino D., Esposito F., Greco A., Masselli C., Minichiello F., "**The energy performances of a ground-to-air heat exchanger: A comparison among Köppen climatic areas**", 2020, *Energies*, 13, 11, 2895
12. D'Agostino D., de' Rossi F., Marino C., Minichiello F., Russo F., "**Double plus-zero energy historic building and improvement of hygrothermal conditions for the Palaeontology Museum of Naples**", 2021, *Journal of Building Physics*, 45 (1), 148,179.
13. D'Agostino D., de' Rossi F., Marigliano M., Marino C., Minichiello F., "**Evaluation of the optimal thermal insulation thickness for an office building in different climates by means of the basic and modified "cost-optimal" methodology**", 2019, *Journal of Building Engineering*, 24, 100743.
14. Renno C., D'Agostino D., Minichiello F., Petito F., Balen I., "**Performance analysis of a CPV/T-DC integrated system adopted for the energy requirements of a supermarket**", 2019, *Applied Thermal Engineering*, 149,231,248.
15. D'Agostino D., Mele L., Minichiello F., "**The contribution of geothermal heat pumps in Net Zero Energy Buildings (NZEBs)**", 2019, *Building Simulation Conference Proceedings*, 7, 4969,4976.
16. D'Agostino D., Marino C., Minichiello F., Russo F., "**Two types of heat exchangers for office buildings in different European climates**",2019, "*Computational Thermal Sciences*", 11,1-2,57,67.
17. D'Agostino D., Daraio L., Marino C., Minichiello F., "**Cost-optimal methodology and passive strategies for building energy efficiency: a case-study**", 2018, *Architectural Science Review*, 61 ,6, 400 ,409.
18. D'Agostino D., Marino C., Minichiello F., Russo F.,"CHT-17: Heat recovery in air conditioning systems for office buildings", 2017,

International Symposium on Advances in Computational Heat Transfer, 869, 880.
19. D'Agostino D., Marino C., Minichiello F., Russo F., "Obtaining a NZEB in Mediterranean climate by using only on-site renewable energy: Is it a realistic goal?", 2017, *Energy Procedia*, 140, 23, 35.
20. D'Agostino D., De'Rossi F., Marino C., Minichiello F., Russo F., "Energy retrofit of historic buildings in the Mediterranean area: The case of the Palaeontology Museum of Naples", 2017, *Energy Procedia*, 133, 336, 348.
21. Ascione F., D'Agostino D., Marino C., Minichiello F., "Earth-to-air heat exchanger for NZEB in Mediterranean climate", 2016, *Renewable Energy*, 99,553, 563.
22. D'Agostino D., Marino C., Minichiello F., "The use of earth-To-Air and air-To-Air heat exchangers for different Italian climates", 2016, *International Journal of Heat and Technology*, 34, 2, S287,S294.

Book Paragraph:

1. "**Scambiatori di calore terra-aria inseriti in impianti di climatizzazione**" D'Agostino D., Marino, C. and Minichiello, F. Book: Progetto Smart-Case, Editor *Giannini*, 2021, ISBN 978-88-6906-161-5 (in Italian).